



11-53-5
 204270
 p. 152

**Configuration Development Study of the OSU I
 Hypersonic Research Vehicle**

**Matthew D. Stein
 Chris Fankhauser
 Warner Zee**

**Melvin Kosanchick III
 Nick Nelson
 William Hunt**

(NASA-CR-195522) CONFIGURATION
 DEVELOPMENT STUDY OF THE OSU I
 HYPERSONIC RESEARCH VEHICLE (Ohio
 State Univ.) 152 p

N94-24591

Unclas

G3/05 0204270

May 31, 1993

Abstract

In an effort to insure the future development of hypersonic cruise aircraft, the possible vehicle configurations were examined to develop a single-stage-to-orbit hypersonic research vehicle (HRV). Based on the needs of hypersonic research and development, the mission goals and requirements are determined. A body type is chosen. Three modes of propulsion and two liquid rocket fuels are compared, followed by the optimization of the body configuration through aerodynamic, weight, and trajectory studies. A cost analysis concludes the study.

May 31, 1993

EXECUTIVE SUMMARY

In an effort to insure the future development of hypersonic cruise aircraft, such as the National Aerospace Plane (NASP), the possible vehicle configurations were examined to develop a single-stage-to-orbit hypersonic research vehicle (HRV). Based on the needs of hypersonic research and development, the mission requirements, goals, and budget were determined. Relying on proven technology, the HRV is required to accelerate test apparatus, including a scramjet propulsion system, to Mach 12, at an altitude of 100,000 feet, for 1 minute. A budget of \$3 billion over 7 years is allowed. The lifting body, due to its good aerodynamic characteristics, and high volumetric efficiency, was chosen as the best body type. Liquid hydrogen and hydrocarbon fuels were then compared in rocket engine and thermal protection system trade studies. Liquid hydrogen, because of its high specific impulse and heat sink capacity, was chosen as the best fuel and most effective means of passive thermal protection. Using AutoCAD, AIREZ, AERO, APAS, ETO, and IDEAS computer codes, an optimum body configuration was obtained. The final vehicle has a total length of 50 feet, wing span of 25 feet, gross take-off weight of 47,800 lbs, and an empty weight of 13,600 lbs. The total cost for three vehicles, completing 70 missions each, is estimated to be \$465 million, which does not include the procurement of three GE scramjet engines. Due to its cost effectiveness, low risk, and capability as a hypersonic test bed, it is recommended that the OSU I HRV, described in this report, be built.

Table of Contents

	Page
List of Illustrations	iv
Introduction	1
Aerodynamics	2
Thermal Protection System	12
Propulsion	13
Engine Inlet	18a
Weight and Structure Analysis	19
Trajectory	35
Longitudinal Stability	37
Cost Analysis	40
Conclusion	42
Appendices	
1. Development of Solid Models	43
2. Weight and Volume Figures	62
3. Stress Contours	68
4. Deflections Plots	82
5. Engineering Analysis of Fuselage Wing Bulkhead	94
6. Force Calculations	102
7. Aerodynamic Characteristics	108
8. Trajectory Data	122
9. Dynamic Analysis of the Wing	131
10. List of Programs	137
References	151

List of Illustrations

	Page
Figure 1. Vehicle Configurations	2
Table 1. Vehicle configurations - advantages and disadvantages	3
Table 2. Static Margin	38
Table 3. Cost Analysis	41

INTRODUCTION

The X-30 program has not been successful, and thus threatened cancellation, because meeting its design goals would require the implementation of technology that has not been tested or proven to this day. The development of future hypersonic cruise vehicles, such as the X-30, requires advances in technology in a number of areas; materials, and propulsion are the prominent ones. Presently, ground testing is relied upon for this development, but this is not sufficient nor even possible for some areas, including propulsion. Thus, a hypersonic research vehicle (HRV) is needed to serve as a test bed for advanced structures, materials, propulsion systems, and data acquisition; and to help us better understand hypersonic flight.

By developing a test vehicle built largely with flight proven materials and concepts, the HRV provides a reliable means of exploring new technologies that is substantially less risky than attempting to launch a vehicle such as the X-30, which relies upon unproven technology. In addition, the HRV would be able to provide hypersonic flight data and advanced systems testing in the near future.

If an optimum configuration is not determined, the X-30 program is virtually assured of being canceled. Money spent on this program will have been wasted, and the possibility of funding for future programs of this kind would be less likely. This could be disastrous to the advancement of aerospace technology and the United States' position at the forefront in this area.

The following text presents a description of the process used in the development of an optimum HRV, and the results obtained.

Aerodynamics

Trade Studies on Vehicle Configuration

Currently, three vehicle configurations are available: wing body, lifting body, and waverider (Figure 1).

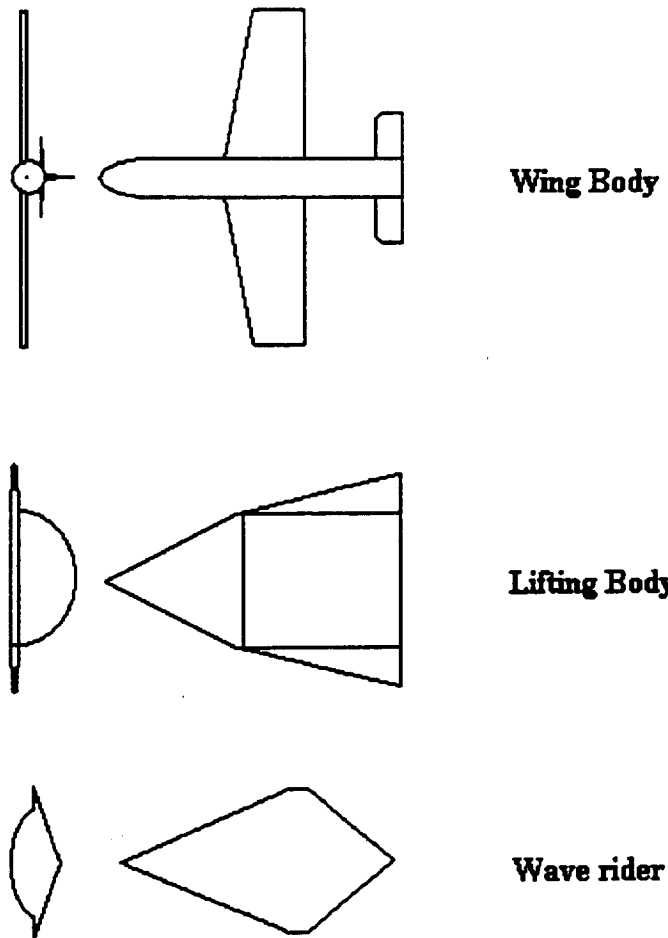


Figure 1. Vehicle configurations

In order to determine the best configuration, the advantages and disadvantages were obtained for each (see Table 1).

Wing Body	
Advantages	<ul style="list-style-type: none"> • Easy to manufacture • Known technology
Disadvantages	<ul style="list-style-type: none"> • Suited only for subsonic and low supersonic • Poor longitudinal and directional stability at hypersonic speeds
Lifting Body	
Advantages	<ul style="list-style-type: none"> • High volumetric efficiency • Higher hypersonic lift to drag (L/D) ratio than wing body • Good longitudinal and directional stability at hypersonic speeds
Disadvantages	<ul style="list-style-type: none"> • Difficult to manufacture
Wave Rider	
Advantages	<ul style="list-style-type: none"> • Higher hypersonic L/D than lifting body • Good cruise vehicle • Optimum operating range
Disadvantages	<ul style="list-style-type: none"> • Very difficult to manufacture • Unproven • Low volumetric efficiency

Table 1. Vehicle configuration advantages and disadvantages

After to reviewing the data in table 1, the lifting body was chosen to be the planform for our vehicle. The wing-body configuration was ruled out because of it's limited flight regime. The low supersonic regime is for Mach numbers less than two, and since our vehicle cruises at Mach 12 the wing body configuration cannot be used.

The wave rider's advantage of high lift to drag ratio is well suited to our mission, because it will reduce the thrust necessary to reach cruising altitude and speed. This produces a substantial decrease in propellant, and results in a substantial decrease in the size and weight of the vehicle. The problem with this configuration is that it is still in the

early research stage and is yet to be proven to work. As a result, this configuration was also ruled out.

The characteristics of the lifting body configuration places it between the wing body and wave rider configurations. It maintains a high lift to drag ratio, although not as much as the wave rider. The high volumetric efficiency, a ratio of the volume and wetted area, shows that it can hold large volumes within the body, as compared to the wave rider, which has minimal space. There is also a lot of proven data from theoretical prediction, wind tunnel experiments, and experimental test flights for the lifting body. The one drawback of this configuration is that it is more difficult to manufacture than a wing body. Since this configuration has none of the major drawbacks of the other configurations and can satisfy our requirements, it was chosen to be used as the vehicle configuration.

Aerodynamic Characteristics

The determination of aerodynamic characteristics is pivotal to the design process. These characteristics determine whether a design will meet certain requirements placed on it. These requirements include time to climb, thrust available, and cruise speed. The efficiency of the design is largely determined by the aerodynamic characteristics. Many barriers exist in determining these values for an arbitrary body configuration, as attempted in this project. The use of empirical formulas combined with aerodynamic formulas becomes very important in the preliminary design process, as will be shown later. The ability to quickly and accurately determine lift and drag coefficients for a given configuration allows changes to be made to the design to improve the efficiency. The design process depends on initial estimates being made with continual updates as other areas such as propulsion and weight determine the factors needed to meet the mission

required. The following pages explain the determination of the aerodynamics for our configuration.

The initial determination of aerodynamic characteristics was done by the AIREZ program. This program was used to get an initial estimate of lift and drag as a function of mach number. The AIREZ program takes simplified aerodynamic theory and combines it with empirical formulas to get agreement with wind tunnel test data. The constants in the empirical formulas were determined using DATCOM methods and data. The drag coefficients were determined using a component build-up method where each part of the design is idealized as a cylinder, cone, etc. The analysis is then done on these sections using simplified aerodynamic empirical formulas. Drag was broken down into several different forms including wave drag, base drag, friction drag, and drag due to lift. For friction drag, a Reynolds number was calculated based on input lengths and a velocity determined by an equilibrium glide trajectory. Several different airfoil shapes were also available for the wing section including biconvex, hexagonal, wedge, and double wedge airfoils. The program was written with the space shuttle Orbiter and the Low-Planform-Loaded configuration designs as test run cases. The ample amount of wind tunnel test data for these designs allowed for comparison between actual and predicted results. Obviously, these configurations are mainly wing-body types. For configurations similar to a wing-body, the AIREZ program will give more accurate results. This is indicative of one of the main problems encountered in doing the aerodynamic analysis for a lifting body configuration. The lack of actual wind tunnel test data on a lifting body made it difficult to get a comparative factor in order to examine a lifting body using a program written for a wing-body configuration. The AIREZ program, however, was only used to get initial estimates, especially in the hypersonic regime. Several examples of input were given in the instruction packet. For the initial analysis, the input for the X-24C was followed as a guide. The geometry for the initial examination of our configuration was estimated by

basically 'scaling' down the X-24C with a total length of 70 feet. Also, the fact that our mission did not have a crew made it so that the body diameter could be made much smaller than the configurations given in the instruction packet.

The output of AIREZ contains aerodynamic coefficients (like C_L and C_D) as function of mach numbers including $M=0.3, 0.6, 0.9, 2, 3, 5, 10$, and 20. These mach numbers are set by the program since the DATCOM data in program is only for these specific mach numbers. The angle of attack (α) is varied from 0 to 30 degrees for subsonic and from 0 to 60 degrees for supersonic/hypersonic speeds. Obviously, the transonic region is 'overlooked' but the results of the program reflect the increased drag of passing through this region. The L/D values calculated show the highest values are at subsonic speeds and that the L/D values slowly increase over the supersonic/hypersonic region after passing through the transonic region. The largest L/D value at the test speed of mach 12 is about 3.0. The aforementioned trends will be used for comparison of results from other methods of analysis. As stated previously, these results were only used as initial estimates of aerodynamic characteristics for our configuration.

With initial estimates in hand, the task of finding a better method to determine the aerodynamic characteristics of our configuration began. The AIREZ program did not allow any variance of the set Mach numbers or the altitude conditions at which the analysis was performed. The AERO program was then experimented with to resolve these problems. The AERO program was designed for preliminary analysis of aerodynamic characteristics for a vehicle in the hypersonic regime. This program was much more flexible than AIREZ since no DATCOM data was needed as input for this program. The purpose of this program was to allow needed characteristics to be calculated quickly and accurately for initial design analysis. There are more accurate programs to perform these calculations but these are often too complex and require more computer time than desired

for a preliminary analysis. Again, this program combined aerodynamic theory and empirical relations to get good agreement with wind tunnel test data, as was the case with AIREZ. The test cases used were the Space Shuttle Orbiter and a Mach 6 Transport Model since both had extensive wind tunnel test results available for comparison. The report for this program showed how well the calculated results agreed with the wind tunnel tests for the test cases.

The program as given did not run and required modification. The program itself is set up to read a data input file containing all the geometry of the configuration to be examined. The example in the packet gave sample input for the Shuttle Orbiter used to get the results given in the report for AERO. This was used as a guideline to locate similar geometry inputs for our configuration. Table 1 in Appendix 7 contains a list of inputs with the values used for our vehicle and a short description for each input. As can be seen, AERO also calculates temperatures in addition to aerodynamic coefficients for a configuration.

Several modifications were made to the AERO program to make performing an analysis much easier. As given, AERO will read in any altitude and Mach number information from a data file called CONT.DAT (contained free stream conditions for one point). The program was changed so that the temperature, pressure, and density were read into arrays for altitudes from sea level to 110,000 feet in increments of 1000 feet. This allowed a large range of altitudes to be examined with the program. Also, the range of Mach numbers and angles of attack to be examined were inputted from the keyboard. These modifications made changing values for the analysis simple and straightforward.

The AERO program is involved and complex; however, the actual run time is relatively short for preliminary design purposes. Several sensitivity studies were done to

see how changing one input affected the output of the program. One variable was changed for each run. These 'sensitivity' variables included the wing area (SW), lifting area (SLIFT), conical semi-vertex angle (DV), and the wing sweep angle (XLW). These studies basically showed that the lifting areas generally greatly affected the output aerodynamic characteristics. Small changes in wing sweep and nose vertex angles did not alter the output significantly. The actual input used for AERO for our configuration contained extra lifting area (SLIFT) added in anticipation of the greater lift expected from a lifting body. All the literature on lifting bodies confirmed this expectation (as compared to a normal wing-body configuration).

The output of AERO had several important features which were used in the design of the vehicle in other areas of study. The most important one was that the L/D maximum was about 2.7 around a four degree angle of attack during test conditions. This was used to position the scramjet on the vehicle for maximum thrust at the test conditions. The typical dive in L/D occurs as the vehicle passes through the transonic region along with the large increase in drag. The L/D values were the greatest for the subsonic region and decreased a large amount in the transonic region. As the Mach number then increased in the hypersonic region, the L/D value gradually increased again. These trends and values were used extensively in the areas of propulsion and trajectory.

As stated in the beginning, the lack of wind tunnel test data for a lifting body made determining the aerodynamic characteristics difficult. The advantages of using a lifting body over a wing body include better L/D characteristics and a better volumetric efficiency. These effects were used to alter the inputs to the programs used whenever possible to get a closer resemblance to a lifting body; however, better estimates were still needed for more accurate characteristics. The Aerodynamic Preliminary Analysis System (APAS) was the tool used to get accurate values for the lifting body configuration. This

computer program allows the analysis of an arbitrary body (not just a wing-body as in AERO and AIREZ). The program was much more complex and time consuming. The APAS program was used to optimize our design and work out any resulting problems. The APAS program figured aerodynamic characteristics for the hypersonic regime needed for our mission. The flexibility of APAS allowed for a more complete analysis of our configuration to be done, all with one program.

The HRV was broken down into several sections including nose, body, inlet, and ramp. These sections were distinguished between the top and bottom of the vehicle. The geometry used was the ellipse for each section. The area and x-coordinate was used as input for APAS for each cross-section that was defined. The areas where the geometry did not change much had a lesser number of cross-sections (as in the body) whereas in areas where the geometry changed quickly, more sections were used (as in the nose). The geometry of the bottom surface did not mirror the top surface which made entering the geometry difficult. A ramp was needed for the inlet into the scramjet which had to be integrated into the bottom surface; hence, the bottom surface was broken down into several different sections. The scramjet module also had to be added to the vehicle. The scramjet was broken into three sections with the last one as the needed exit ramp to accelerate the flow. The wing on the HRV was a hexagonal airfoil with a 75° sweep. The area, aspect ratio, and taper ratio were all input to create the wings. Since the wings on the HRV do not 'touch' each other, the geometry had to be edited to create the wings as shown in the three-view drawing. The vertical tails were created in the same fashion except these were reflected over the centerline to create the set of twin tails.

With the geometry in APAS, the analysis of our vehicle could begin. The first analysis done was the VISCOUS routine. This gave the volume and wetted area as a function of the x-coordinate. The volumes and wetted areas were then totaled for each

section of the vehicle. The totals were very close to the volumes predicted by the I-DEAS program, as will be discussed later in this report. The skin friction coefficient is also predicted in this routine at certain specified conditions. The WAVEDRAG routine was not used due to problems in running the routine. This routine like VISCOUS gave estimates of the wave drag at certain specified conditions as a function of roll angle.

The actual analysis of the HRV was setup in the APAS program by specifying a Mach number, altitude, and certain angles of attack (α) or sideslip angles (β). For each analysis run, a certain configuration was used. This allowed different geometries to be used and compared. In order to set up an analysis run, several parameters must be input including the center of gravity location, planform area, chord length, and vehicle span. These reference numbers are used to figure the non-dimensional coefficients (such as lift, drag, and moment coefficients). The Hypersonic Arbitrary Body Program (HABP) was used to analyze the vehicle. This program requires the different methods of analysis be specified in APAS before the program is run. There are two methods specified for each section, one for impact flow and one for shadow flow. Impact flow is where the flow directly hits the panel, and shadow flow is where the flow does not come into contact with the panel. For the forward part of the vehicle, the empirical tangent cone method for impact flow was used due to the shape of the vehicle. The main body of the HRV used the modified Newtonian method for impact flow. The wings and tails used the empirical tangent wedge method for impact flow due to the 2-D nature of these sections. For shadow flow, the Prandtl-Meyer expansion method was used everywhere on the vehicle except at the base of the HRV. Here, a high mach number base pressure method was used. There are several options which need to be set to run the HABP program. These include whether sheilding effects are to be considered. For the nose, a hemispherical nose cap is added to configuration. Sheilding effects can also be considered on any component. For the HRV, no sheilding effects were considered. The last option considered was with

regard to skin friction effects. For the HRV, skin friction effects were included using turbulent flow over the whole vehicle. Turbulent flow was used as a 'worst' case for the vehicle since the drag will be greater for this type of flow. There are also options for a laminar to turbulent transition based on several different parameters but the design of the HRV was based upon turbulent flow. With all the needed information specified, the HRV was analyzed.

The results of HABP can be seen in Appendix 7 for our configuration. The L/D at the test conditions was around 2. This is lower than predicted by the AERO program. Also, there was a problem in trimming the vehicle at the test conditions. From the moment coefficient graph, the vehicle was stable but unbalanced, i.e. the C_{mo} was not positive. Several different ideas were attempted to get the C_{mo} positive including giving the wings incidence and dihedral. The twin tails were also rotated to see the effect on the moment coefficient. The basic result was that giving the wing incidence gave the needed positive C_{mo} . There was an attempt to move the maximum cross-sectional area to the midpoint of the vehicle giving it a 'hump' in the middle. This actually decreased the moment curve even more since the CG location was behind the midpoint.

In the end, the HRV was made balanced and stable. The moment, lift, and drag coefficients can be seen in Appendix 7. The AIREZ program was used for the subsonic regime since its data matched those in papers better than the subsonic data from AERO. AERO predicted much lower L/D for the subsonic region than AIREZ. All the curves in Appendix 7 are shown at Mach numbers of 0.3, 0.6, 0.9, 3, 6, and 12. Each has been divided up into several graphs for clarity.

Thermal Protection System

The temperature contours obtained from APAS, see Appendix 7, indicate that a passive system can be used all over the plane except for the nose and leading edges. Multi wall TPS panels were selected for the passive system. These panels can withstand temperatures of approximately 2400 degrees Fahrenheit. These panels were selected for their high mechanical strength, light weight, and flexibility. The only disadvantage to these panels is that they have a high thermal expansion coefficient.

Several active thermal protection systems were studied. The active systems that were studied included a transpiration system, a direct cooling system that circulates the fuel through the leading edges and a heat exchanger system, which utilizes a secondary coolant. The direct system and heat exchanger system were ruled out because of their complexity and high component weight.

The transpiration system injects liquid hydrogen into the boundary layer at the leading edges and nose. Although the transpiration system can not utilize the engine fuel as coolant, it was chosen because of the very short time that active cooling will be required during the mission. □

Propulsion

Turbojet to Ramjet to Scramjet

The turbojet to ramjet to scramjet option offers minimum thrust specific fuel consumption. The turbojet is the most efficient means of propulsion under Mach 3. Turbofan and turboprop engines are more efficient than the turbojet, but, these two engines usually operate in the subsonic regime. Since the turbofan and turboprop operate over a very limited speed range, they were not considered as a first stage propulsion alternative.

A typical turbojet will have a thrust specific fuel consumption between 1 and 2 pounds of fuel per pound thrust per hour. The typical turbojet weighs approximately 2000 pounds.

The ramjet is the most efficient means of propulsion between Mach 3 and Mach 6. Turbojets can not be used in this region because the turbine would melt at the temperatures that would be necessary to produce thrust. The ramjet overcomes this problem by not using compressors or turbines. Typical ramjets have thrust specific fuel consumptions of 1.7 to 2.6 pounds of fuel per pound thrust per hour.

Theoretically, the scramjet is the most efficient means of propulsion from Mach 6 to Mach 15. The scramjet has a specific impulse of approximately 1500 seconds at Mach 12.

This configuration has a high component weight. This increases the empty weight of the aircraft. This configuration would require two turbojets, two ramjets, and two

scramjets. This does not include the weight of the heavy variable geometry inlets that would be required. Turboramjets were not considered because they will not be ready by 1998, the required operating date for the aircraft.

This configuration is very complex. No aircraft have been built that utilize three different propulsion systems in this manner. No work has been done with variable geometry inlets that operate from Mach 0 to Mach 12. This configuration, in addition to being heavy, would take up a lot of volume. Finally, this option offers a very low reliability due to all of the moving parts involved in the engines and inlets.

Due to the high component weight, and enormous complexity of this option, it was ruled out.

Rocket

The rocket option is the simplest of all options considered. Rockets can operate over all Mach numbers. Unfortunately, the rocket offers the lowest specific impulse of all alternatives considered. The weight of the engines would be 1,140 pounds. Additionally, since the rocket carries its own oxidizer, inlets are not required.

The one propulsion system and no inlet features combined make the rocket option the most reliable of the alternatives considered. There have been a lot of rockets developed for previous projects that could be suitable for this project. Using a previously developed engine could drastically reduce the cost of the propulsion system. Using a previously developed engine will also decrease the propulsion system design time.

Turbojet to Rocket

The turbojet to rocket mode may offer the best of both worlds. The turbojet is 8 to 12 times as efficient as the rocket in the Mach 0 to Mach 3 regime. This could drastically reduce the fuel required to get to Mach 3. Unfortunately, this option also requires variable geometry inlets for the turbojets, which would have to be closed once the rocket engine(s) started at Mach 3.

The weight of the turbojets plus the turbojet fuel may exceed the weight of the rocket fuel required to propel the vehicle from Mach 0 to Mach 3. This will depend on gross takeoff weight. As gross takeoff weight increases, the turbojet to rocket option becomes more attractive. Most turbojets are fueled by JP. If a Hydrogen Oxygen rocket is selected, the vehicle would have to carry multiple fuels for the propulsion systems.

Hydrogen Oxygen Fuel

Hydrogen Oxygen fuel provides the maximum specific impulse possible. Theoretically, Hydrogen Fluorine provides the highest specific impulse, but Fluorine is highly reactive, making it impractical as a rocket oxidizer. Although Hydrogen has a high heat capacity per pound of fuel, it has an extremely low density. Hydrogen Oxygen has twice the volume of alternative fuels.

Hydrogen Oxygen fuel is very difficult to store. Hydrogen and Oxygen are cryogenic liquids. Hydrogen is particularly difficult to store. Hydrogen has a high heat capacity, which makes it an excellent coolant for an active thermal protection scheme. Finally, the scramjet uses Hydrogen as well, making a multiple fuel system unnecessary.

The specific impulse for the RL-10 35K Hydrogen Oxygen rocket engine is 415 seconds. The average bulk propellant density is 20 pounds per cubic foot.

JP Oxygen Fuel

JP Oxygen fuel is only 60% as efficient as Hydrogen Oxygen fuel. JP Oxygen fuel is dense, so the required volume is a lot less compared to the Hydrogen Oxygen fuel. Since JP is not cryogenic, it can not act as a coolant in any active thermal protection scheme that might be necessary. The specific impulse for the H-1 JP Oxygen rocket engine is 295 seconds. The average bulk propellant density is 64 pounds per cubic foot.

Propulsion Selection

After reviewing all pertinent data, a Hydrogen Oxygen rocket propulsion system was selected. The rocket propulsion system offers the best reliability. Although the turbojet is much more efficient at lower Mach numbers, it was determined that the weight of the turbojets exceeded the weight of the rocket fuel required to propel the vehicle from Mach 0 to Mach 3. If the vehicle weighed more than 65,000 pounds at takeoff, the turbojet to rocket option would have been viable.

Hydrogen Oxygen fuel offers the lowest fuel weight for a rocket system. Hydrogen Oxygen offers a high enough specific impulse to make up for its low density. The lifting body configuration is well suited for Hydrogen Oxygen fuel, due to its high volumetric efficiency. Hydrogen Oxygen fuel was also selected because Hydrogen is an excellent coolant.

The rocket's low cost, low complexity, and high reliability made it the clear choice for propulsion. The best rocket for the vehicle is the Pratt and Whitney RL-10 rocket engine. The RL-10 is a proven Hydrogen Oxygen fueled rocket. The RL-10 35K provides 34,000 pounds of thrust. The RL-10 has a specific impulse of 415 seconds. Three RL-10 engines will be required, giving a combined thrust of 102,000 pounds. Each RL-10 has an exit diameter of 28 inches. The combined weight of all three engines is 1140 pounds.

The rocket will require 33,700 pounds of fuel for a 47,810 pound vehicle, leaving an initial cruise weight of 14,020 pounds. The fuel and oxidizer combined will occupy a volume of 1492 cubic feet. The weight of the Hydrogen required for the rocket phase is 4,814 pounds, which occupies a volume of 1,094 cubic feet. The weight of the Oxygen required is 28,886 pounds, which occupies a volume of 398 cubic feet.

Scramjet Propulsion

Only one scramjet, producing 7,000 pounds of thrust will be required for the test. According to the General Electric Aircraft Engine scramjet data, 420 pounds of Hydrogen will be needed to power the scramjet for a 1 minute test. This will occupy a volume of 95 cubic feet.

Methods

After ruling out the turbojet to ramjet to scramjet option, a program was developed to analyze rocket fuel consumption. The program assumed level flight and a constant lift over drag. The program asks for initial velocity, final velocity, thrust available, gross weight, and a time step. The program uses this information combined

with specific impulse and propellant density information for Hydrogen Oxygen and JP Oxygen fuels to arrive at a fuel weight and volume for each fuel. Basically, the program applies $F=ma$ for each time step.

The most interesting thing learned from this program is that if you increase thrust available, you decrease fuel required. This is due to the fact that more thrust results in a smaller distance traveled, which results in lower work against drag.

Once it was determined that the rocket might be viable for the entire mission, the program was modified to take into account climbing flight. As a rough approximation, a constant climb angle was assumed. The program proved that there was enough volume available in the plane to allow the use of a Hydrogen Oxygen rocket for the entire mission.

Once the RL-10 35K engine data was obtained, the program was modified one final time to account for thrust variations due to altitude. The exact specific impulse of the RL-10 was also used in the final version.

The propulsion program proved to be invaluable in determining the feasibility of rocket propulsion for this mission. Even with some of the crude assumptions, it still gave remarkably accurate results.

Engine Inlet

The engine inlet is used to supply the needed air to the scramjet engine. The major performance characteristics of the engine inlet are pressure recovery and air quality. An external compression inlet was used because the design was easier. An internal compression inlet may have been better suited for the shortness of the inlet, but no information on design could be obtained. For the initial inlet design the CONIC and GEOM computer codes were used. This gave a starting point for the design. The final inlet was designed using the method of characteristics and geometry.

The inlet that was chosen consisted of two compression ramps. This was chosen, because the inlet needed to be short, but still provide an acceptable pressure recovery. The inlet was designed to begin at approximately two feet behind to nose of the aircraft. This gave a small amount of lifting surface on the front of the aircraft. It also provided a fairly two-dimensional inlet surface. The oblique shock from the nose of the aircraft gave a Mach number of 8.4 at the first ramp. Because of this distance the first inlet ramp was at an angle of about nine degrees. The second ramp began at about 330 inches from the first ramp.

The inlet provided conditions at the engine face of Mach 5.5 and a pressure recovery ratio of 0.41. The cowl lip of the inlet is used to straighten the flow to provide clean air to the engine. The cowl lip is also used to cover the engine while the aircraft is climbing to the test altitude.

Weight and Structure Analysis

The optimization of the hypersonic test vehicle, OSU I, is basically an optimization of the weight of the vehicle. The weight is the driving parameter in the design of any aircraft. A reduction in weight results in an increase in performance and efficiency, while decreasing fuel weight and cost. Lighter engines, fuels, structures, and materials are always preferred when designing an aircraft. With a hypersonic aircraft, the weight becomes even more important. Due to the complexity of hypersonic aircraft, their weight tends to be enormous. Some total gross take-off weights for various proposed and operational hypersonic vehicles are listed below:

Lockheed Hycat-1	773,706 lb
Lockheed Hycat-4	959,426 lb
Space Shuttle Orbiter	255,170 lb
General Dynamics Orbiter	891,795 lb
H ₂ Fighter (M = 6)	320,000 lb

The payload weights of these vehicles range from 42,000 lb to 80,000 lb.

The hypersonic vehicle under consideration in this design has a payload of 1,000 lb. Common sense says that the weight of OSU I should be meager in comparison. The problem with determining the weight of a hypersonic vehicle, especially one that has no comparison to either operational or theoretical designs, is the method to be used in calculations.

Methods for Calculating the Weight of a Hypersonic Vehicle

There are a few analytical computer programs available to calculate the weight of a hypersonic vehicle. Hypersonic Aerospace Sizing Analysis for the Preliminary Design of Aerospace Vehicles (HASA) and Weights Analysis of Advanced Transportation Systems

(WAATS) were the only two considered. WAATS was discarded due to problems obtaining access to the computer system to run the program. However, HASA was run and results were analyzed. Another method would be to break the vehicle down into components and determine their individual weights from analytical calculations or comparisons with similar structures.

HASA

HASA is a program written in Fortran that first iteratively solves for the size of the vehicle, breaks it down into 14 individual components and then weights each of them. The program uses statistical weight equations to solve for the 14 individual components. These components include the propellant, body, wing, horizontal and vertical stabilizers, thrust structure, propellant tank, landing gear, propulsion, thermal protection system, avionics, hydraulics, electronics, equipment, and payload. The program has various inputs for fuel types and their mass fractions, geometry, payload weight and volume, and the number and types of engines.

The program met with limited success. Almost all the configurations tried resulted in take-off weights of 100,000 lb to 200,000 lb. The reason for this is that the program was written for large vehicles and certain values in the program are hard coded with this in mind. In order to change these values extensive work would be required. It was determined that time could be better spent on the component build up method.

However, HASA did reveal that vehicles that used large fuel mass fraction on the order of 0.6 to 0.8 produced the heaviest vehicles. Also, vehicles that used liquid hydrogen as fuel were nearly 1.5 times heavier and 3.0 times as large as vehicles that used the same mass fraction of JP. Vehicle configurations that used just rocket propulsion

were slightly lighter than vehicles that used other configurations, such as; turbojet/ramjet, turbojet/scramjet, turbojet/rocket, and turbojet/ramjet/scramjet.

With the unsuccessful try at using HASA as a means of calculating the vehicles weight, a component build-up method was employed.

Component Build-up Method

The component build-up method entails breaking down the vehicle into several components, determining their weight, and then summing the weights together. How to obtain the weights of the individual components is the major stumbling block. This problem was solved by developing a solid model of OSU I on SDRC's *solid model and finite element analysis program*, I-DEAS.

The reason for using I-DEAS to do the solid model was that it could calculate the properties of the mode quickly and accurately. The break down of components used follows:

Internal Structures:

- Fuselage frame
- Wing frame
- Vertical tail frame
- Longerons

Surfaces:

- Fuselage
- Wings
- Vertical tail

Components:

- Rocket engines
- Scramjet

- Fuel tanks
- Landing gear
- Payload
- Pressurization System
- Power Supply
- Control Systems

Development of Solid Models

From the components list the necessary solid models broke down in two main models. The first and most complicated model was the internal structure solid model. The next was the outer surface model. Also, solid models for the rocket engines and scramjets were necessary. The solid models for the landing gear, payload, and fuel tanks are too simple to mention.

Fuselage Design

The fuselage design for the internal structure entailed the creation of 16 bulkheads along the length of the vehicle from 0.3048 m to 15.24 m. The profiles were created using the known points of the outside shape of the vehicle (profiles for the top and bottom of the vehicle were treated separately). Then each profile was extruded 76.2 mm and a solid object of the profile was created. The solid object of the profiles was then scaled down by 90% in both the x and y directions. This new object was then used to cut the original object. This resulted in either the top or bottom portion of the fuselage bulkhead. Finally, the top and bottom bulkheads were joined and the result of creating one bulkhead can be seen in Appendix 5. Once all the bulkheads were created, they were placed at the correct locations and then joined to one another in order to create the fuselage. For the outer surface of the fuselage, only the profiles were necessary. The profiles were placed in the correct locations and a skin was drawn over them.

The next step was to make four 15.24 m long beams called longerons. These were created using three square profile sections of variable size, (6.35 mm x 6.35 mm, 12.7 mm x 12.7 mm, and 25.4 x 25.4 mm). The profiles were then placed at the correct x,y, and z locations and a skin was created along the path. The longerons were then joined to the fuselage, Figure 3. These longerons were not used in the development of the solid model of the outer surface.

Wing and Vertical Tail Design

The procedure for creating the wing and vertical tail structures is the same, so only the procedure for the creation of the wing will be discussed.

The solid model of the outer surface (Figure 8) of the wings was created by using two biconvex airfoil shapes for the root and tip of the wing. Between these profiles a skin was drawn. Starting with the outer surface, the internal structure of the wing was created by using a cutting block. Once the block was moved to the appropriate location, a cut was made and one of the vertical spars was formed. The result of six cuts produced six vertical spars. Then the outer surface of the wing was cut horizontally by another cutting block. The result of nine cuts produced nine horizontal spars. Finally, a large cutting block was oriented so that the leading edge of the wing could be obtained. Finally, the vertical and horizontal spars and the leading edge were all joined together. The final internal structure of the wing is shown in Figure 10. The vertical tail was created by using different cutting blocks, but the same method was applied. The result of the vertical tail structure is shown in Figure 12.

Scramjet and Rocket Engine Design

The scramjet was designed using a profile of appropriate dimensions and then an extrusion was made in order to obtain the solid model. The rocket engines were created using the top half of the profile of the engine. The corners were filleted for a more realistic effect, and then the entire profile was revolved 360 degrees to form the solid object.

Assembly of the Hypersonic Test Vehicle Structure

The procedure for assembling the structural solid model and the outer surface solid model was the same except for the scramjet and the rocket engines. With the fuselage, the two wing halves, and the two vertical tails, the final hypersonic test vehicle structure could be assembled. First, the wings were translated to the correct location and then joined to the fuselage. Next, the two vertical tails were rotated 15 degrees from the vertical and translated to the correct positions on the hypersonic test vehicle. Then the vertical tails were joined to the fuselage. The scramjet and the rocket engines were moved to appropriate locations and joined only to the outer surface solid model. The final internal structure of the hypersonic test vehicle is shown in Figure 13 and the final outer surface solid model is shown in Figure 14.

Weight Calculations from the Solid Models

The weight calculations were obtained directly and indirectly from I-DEAS. Within I-DEAS, the properties of each component were calculated and are listed in Table 2.1. Note, only the information necessary for the calculation of the weight, volume, and center of mass is listed. By imputing the density of titanium (281 lb/ft^3) the weights for

the internal structures was obtained immediately. The weight of the other components were determined by using trade study data and data obtained from I-DEAS.

The weights of the outer surfaces of OSU I were determined by trade studies and the surface area of the object as determined by I-DEAS. From various aircraft, such as the SR-71 and the Space Shuttle Orbiter, the thickness of the fuselage skin was determined to be 1/8 " and the thickness of the wing and vertical tail skin was determined to be 1/16". These values of skin thickness were averages for the skin thickness over the entire surface. Titanium was used because it is a common material in aircraft construction, and follow the idea that the plane must be low cost and operational by 1999. The procedure for calculating the weight of the wings follows:

1. Obtain the surface area of the wings from Table 1.
2. Convert the 1/16" thickness to feet.
3. Obtain the volume of the material necessary by multiplying the thickness by the surface area.
4. Multiply the volume by the density of titanium.

(Note: The actual calculation gives the mass, but the mass is in lb_m , so the conversion to lb_f is straight forward)

The weights of the landing gear were obtained from a trade study discussed at the end of this section. The weight of the rocket engine was obtained from NASA, and the weight of the fuel tanks were obtained by scaling the main fuel tanks on the Space Shuttle.

The weight of the fuselage's internal structure was obtained by an iterative process using I-DEAS *finite element analysis* (FEA). This process was performed on a fuselage bulkhead attached to the wing. The objective of this iteration using I-DEAS was to reduce the weight of the member as much as possible while meeting certain design

requirements. The specifics of this analysis are in the section Engineering Analysis of Fuselage Wing Bulkhead.

A complete list of the weights calculated for each component and the fuel weights are in Table 2.1 and a partial weight pie chart can be seen in Figure 2.1. From the pie chart one can see that the fuel is 74% of the total weight. The structure of the plane is the next largest at 17%. The remaining weight is taken up by the fuel tanks, payload, engines, and landing gear.

Engineering Analysis of Fuselage Wing Bulkhead

Static analysis was performed on a fuselage bulkhead in particular the second to the last bulkhead on the vehicle. This particular bulkhead was attached to the wing. The material used for the bulkhead was a titanium-carbon fiber alloy with a density of 281 lb/ft³, a Poisson's ratio of 0.33, and a Young's Modulus of 1.1×10^{11} Pa.

To minimize computer resources, only half of the bulkhead was modeled. This was a viable assumption, which can be validated by looking at the stress contours and deflections for both the half and whole initial bulkhead configurations (see Appendix 5 and 6, initial bulkhead configurations). These figures show that the whole bulkhead is stressed and deflected in the same manner as the half bulkhead. After the initial configuration, modifications were made to increase the stress over the entire bulkhead, while still remaining below the design requirements of maximum deflection of 6.5 mm, and maximum allowable stress of 500 MPa. Modifications could be made to any part of the bulkhead, except the outside shape. The outside of the bulkhead had to maintain the dimensions shown in Figure 3.5. The various configurations that were analyzed during the

optimization process along with their corresponding weights are shown in Appendix 3. Stress contours and deflection plots can be seen in Appendixes 5 and 6, respectively.

A section of the wing bulkhead is connected to the fuselage bulkhead as shown in Figure 5. During flight, lift, drag, and moments acting on the wing are transmitted to the fuselage bulkhead via the wing clamp. For this study only forces due to lift and drag and moments due to lift were considered. The derivation of these forces is in Appendix 6. The magnitude and direction of the loads applied to the clamp can be seen in Figure 5.6. Even though the case of the pin carrying half the moment is more realistic, the worst case of the clamp carrying all the forces was chosen as an extra margin of safety, . Also a load factor of 9 was chosen to represent the maximum loading the wing clamp would encounter during flight..

The restraints were applied to the top and bottom beams of the bulkhead for configurations 1, 2, and 4A. An additional restraint in the form of a longeron was applied to configuration 3 and B-10. These restraints are shown in Figure 5.7.

The following is a brief description of the major changes made during each iteration and the corresponding results:

Configuration 1

This initial design had a thickness of 101.6 mm and a weight of 771.0 kg. This configuration was considered to bulky. The deflection was 0.12 mm and the maximum tensile and compressive stresses were 3.18 MPa and -1.3 MPa, respectively. A high tensile stress could be seen on the top beam, lower surface, and near the upper corner of

the clamp. This high stress should have been in the corner of the overhand of the clamp. The reason for it not being there is that the mesh on the clamp area was too coarse.

Configuration 2

The upper and lower beams were thinned while the thickness of the bulkhead was reduced to 89 mm. The resulting weight was lowered to 494.2 kg. The resulting deflection was 7.1 mm and the maximum and minimum stresses were 43.3 MPa and -9.39 MPa, respectively. Although the increase in the stress over the bulkhead due to the reduction in weight is tolerable, the deflection is above the design goal.

Configuration 3

The inner surface was rounded near the clamp and the bottom beam was shaped to conform more to the outside shape of the fuselage. The rounding of the clamp area was intended to decrease the deflection while still decreasing the weight. The addition of a longeron was placed above the clamp in another attempt at decreasing the deflection. This was modeled by using restraint C (see Figure 15, page). While the maximum and minimum stresses were increased to 45.1 MPa and -13.6 MPa, respectively, the reduction in weight was lowered to 318.8 kg. The addition of the longeron proved effective in reducing the amount of deflection in the z-direction. The maximum deflection was reduced to 4.7 mm.

Configuration 4A and B

These configurations show a much slimmer overall bulkhead along with a reduction in thickness to 63.5 mm, and an overall weight reduction to 181 kg. A 0.1 m

fillet at the inside corners of the clamp was added in order to spread out the high stress regions near the corners. The purpose of these two configurations is to demonstrate the effectiveness of the longeron over the clamp. Configuration 4A has no longeron and its maximum deflection is 45.0 mm, whereas configuration B has a longeron placed just above the clamp and its maximum deflection is 16 mm.

Configuration 5

This configuration was an attempt to thicken the beam above the clamp in order to reduce the deflection in both the y and z direction without the use of the longeron. Thickness and weight of this configuration were 50.8 mm and 177.4 kg, respectively. A quick look at the maximum deflection shows that this configuration was a failure because it was much worse than the last configuration, B. The addition of the longeron above the clamp seems to be the only viable solution to keeping the z-direction deflection down. This iteration is shown because it represents the fact that not all of the ideas that were used worked. There were many other configurations that produced worse results than their corresponding previous configuration. However, these configurations were important because a great deal of knowledge was acquired from their failures.

Configuration 6

Configuration 6 shows a greatly increased width in the beam above the clamp. Since the longeron is going to be used to limit the z-direction deflection, a reduction in the overall thickness to 44.5 mm was made. The result was still another reduction in weight to 135.4 kg. The deflection of this bulkhead, 40 mm, was still way to high. From the 3-view deflection plot one can see that this 40 mm deflection must be in the y-direction. The bulkhead is almost entirely in compression except near the cantilever top beam, the

rounded corner of the top beam, and the upper inside corner of the clamp. There are also very high compression spots all over the beam. From this configuration and the two previous configuration, a conclusion was made that the only way to reduce the y-direction deflection is to increase the width of the upper and lower beams.

Configuration 7

With configuration 7, another reduction in overall thickness to 38.1 mm was made for a reduction in weight of 159.2 kg. This configuration was a success because the maximum deflection was reduced to 9.8 mm, the weight was reduced, and the stress over the entire bulkhead was more proportional. This configuration would have a much longer life span than configuration 6. The deflection around the longeron is more noticeable in this configuration. Looking at the x-view, the bulkhead deflects about the longeron location. This deflection is due to the drag forces.

Configuration 8

In an attempt to reduce the weight even further the beam thickness was cut to 31.75 mm and the lower beam width was reduced. This configuration at a weight of 123.3 kg was the lightest configuration tested. Like configuration 6, this configuration was a failure. The deflection jumped up to 12.5 mm. This meant that the lower beam width had to be increased.

Configuration 9

This was the final configuration because it was below the design limit of a maximum deflection of 6.5 mm. The thickness was cut to 25.4 mm, but the lower beam

width was increased to the size of configuration 7. Also the width around and above the clamp was increased. This resulted in a weight of 141.0 kg, and the final deflection of 6.458 mm.

From the x-view of the deflection plot, one can see how the beam deflects around the longeron. This is also represented in the stress contour; the front or left view shows the tension on this face due to the deflection resulting from the drag forces applied to the clamp. The back view or right view shows the corresponding areas in compression. The majority of the beam ranges from stress values of 30 MPa to -14.3 MPa. A blow up of the clamp shows the high tensile stress, 118 MPa, in the upper inside curve of the clamp. This high stress could be alleviated by increasing the fillet size of the clamp. The top of the bulkhead is blown up in the right view. This view shows the greatest rate of change in stress on the bulkhead. From the bottom, the stress ranges from a tensile stress of 96 MPa to a maximum compressive stress of -36.3 MPa.

The overall optimization process resulted in a reduction of weight from the initial configuration to the final configuration of 81%. This reduction in weight is mainly due to the reduction of the bulkhead thickness from 101.6 mm to 25.4 mm. Alone, this is a reduction in weight of 75%. The more proportioned stress contours will result in a longer usable lifetime for the bulkhead. As a whole the optimization process resulted in a more fully stressed structure. The main design barrier was the deflection of the beam. The maximum allowable stress of 500 MPa was never reached. With new modifications, a further reduction in weight could be achieved if methods for reducing the deflection in the y-direction could be implemented. Possibly a vertical spar could be used to decrease this deflection. If this vertical spar was used, a buckling analysis would have to be performed to guarantee that the spar would maintain its shape. Additional longerons could be used to reduce any further increase in z-direction deflection. The optimum goal would be a

fully stressed structure that had the lowest possible weight. With further time and new ideas, this optimum structure could be achieved using I-DEAS.

Volume

The configuration chosen for OSU I was a lifting body. One of the biggest advantages of a lifting body is its volumetric efficiency. OSU I is almost an ellipse. This allows for a large volume of components to fit inside the vehicle. The volume for each component is listed in Table 1 and was calculated by I-DEAS. An inboard platform of OSU I is shown in Appendix 2.

The most challenging structures to fit inside OSU I were the hydrogen and oxygen fuel tanks. Attempts a conventional cylindrical tanks was attempted, but not enough volume was produced to hold the 1,189 ft³ of hydrogen fuel. The only immediate solution that presented itself was to scale down the body of OSU I by a factor of 0.9. This resulted in the shape of the fuel tanks seen in the inboard platform. These tanks were a little to big, but fit fine inside the fuselage. The shape of the fuel tanks is questionable. Due to the high pressure of the liquid hydrogen, cylindrical tanks are preferred. An analysis of the shape of these fuel tanks must be performed in order to determine their practicality. All other components in the inboard platform were checked to make sure they fit inside the vehicle.

A breakdown of the volume can be seen in the volume pie chart Figure 2.2. The volume of the hydrogen fuel is almost half to total volume. The oxygen fuel is about a fifth of the total volume, and the rest of the components occupies 3% of the total volume. The remaining 30% is due to unusable space, and to components not added to the vehicle.

Landing Gear

The landing gear for the aircraft was required to be rugged, sturdy, lightweight, and compact. It had to be sturdy due to the fact that the craft is remotely piloted and landing without power. Both of these factors lead to the possibility of hard landings. At the same time the gear must be light and compact so as not to use excessive space and weight which could be more readily used for increased fuel and/or other component storage.

In order to minimize the weight of the gear, unnecessary features and components were omitted. For example, since this is a test aircraft, it will most likely not be flown at night, during inclement weather, or at any other less than optimum condition. This led to the omission of lights on the nose gear. Since the plane is pilotless, it will most likely be taxied to and from the runway, tarmac, and hanger. Because of this no steering actuator was incorporated into the design. The nose wheel, however, can be unlocked for full 360° rotation during taxiing. This reduction in features lead directly to weight savings which allow the gear to be built within weight limitations without sacrificing strength.

The nose gear is rearward retracting with twin wheels and a shock strut. The rearward retraction allows the gear to be located farther forward in the nose. Each of the twin nose tires is a 20 ply 20 x 6.6 -10 manufactured by B.F. Goodrich and inflated to 150 pounds per square inch. The main gear is forward retracting to allow placement farther aft to allow an acceptable maximum rotation upon take-off. The main gear also incorporates a shock strut and is capable of withstanding a maximum descent rate of twenty-one feet per second. Each main gear tire is a 24 ply 30 x 11.5-14.5 manufactured by B.F. Goodrich and inflated to 200 pounds per square inch. The nose gear weighs 150

pounds and each main gear weighs 200 pounds, including local hydraulic components, for a total gear system weight of approximately 550 pounds.

Trajectory

Given predetermined mission requirements and goals, a trajectory that minimized empty weight was needed. The goals and requirements are as follows: accelerate from conventional ground take-off to a Mach 12 cruise at 100,000 feet altitude; test a scramjet for one minute at equilibrium conditions; carry 1000 lbs and 35 cubic feet of payload; and land conventionally. It was decided that an unpowered landing was both feasible and necessary in order to minimize weight.

An optimized ascent trajectory was determined through the use of a computer program called, "ETO - A Trajectory Program for Aerospace Vehicles," which was developed at the Aero Propulsion and Power Laboratory of the Wright Research Development Center, Wright-Patterson Air Force Base. This program, which is based on equations of motion and forward time iteration, requires aerodynamic data, propulsion data, initial conditions, and phase parameters as input in a particular form text file. Out of five flight phases available in the ETO program, it was found that Phase I, II and V provided the best results. Phase I is the take-off ground roll. Phase II is a Rutowski climb at a commanded load factor and axial acceleration. Phase V is a pull up to ballistic ascent. The input file used for the final ascent trajectory analysis can be found in Appendix 8. This file was produced by the FORTRAN code called SORT.FOR, which reads aerodynamic data produced by the AERO FORTRAN code and writes it, along with the propulsion data, into an input file that can be read by ETO. For the final trajectory, Phase II is initiated at $V_{t0} = 450$ ft/s and concluded at a velocity of 900 ft/s and altitude of 5,000 feet, incurring a maximum load factor, $L/W = 1.6$. At this point Phase V is initiated, at which point the vehicle pulls up to a climb angle of 54 degrees and follows a ballistic ascent until leveling at 106,000 feet altitude and Mach 12. 33,700 lbs of LH2/LO2 fuel is

required for climb, giving the vehicle a total take-off weight of 47,810 lbs. A maximum dynamic pressure of $q = 1,960$ psi is encountered during this phase.

The unpowered glide descent trajectory was determined from the FORTRAN code called GLIDE.FOR. The code determines the maximum range glide descent using L/D_{max} values, which were determined by the AERO FORTRAN code (with base drag). A maximum range of 783 nautical miles and total mission time of 27 minutes were calculated. Graphical representation of the trajectory analysis can be found in Appendix 8.

Take-off and Landing

The take-off performance parameters of the OSU 1 was calculated by ETO. Under full power of three RL-10 rocket engines, the rolling distance needed is 2,130 feet. The velocity at this point is 460 ft/s. The distance needed to clear a 50 foot obstacle is 4,250 feet. The velocity at this point is 600 ft/s.

The program, GLIDE.FOR, calculates the landing parameters. After clearing a 50 foot obstacle at 210 ft/s., the vehicle travels 628 feet before touch down at 211 ft/s. Based on an 8 deg/s second rotation to nose down, the vehicle rolls another 209 feet, and then brakes from 208 ft/s to stand-still in 2,788 feet. This braking distance is based on a rolling coefficient of 0.2, whereas a typical value for a paved runway is 0.4.

Longitudinal Stability

Several parameters were needed to calculate the longitudinal stability of our vehicle. These included the mean aerodynamic chord (MAC), aerodynamic center, tail volume ratio (V_H), taper ratio (λ), and the center of gravity (CG) location. There were several assumptions made in this initial stability analysis. The planform used was simply a delta wing covering the entire vehicle. The twin tails located on top of the vehicle are at a 15° slant with respect to the vertical. For longitudinal analysis, an effective horizontal tail was assumed to be simply the sine of that angle times the height of the tail. This gives the length of the horizontal tail, and the same width was used. As is common in aircraft analysis, the z-component (vertical) of the tail above the CG was assumed small relative to the x-component (axial). This indeed was the case as the numbers show. Last, the lift curve slopes of the wing and the tail were assumed the same since each is the same type of airfoil.

The analysis began by calculating a MAC. This was done using a formula found in Dynamics of Flight: Stability and Control by Bernard Etkin. The MAC was found as follows:

$$MAC = \frac{2c_r (1 + \lambda + \lambda^2)}{3(1 + \lambda)}$$

This formula was for a planform with constant taper and sweep with any loading distribution. This book also contained graphs which gave the distance of the tip of the MAC from the apex of the planform. These values were found using the following parameter:

$$AR \tan \Lambda_{1/2}$$

where the L is the sweep angle of the half chord line. This factor then along with the taper ratio gave the distance from the apex in terms of the MAC. The tail volume ratio was then calculated using the CG location, wing area, and tail area. The neutral point is then found using the following:

$$h_n = h_{nw} + V_H$$

The static margin is then found by taking the difference between the neutral point and the CG location as a percent of the MAC. The following table gives the resulting values for our vehicle.

	Take-off	Cruise
hCG	0.33	0.27
hn	0.36	0.36
Staic Margin	0.029	0.094

As can be seen, our configuration is stable since the static margin varies within allotted limits. The tail planform area was found using the X-24 as a guide. The tail area was within 4% of the planform area for the X-24 again confirming the tail volume ratio found.

The APAS program was used to perform some stability analysis. The moment and lift coefficients were used to find our static margin. As discussed in the Aerodynamics section, the APAS program was used only for the hypersonic regime. The stability analysis here is only for the test conditions where the HRV is practically empty of all fuel. Using the appropriate CG location, the $\delta C_m / \delta C_1$ curve was made. From the equations on the following page, the static margin can be derived from this graph.

$$\begin{aligned}
 C_{m\alpha} &= C_{L\alpha} (h - h_f) \\
 C_{m\alpha} &= \partial C_m / \partial \alpha \\
 C_{L\alpha} &= \partial C_L / \partial \alpha \\
 SM &= -(h - h_f) \\
 &= -C_{m\alpha} / C_{L\alpha} = -\partial C_m / \partial C_L
 \end{aligned}$$

As can be seen, the value of $\delta C_m / \delta C_L$ is the negative of the static margin. From the graph included in Appendix 7, the value of our static margin at the test conditions is around 30%. This shows that our vehicle is stable.

Cost Analysis

A cost analysis was performed using the method described on pages 24-8 through 24-19 in the course text, Fundamentals of Aircraft Design (Nicolai), with one modification. This method consists of a series of equations that determine the number of hours required for a particular aspect of the development phase. This number is then multiplied by the current cost rate for that particular aspect. For example, the equation that determines the number of engineering hours required is:

$$E = .0396 A^{.791} S^{1.526} Q^{.183}$$

where A is the empty weight, S is the maximum speed in knots, and Q is the number of aircraft to be developed. However, this method was not developed for hypersonic cruise vehicles, so a correction factor was introduced so that the method gave figures that was in close agreement with cost figures for the X-24C. It turned out that if the exponent of the S term is multiplied by 0.7 wherever it appears in the method, the cost estimate for the development phase is \$245 million in 1986 dollars, which is close to the estimate determined by Lockheed "Skunk-Works" (NASA CR-145274). Therefore, this 0.7 correction factor was used for the developmental cost determination of the OSU I vehicle, and a total of \$465 million was found. It is important to note that this figure is 1993 dollars, and that it does not include the procurement of three GE scramjet engines.

An operational cost of \$15 million was determined based on 60 maintenance hours per flight hour, \$60 per maintenance hour, 0.45 flight hours per mission, a total of 210 missions, and \$6 per gallon for liquid hydrogen. A cost analysis is shown in the following table.

Airframe Engineering		33
Development Support		22
Flight Test Airplanes		
Engines & Avionics		37
Manufacturing Labor		51
Materials & Equipment		76
Tooling		47
Quality Control		66
Flight Test Operations		66
Manufacturing Facilities		15
	Subtotal	413
	Profit (9%)	37
Figure in Millions of Dollars (1993)	Net Total	450
	Mission Operations	15
	Gross Total	465

Table 3. Cost Analysis

Conclusion

From the studies and analysis described in this report, a final research vehicle was obtained. It has an overall length of 50 feet, wing span of 25 feet, take-off weight of 47,810 lbs, and empty weight of 13,600 lbs.

A detailed analysis of the air flow into the scramjet, as well as the exhaust diffuser, needs to be performed. A more detailed stability and control analysis needs to be performed, including C_m/C_l versus M , stability and control derivatives, and control block diagrams.

Overall, the hypersonic test vehicle described in this report represents a reliable, near-term, feasible, and cost efficient means of hypersonic research. It is recommended that, in order to insure the future development of hypersonic cruise vehicles, this vehicle be developed and built.

APPENDIX 1: Development of Solid Models

1. Figure 1: Bulkhead profile
2. Figure 2: Solid object of bulkhead profile
3. Figure 3: Cut object of top bulkhead
4. Figure 4: Joined bulkhead
5. Figure 5: All bulkheads in correct z-depth position
6. Figure 6: Longerons
7. Figure 7: Longerons joined to fuselage
8. Figure 8: Solid object of the wing
9. Figure 9: Vertical spars
10. Figure 10: Vertical and horizontal spars joined together
11. Figure 11: Solid object of the vertical tail
12. Figure 12: Vertical tail structure
13. Figure 13: OSU 1 internal structure
14. Figure 14: Color Iso
15. Figure 15: Iso 1
16. Figure 16: Iso 2
17. Figure 17: 3-view drawing
18. Figure 18: Landing gear

1. Bulkhead profile

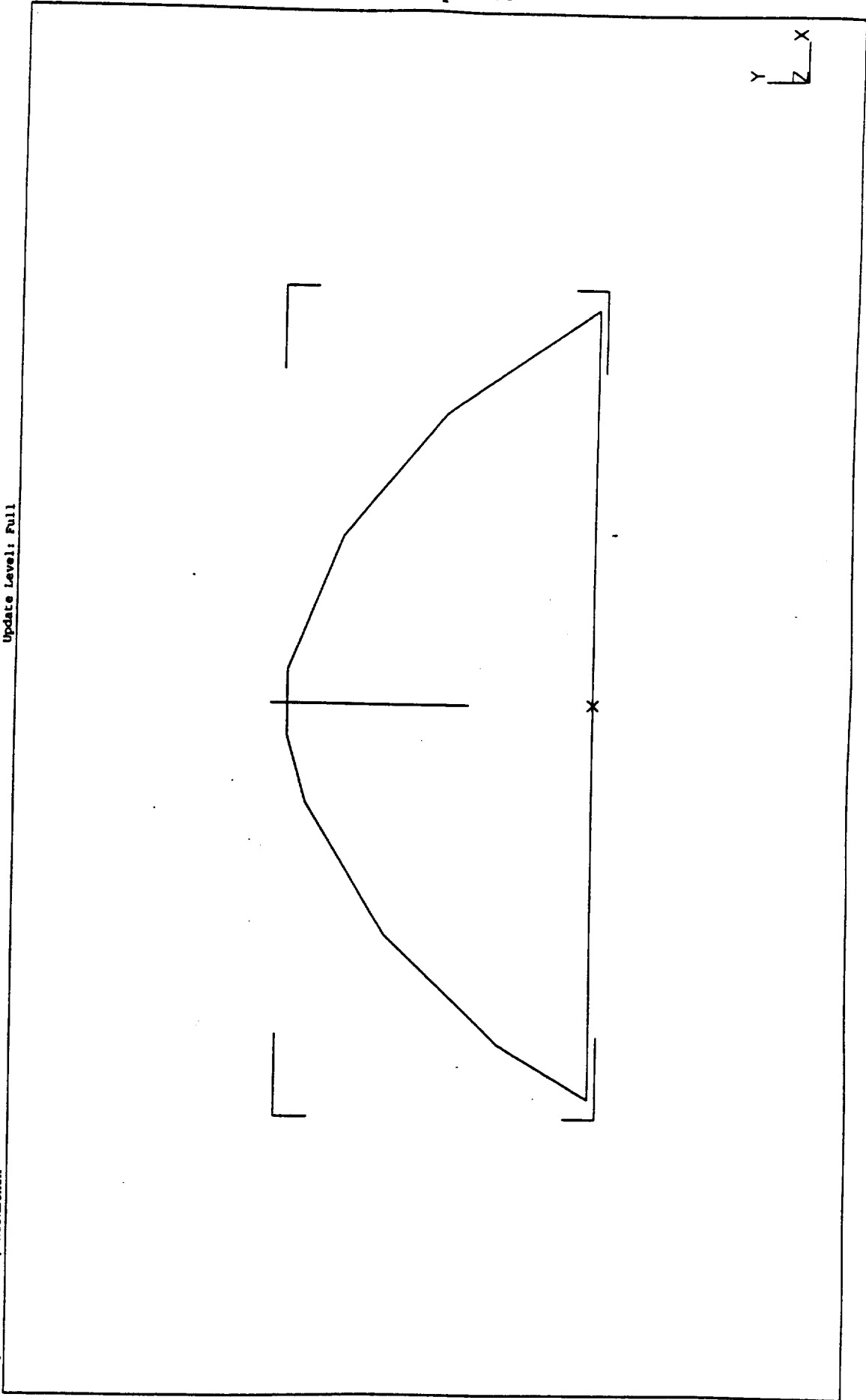
CAEDS V4R2H0: Solid_Modeling

17-FEB-93 10:34:38

Database: toprib
View : No stored View
Task: Object
Object: 1-WORK1, Workbench

Units : IN
Display : No stored Option

Bin: 1-MAIN
Update Level: Full



2. Solid object of bulkhead profile

CAEDS V4R2H0: Solid_Modeling

17-FEB-93 10:43:17

Database: toprib

View : No stored View

Task: Object

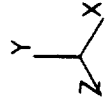
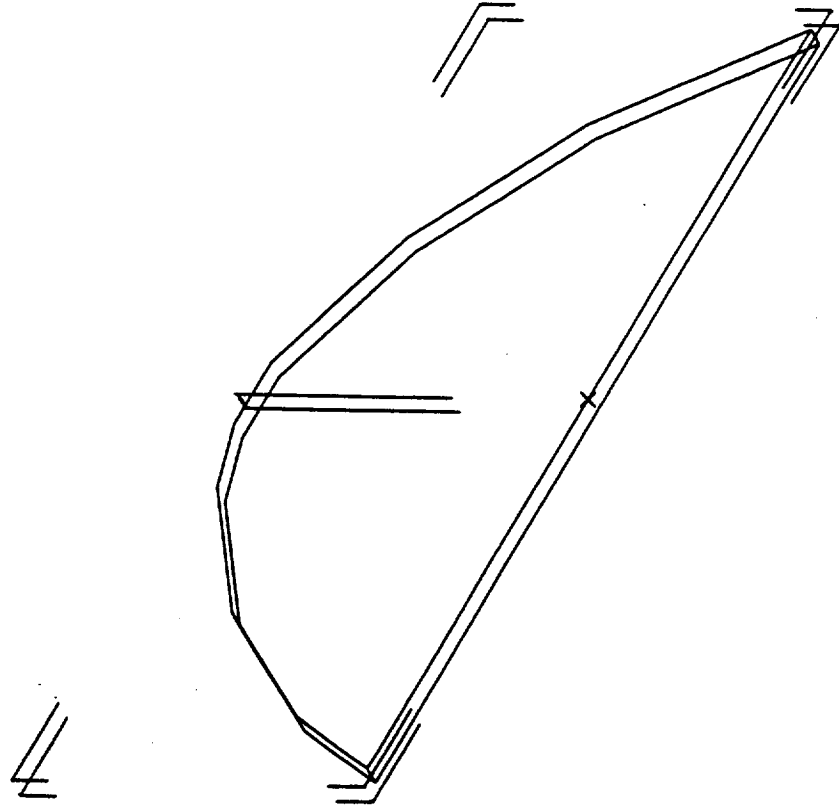
Object: 1-WORK1, Workbench

Units : IN

Display : No stored Option

Bin: 1-MAIN

Update Level: Full



3. Cut object of top bulkhead

CARDS VAR2M0: Solid_Modeling

17-FEB-93 10:48:46

Database: toprib

View : No stored View

Task: Object

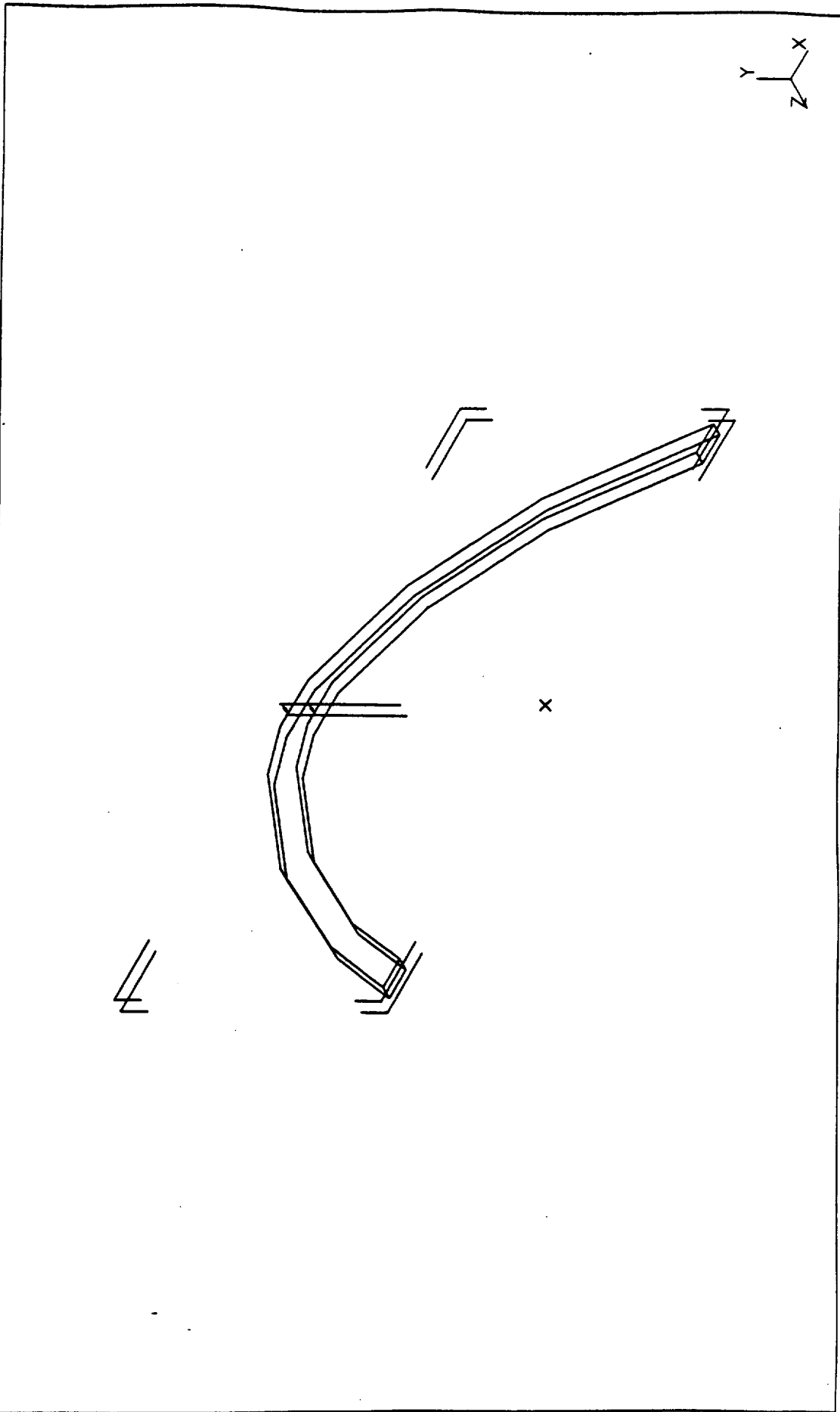
Object: 1-WORK1, (TOPRIB5, Bin1)

Units : IN

Display : No stored Option

Bin: 1-MAIN

Update Level: Full



4. Joined bulkhead

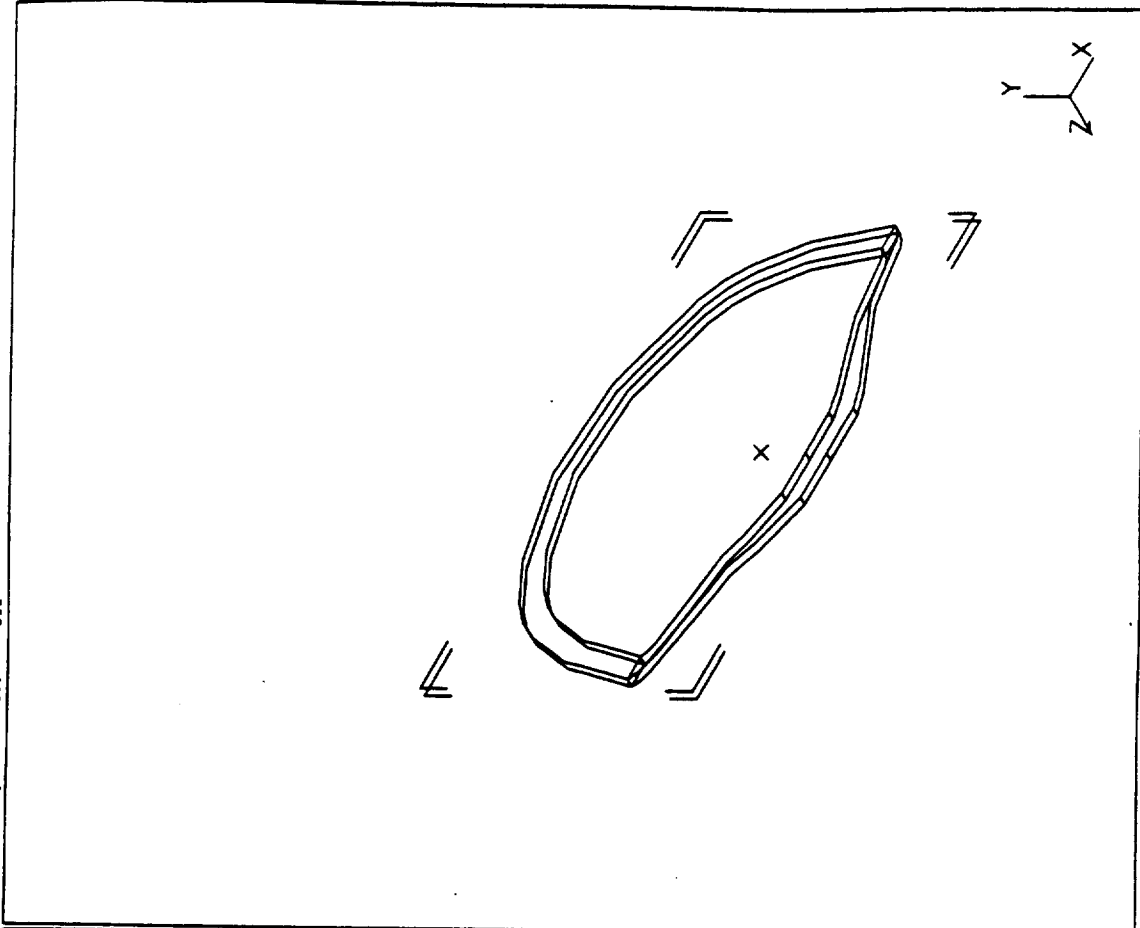
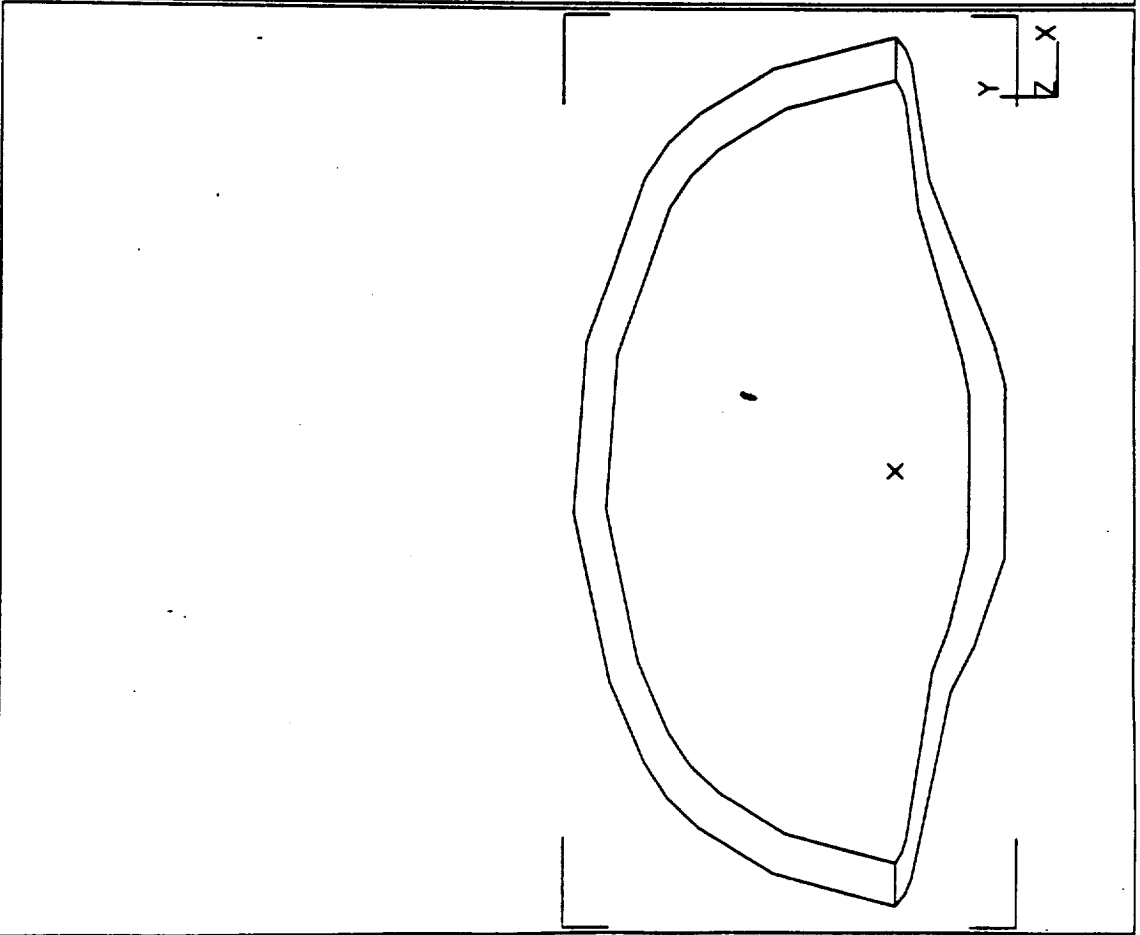
CAEDS V4R2M0: Solid_Modeling

17-FEB-93 10:33:37

Database: hyper
View : none, none
Task: Object
Object: 1-WORK1, (RIB16, Bin1)

Units : IN
Display : none, none

Bin: 1-MAIN
Update Level: *** Off ***



5. All bulkheads in correct z-depth position

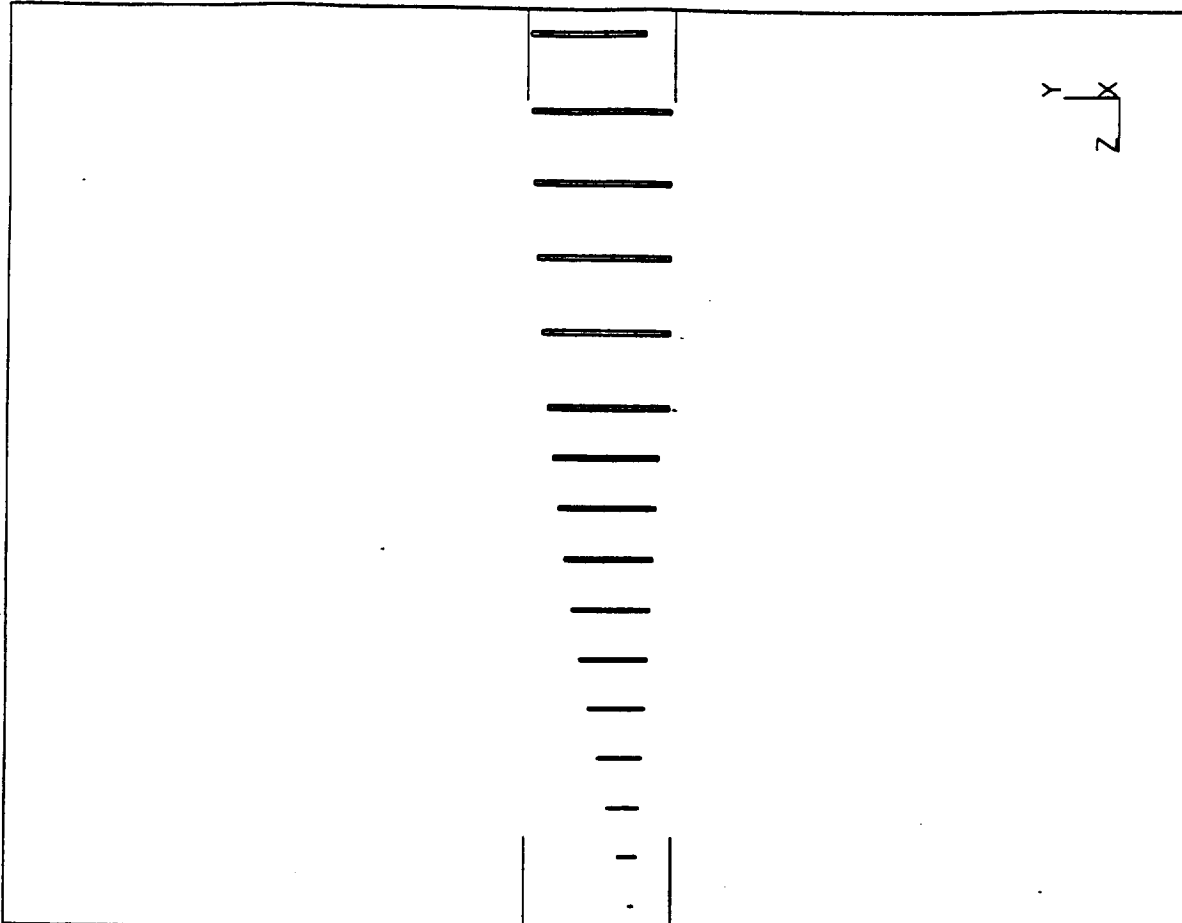
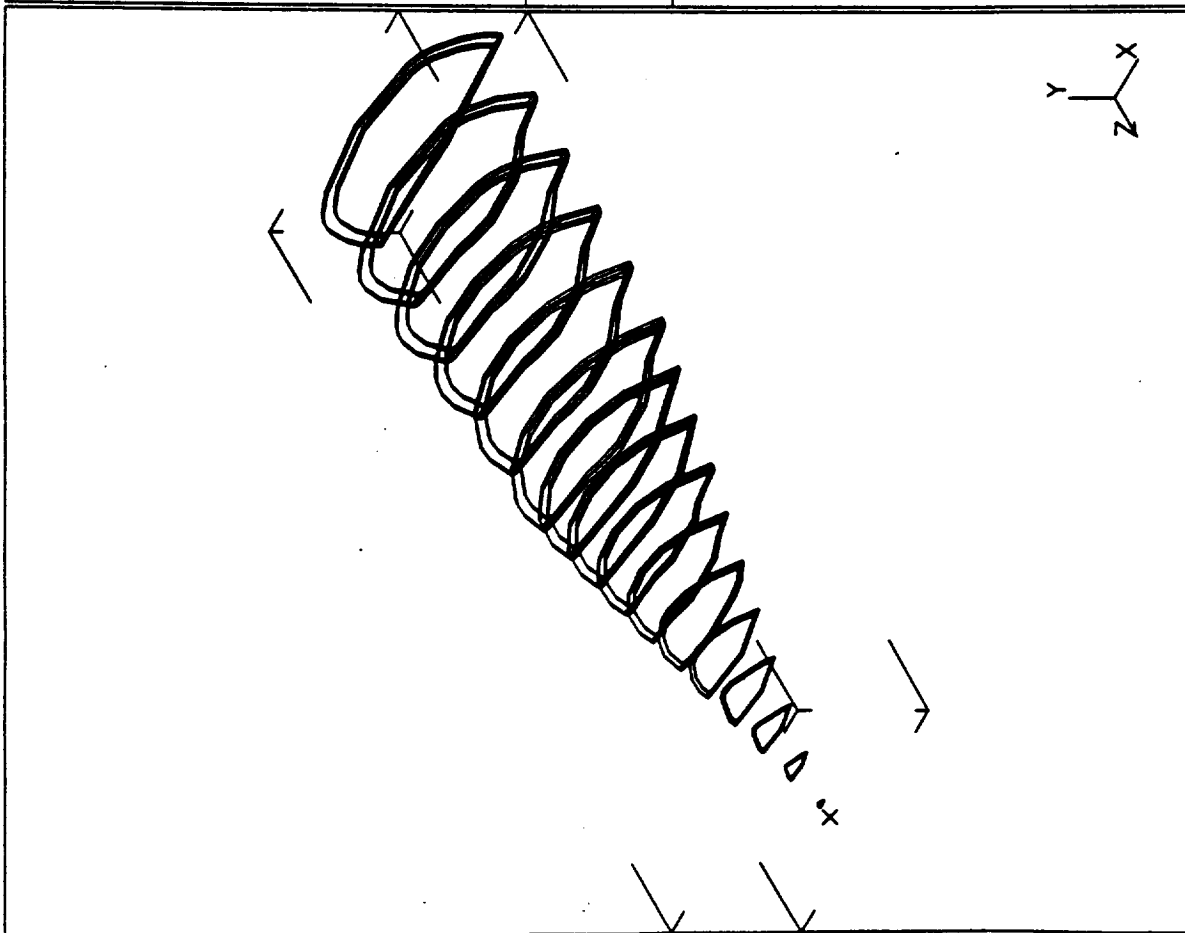
CAEDS V4R2M0: Solid_Modeling

00:13:41

18-FEB-93

Database: frame
View : none, none
Task: Object
Object: 1-MONK1, (BODY)001M, (ini)

Units : IN
Display : none, none
Bin: 1-MAIN
Update Level: ... Off ...



6. Longerons

18-FEB-93 01:23:15

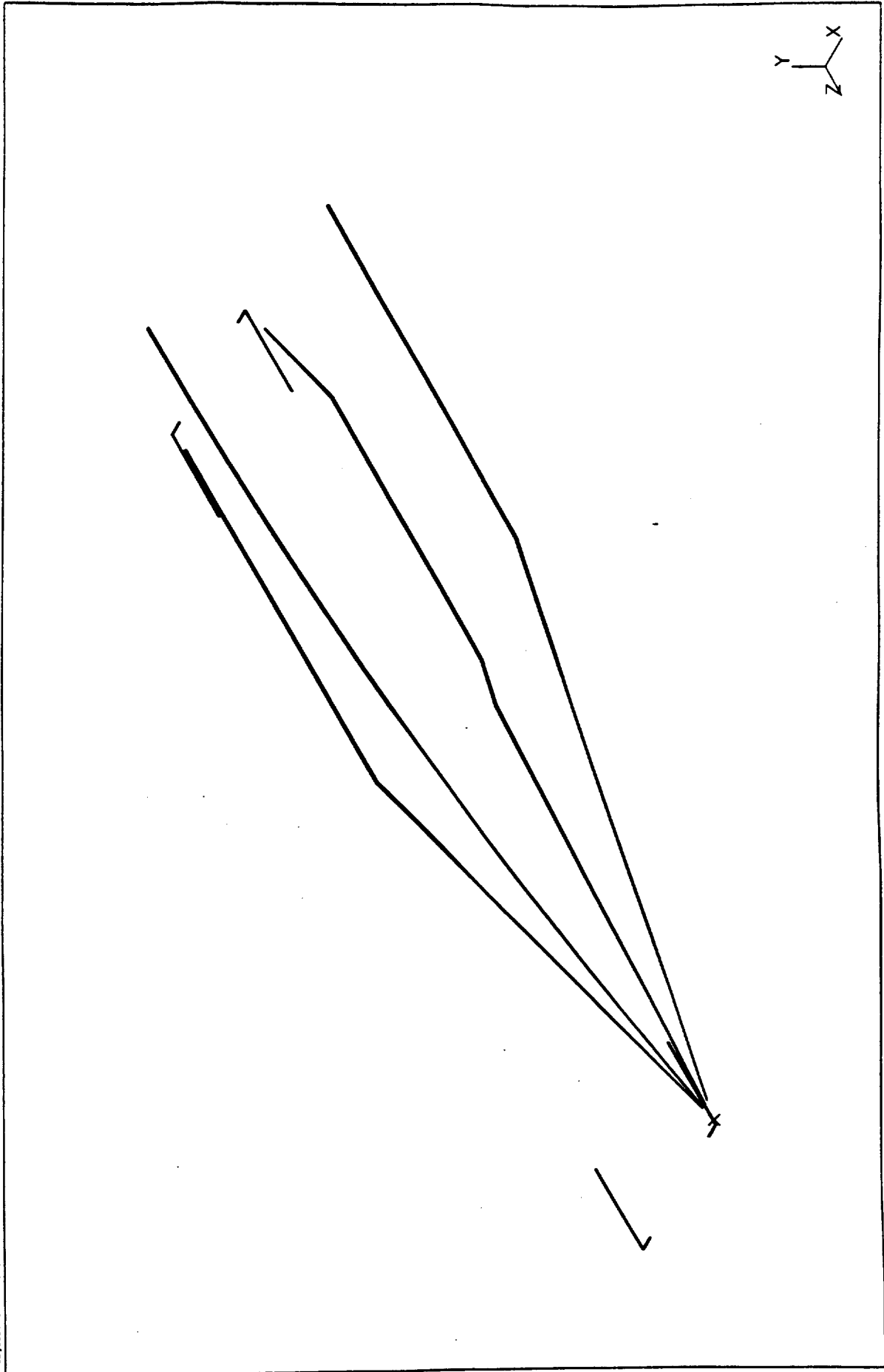
Units : IN
Display : No stored Option

18-FEB-93

Bin: 1-MAIN
Update Level: Full

CAEDS VAR2M0: Solid_Modeling

Database: frame
View : No stored View
Task: OBJECT
Object: 4-MORE4, (LONGERONS, Bin1)

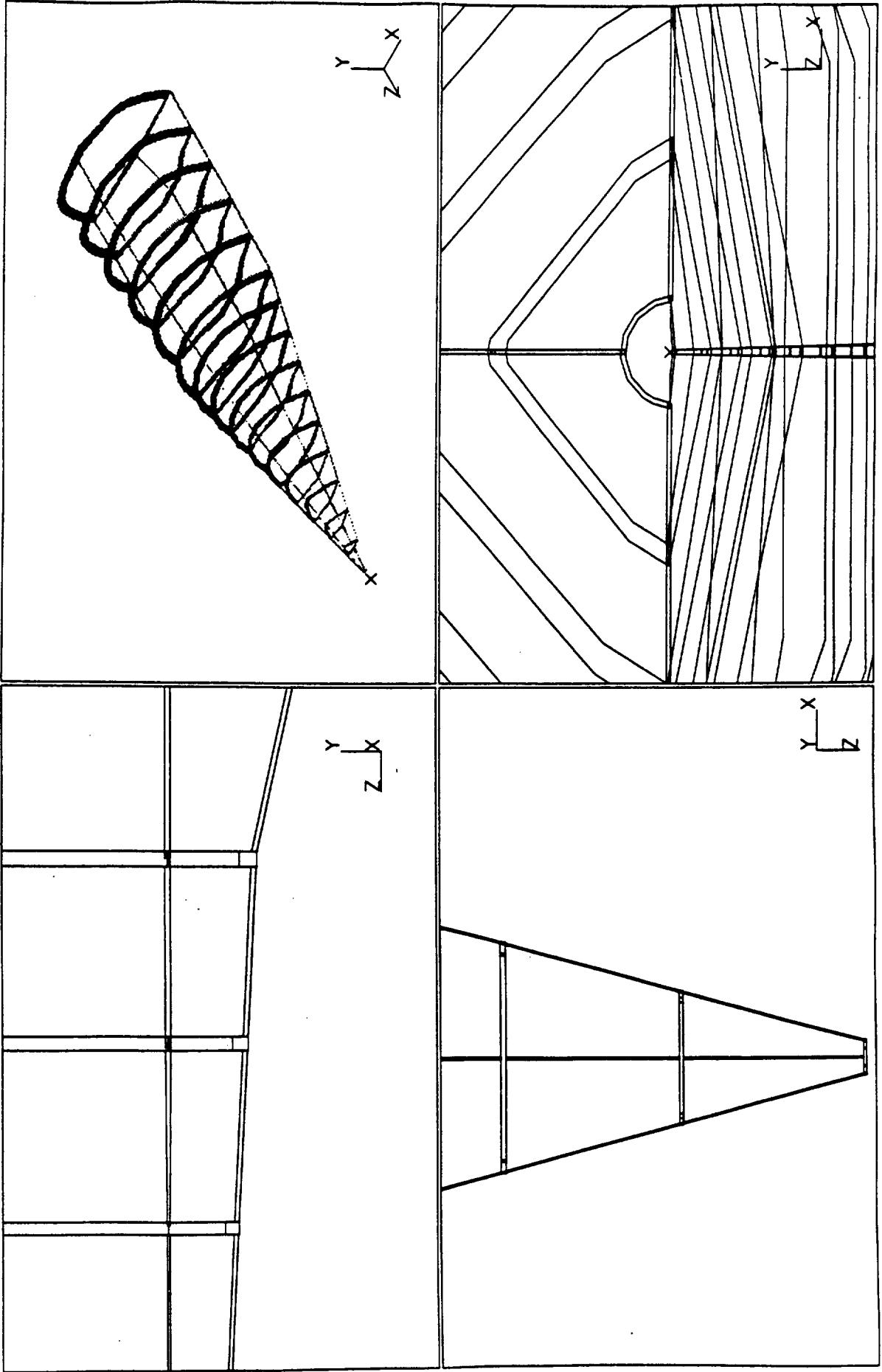


7. Longerons joined to fuselage

18-FEB-93 01:40:44
Units : IN
Display : none, none, none, none
Bin: 1-MAIN
Update Level: ... Off ...

CAEDS V4R2M0: Solid_Modeling

Database: frame
View : none, none, none, none
Task: OBJECT
Object: 1-MORR1, (BODYJOIN, Bini) (Mod)



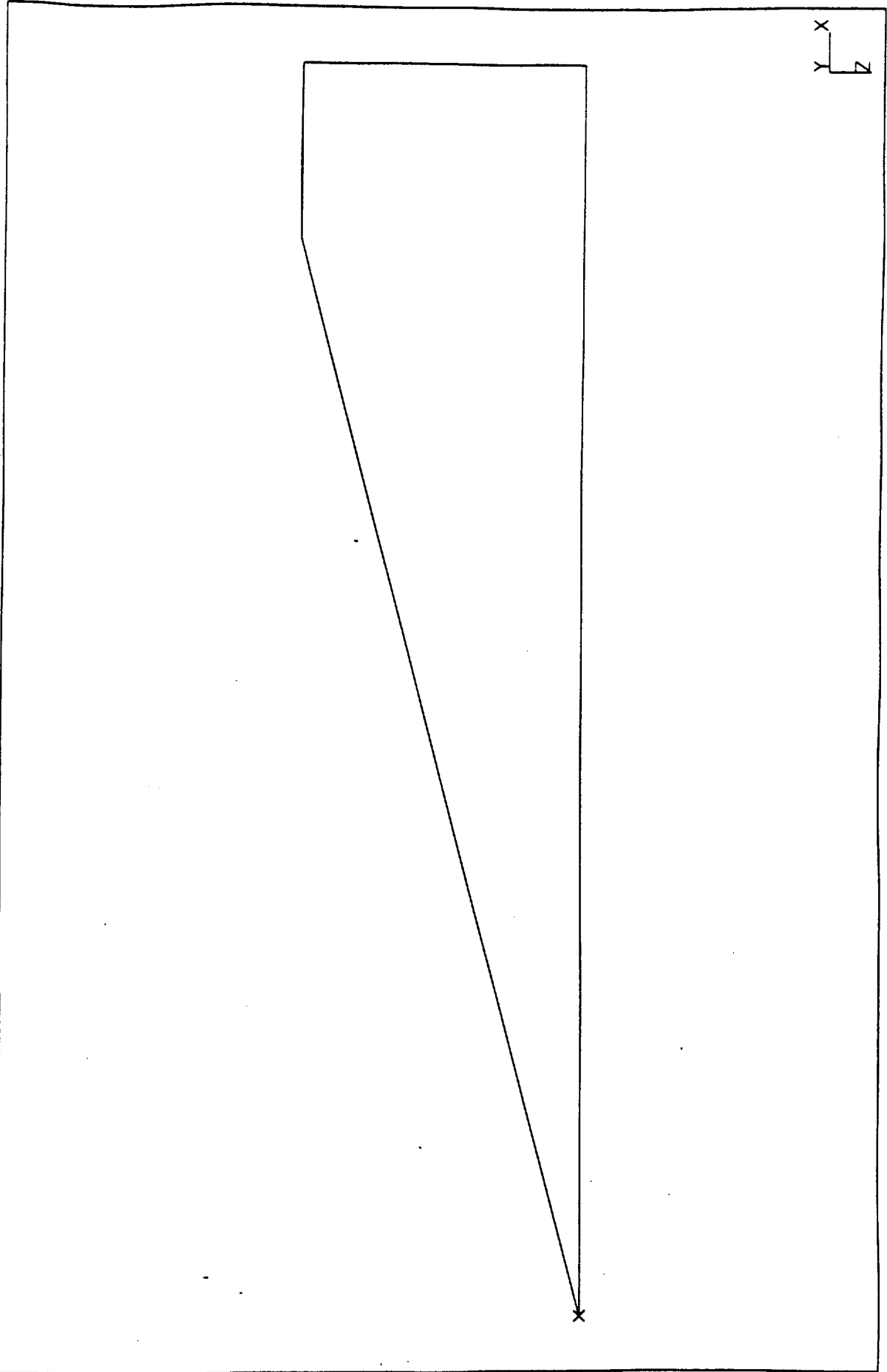
8. Solid object of the wing

CAEDS VAR2ND: Solid_Modeling

11-MAR-93 23:36:20

Database: plane
View : No stored View
Tidff: Object
Object: 1-MORPH. (WING, Bin1)

Update Level: Full
Bin: 1-MAIN
Display : No stored option
Units : SI



9. Vertical spares

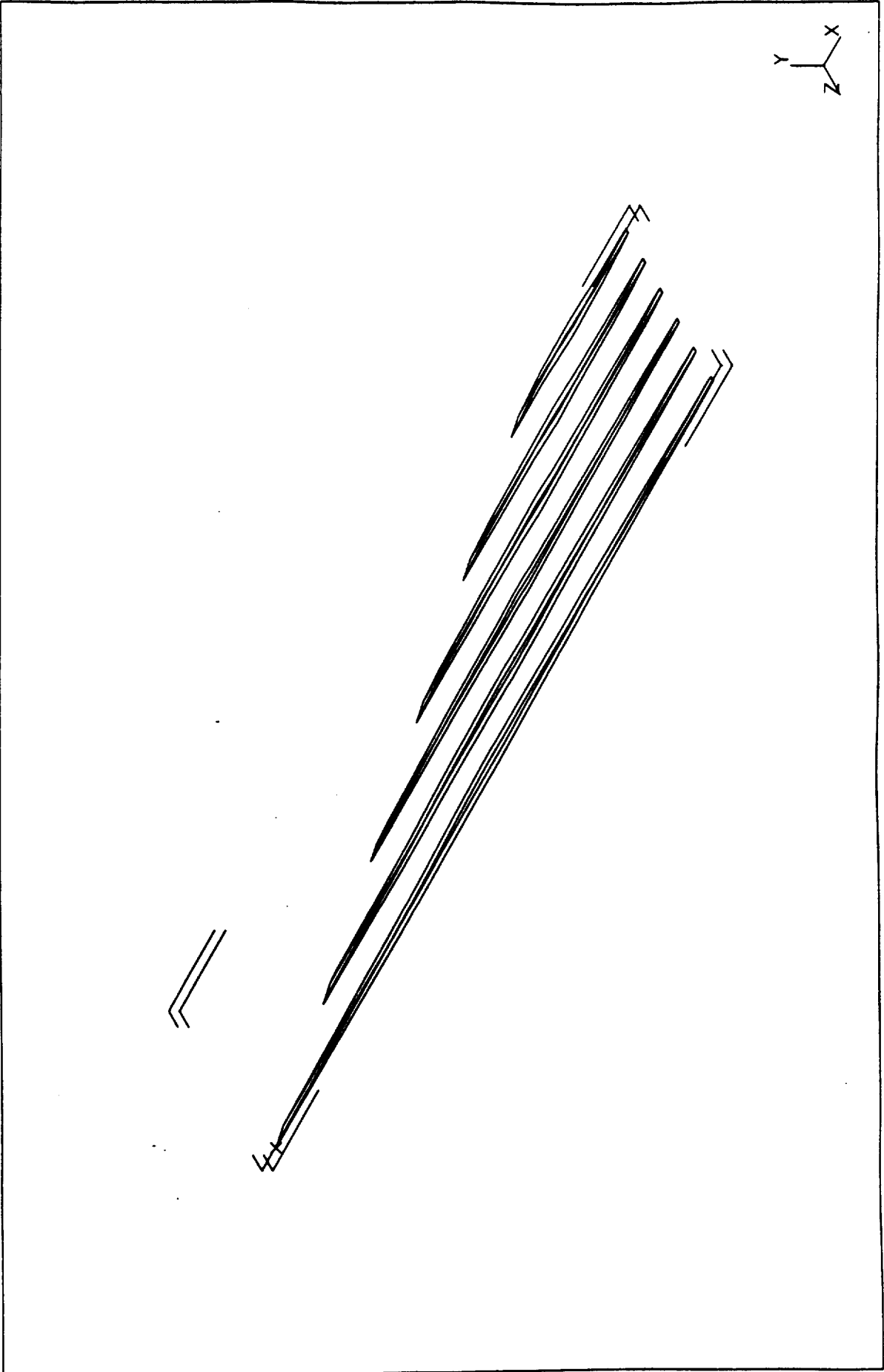
CAEDS VAR2M0: Solid_Modeling

18-FEB-93

00:45:40

Databases wing
View : No stored View
Tech: Object
Object: I-WORK1. (MINGEBC. Sini)

Units : IM
Display : No stored Option
Sini: I-WORK1
Update Level: Full



10. Vertical and horizontal spars joined together

CAEDS VAR2H0: Solid_Modeling

18-FEB-93

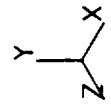
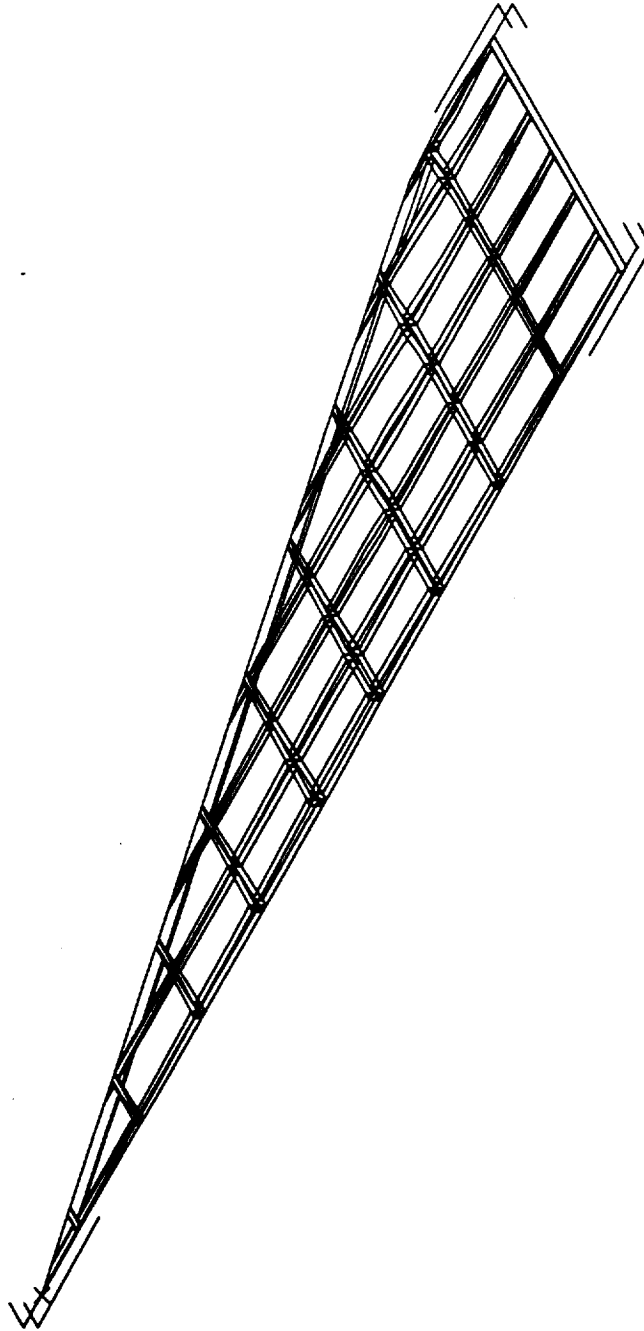
02:33:08

Database: wing
View: No stored View
Task: Object
Object: 1-MORSE1, (MORSE005, Bini)

Bin: 1-MAIN
Update Level: Full

Display: No stored Option

Units: IN



11. Solid object of the vertical tail

CAEDS VAR2H0: Solid_Modeling

11-MAR-93 23:37:04

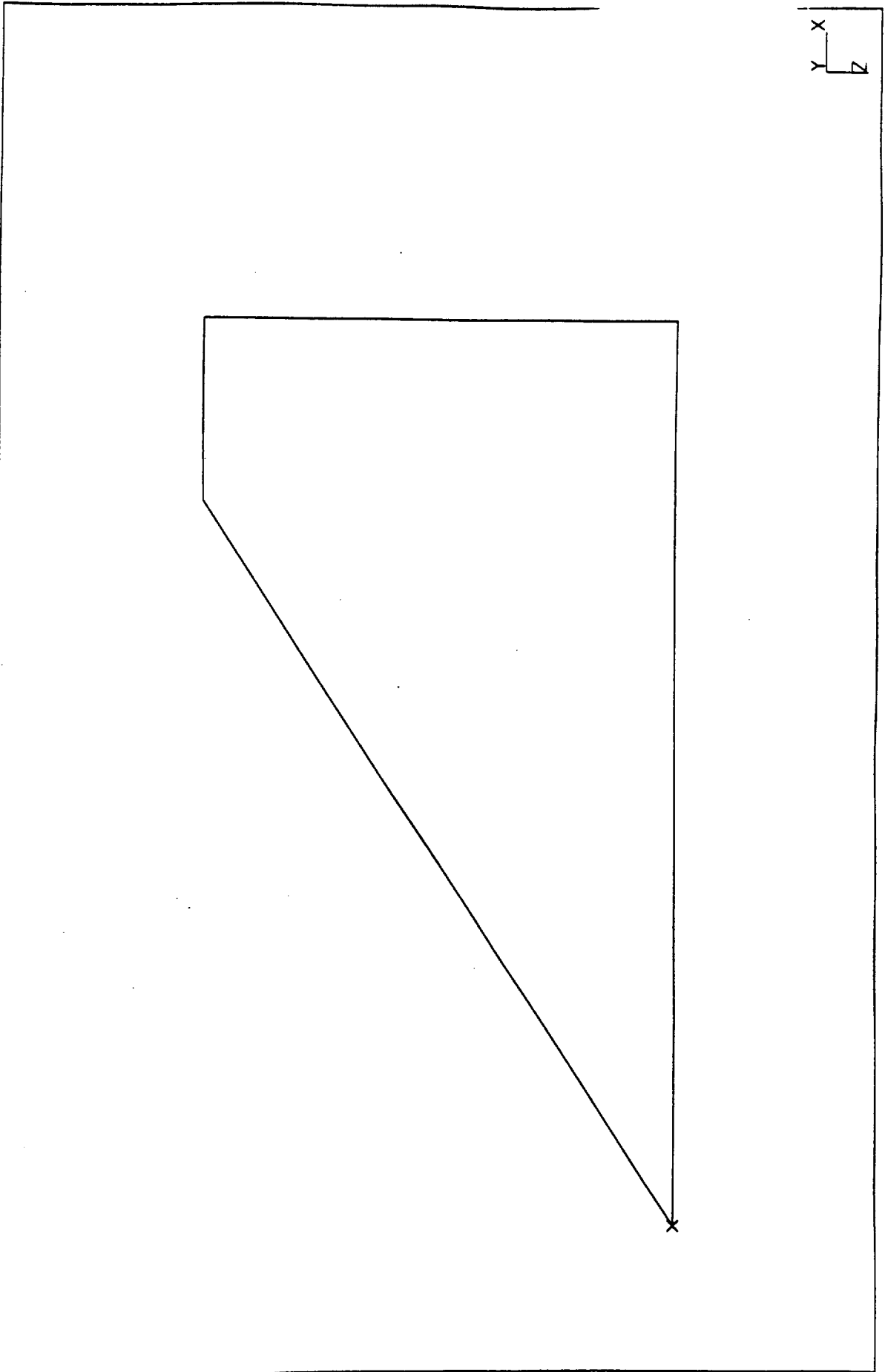
Units : SI

Display : No stored Option

Bin: 1-MIN

Update Level: Full

Database: plane
View : No stored View
Task: Object
Object: 1-MORE1, 1-TAIL, Bin1



12. Vertical tail structure

CAEDS VAR2M0: Solid_Modeling

02-MAR-93 16:45:25

Database: plane

View : No stored View

Task: Object

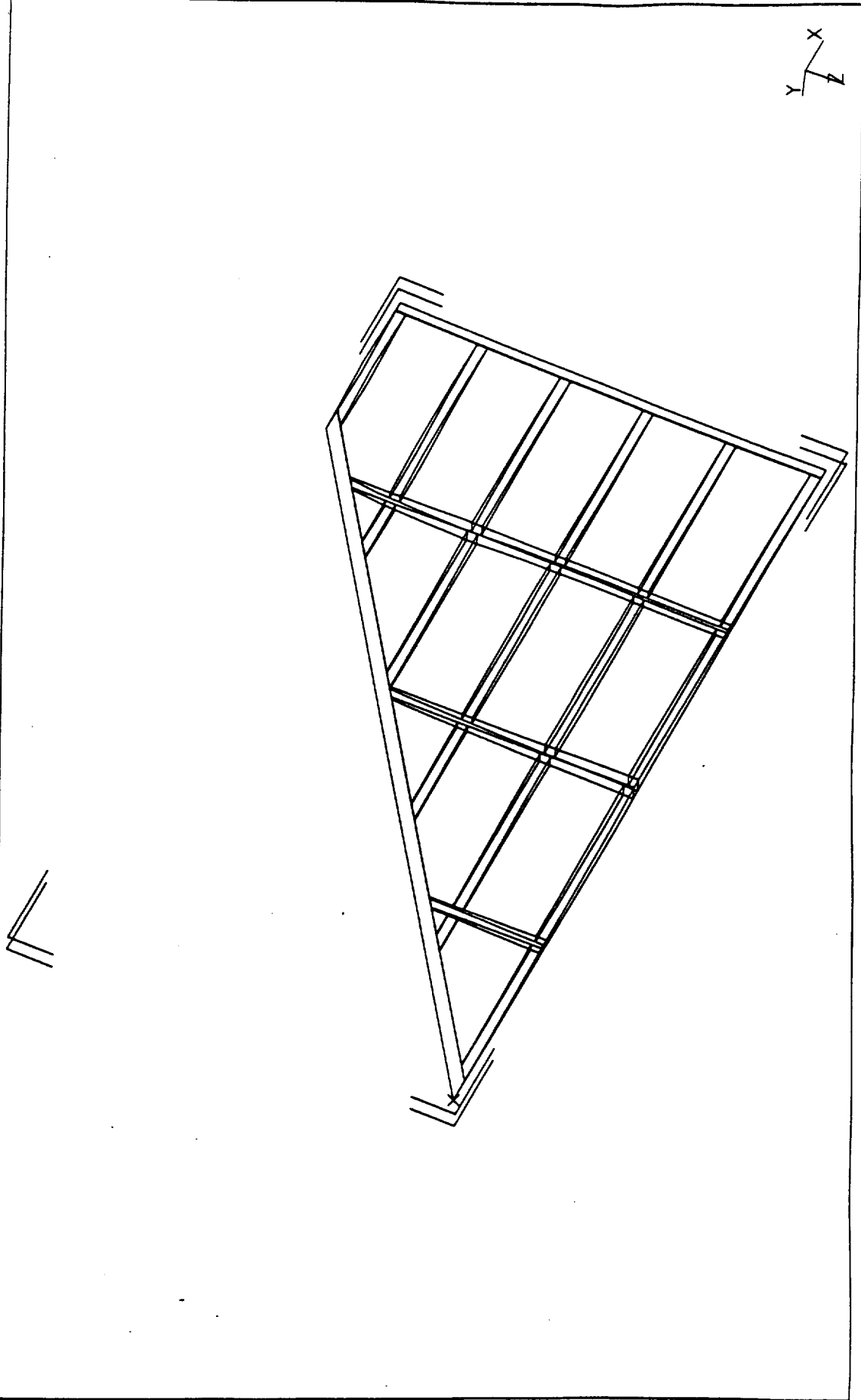
Object: 1-MORK1, (VTHCROSS, Bini)

Units : IN

Display : No stored Option

Bin: 1-MAIN

Update Level: Full



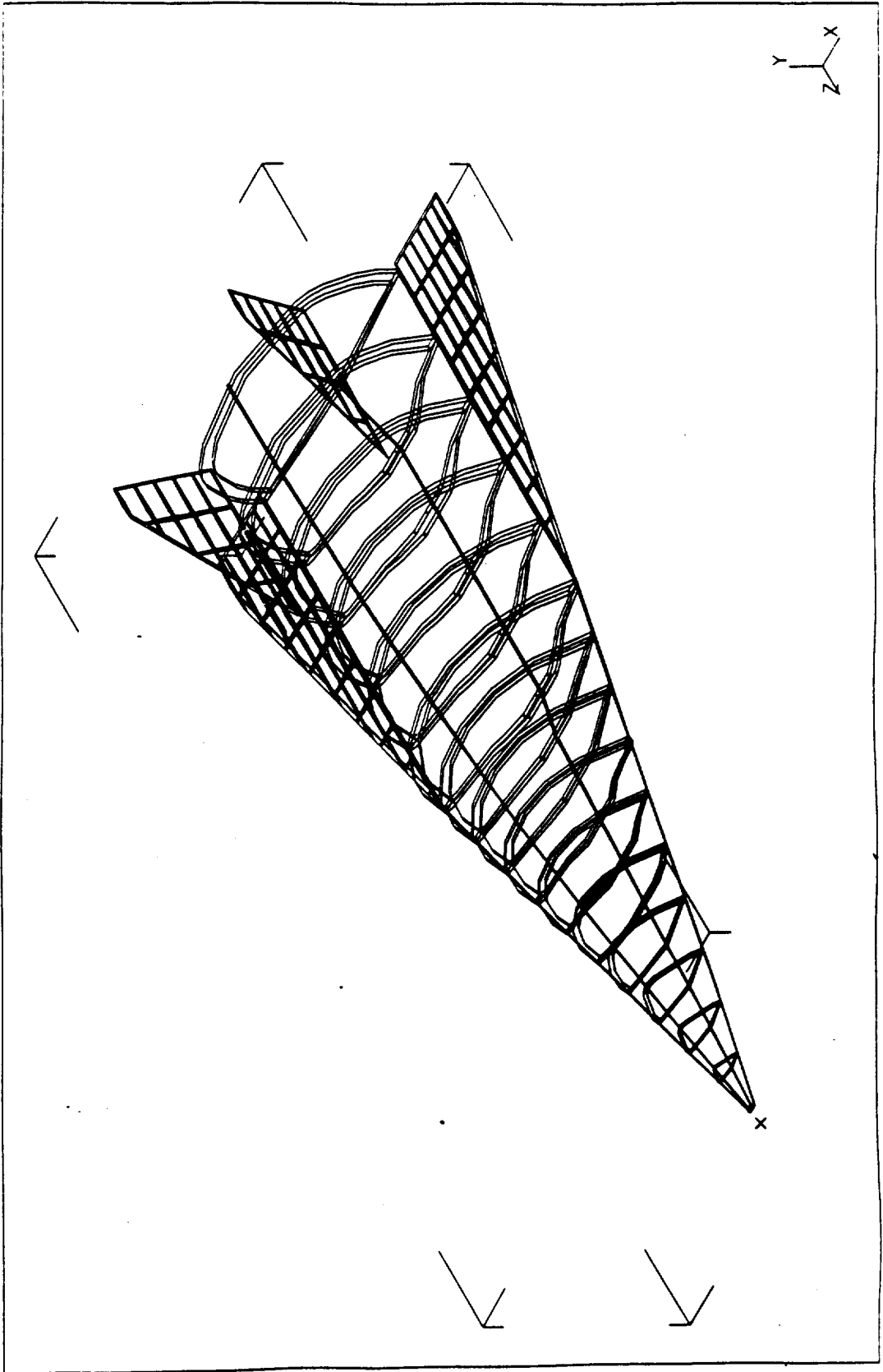
13. Hypersonic Test Vehicle's Internal Structure

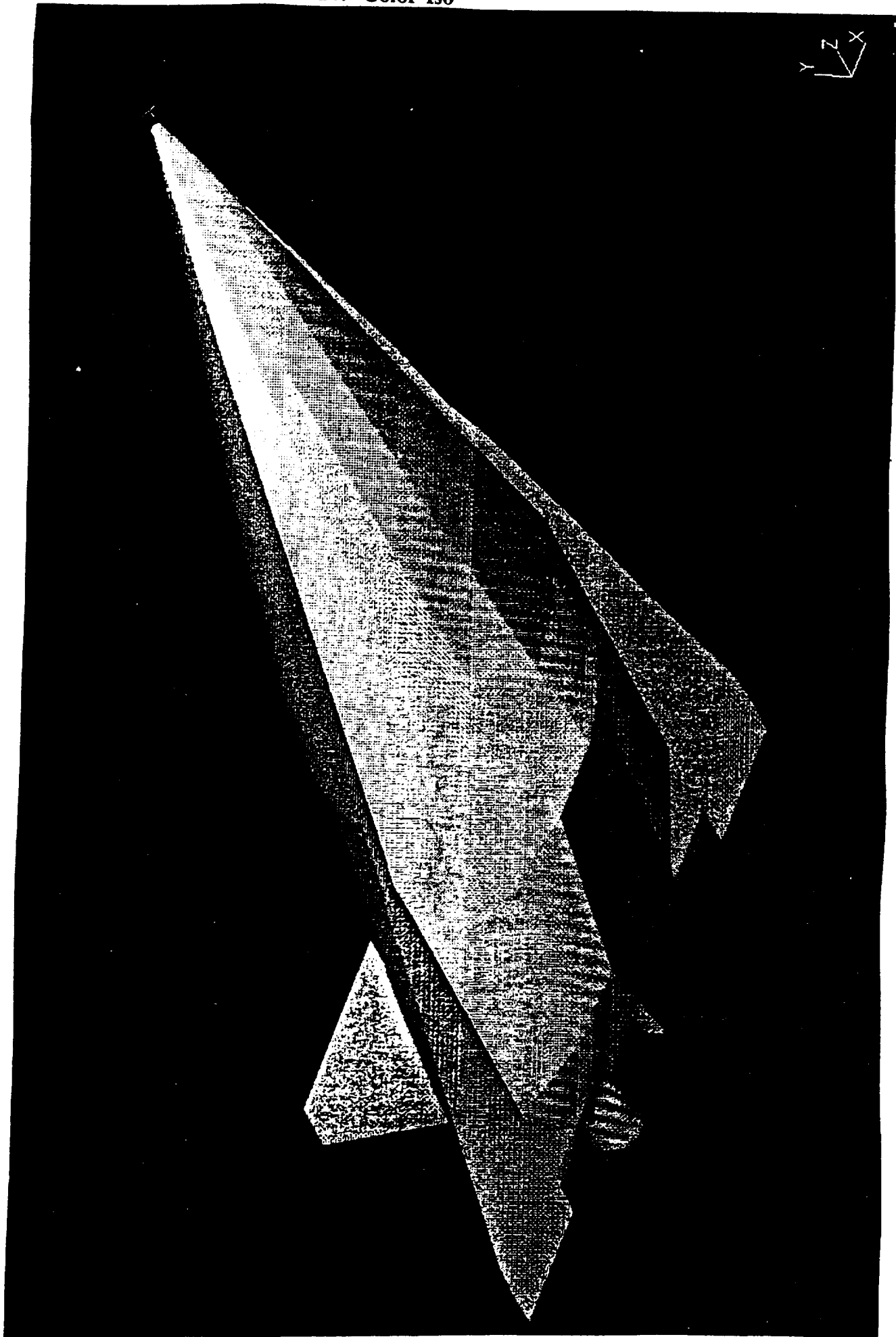
CAEDS V4R2M0: Solid_Modeling

08-MAR-93 22:49:52

Host: I MAIN
Model Level: Full
Display: Isometric
Date: 03/08/93

Model: Solid
View: Isometric View
Task: Object
Object: MODEL, (MODELING, BINIT)





15. Isometric 1

CAEDS VAR2M0: Solid_Modeling

11-MAR-93 02:11:16

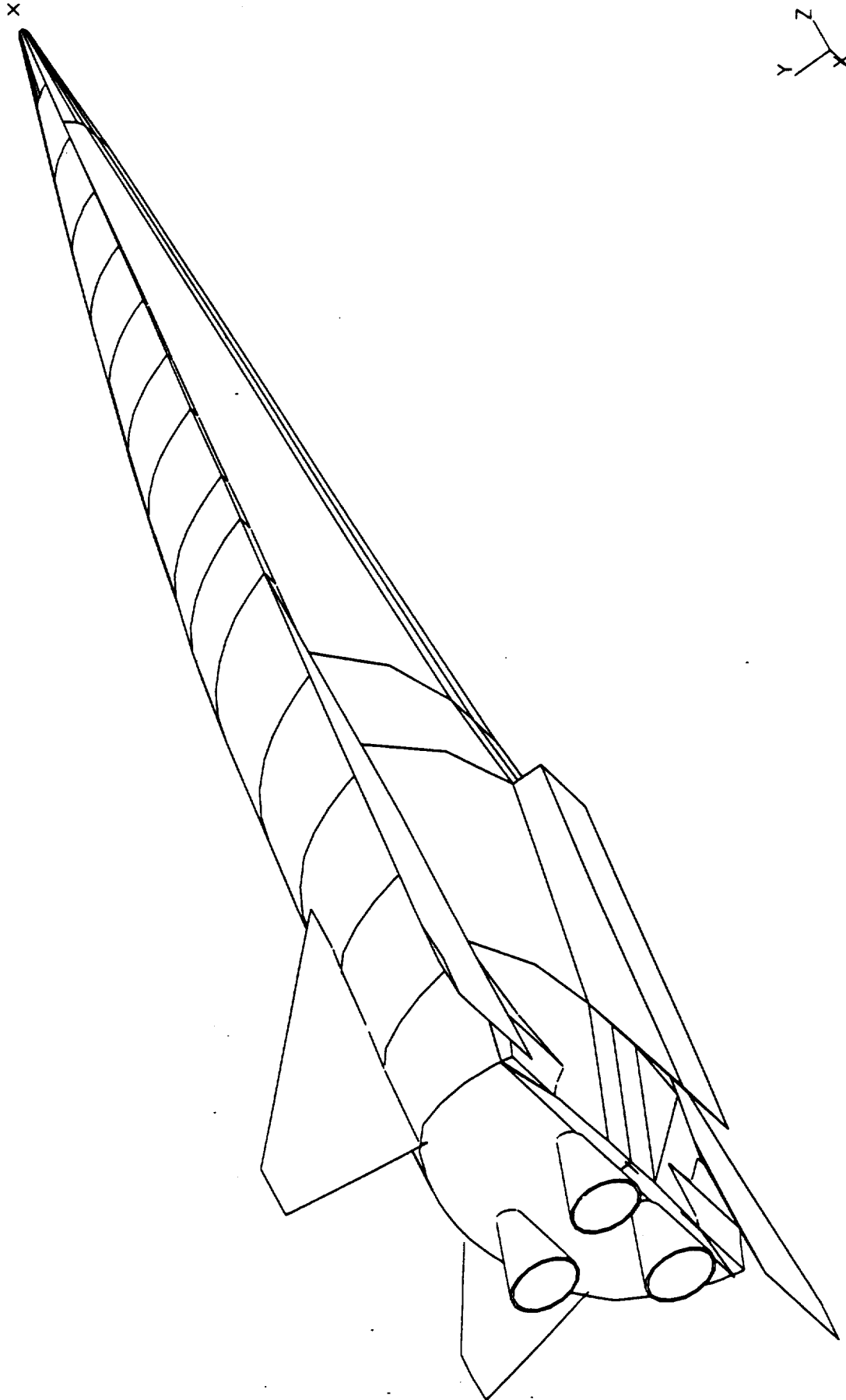
Name : IN

Display : PLANFORM (modified)

Bin : MAIN

Update Level: Full

Database: hyper
View : No aligned View
Task: Object
Object: 4 WORKS. (3:RANKIT. Nint)



16. Isometric 2

CAEDS V4R2M0: Solid_Modeling

11-MAR-93 02:09:02

Host: IN

Database: hyper
View: No. mirrored View

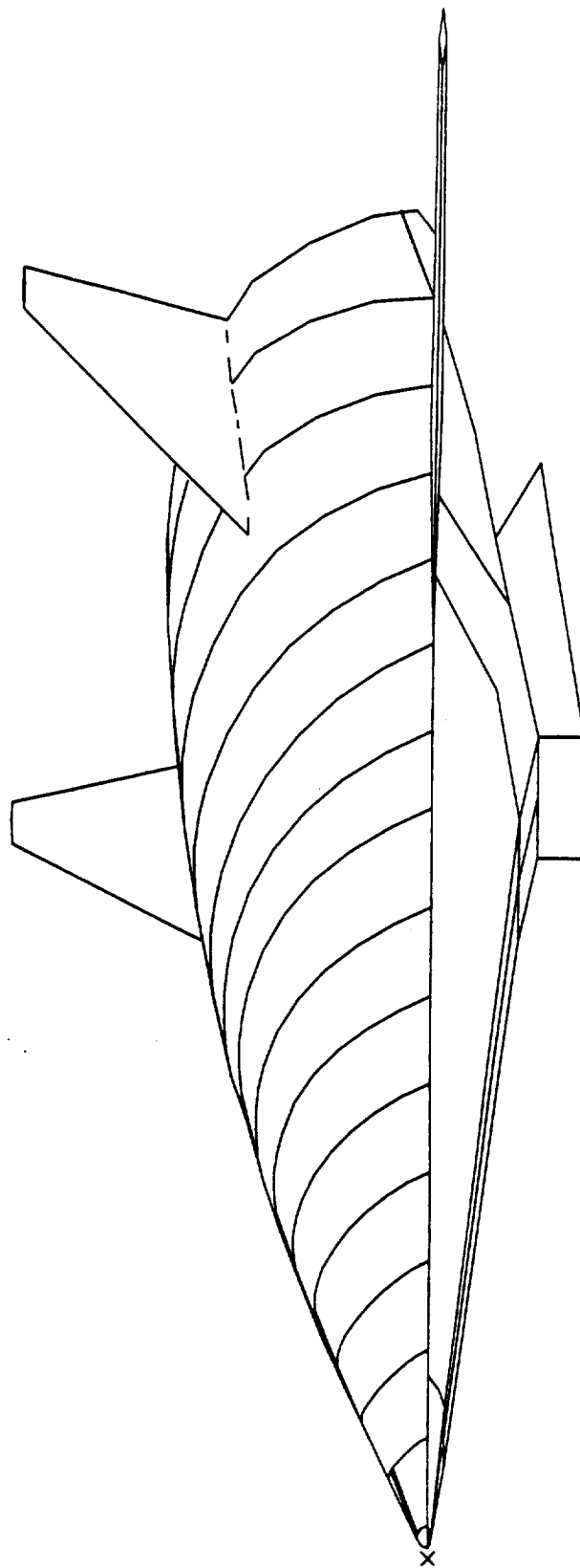
Display: PLAINFORM (modified)

Task: Object

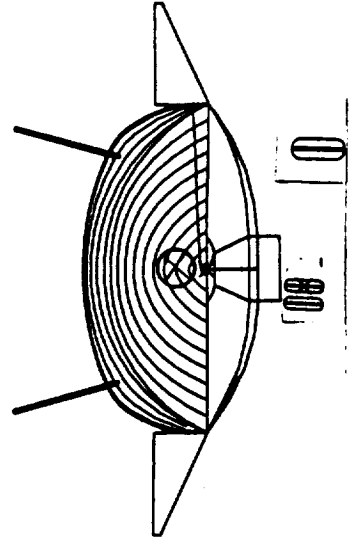
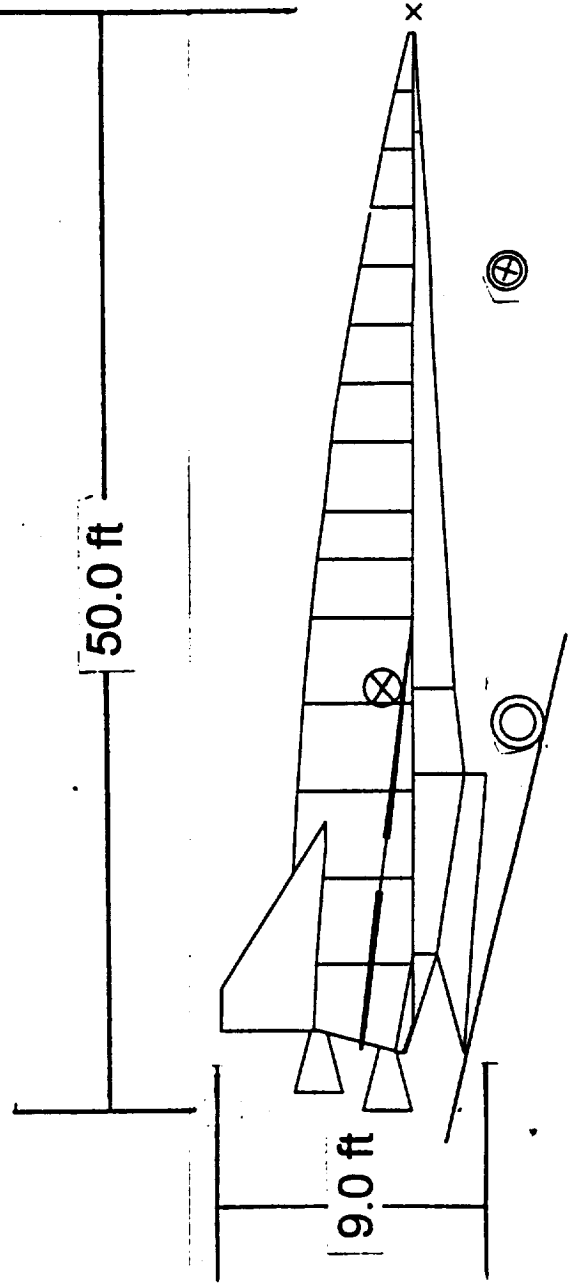
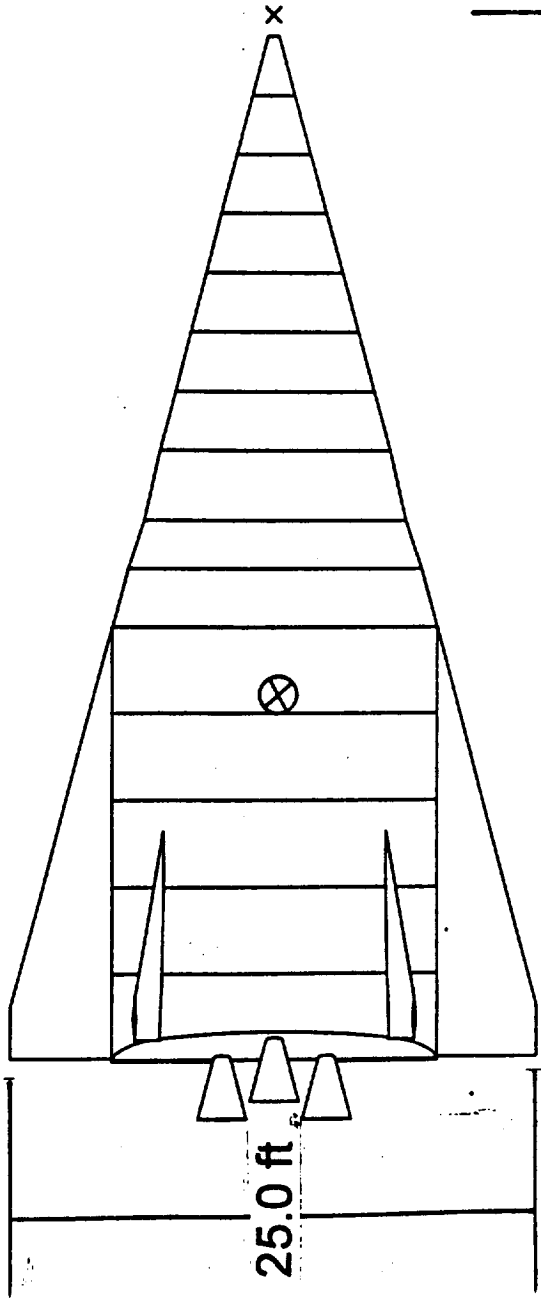
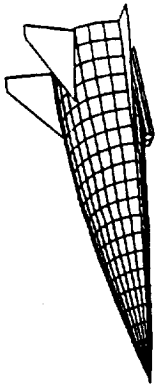
Bin: 1 MAIN

Object: 4 WORKG. (STRANJET. Bin1)

Update Level: Full

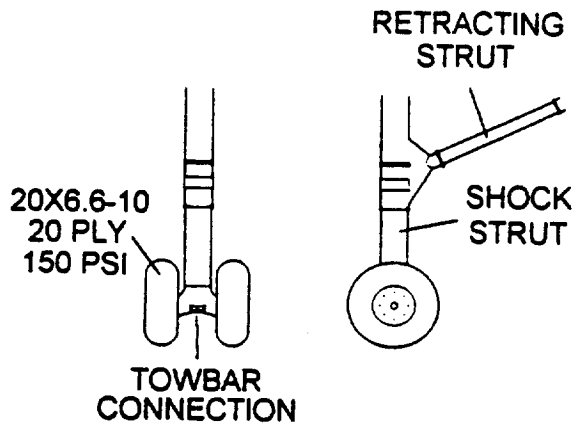


3-View

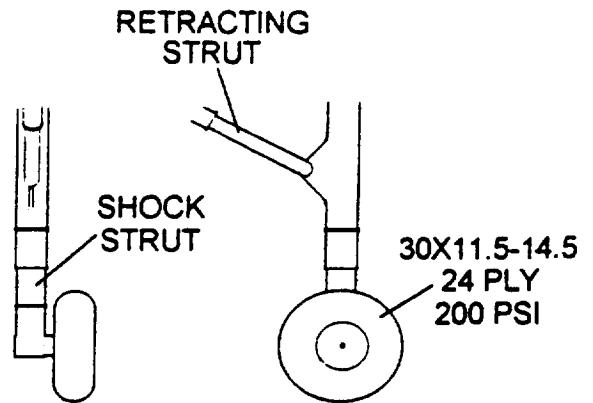


18. Landing Gear

NOSE GEAR:



MAIN GEAR:



- REARWARD RETRACTING TWIN NOSEWHEEL WITH SHOCK STRUT
- NO LANDING OR TAXI LIGHTS
- NO STEERING ACTUATOR
- FREE 360° ROTATION WHEN UNLOCKED

- FORWARD RETRACTING MAIN GEAR
- MAXIMUM DESCENT RATE OF 21 FT/SEC

Appendix 2: Weight and Volume Figures

1. Table 2.1. I-DEAS Properties
2. Figure 2.1. Weight Pie Chart
3. Figure 2.2. Volume Pie Chart
4. Table 2.2. I-DEAS vs. PPDWAP Weight Comparison
5. Figure 2.3. Inboard Planform

Table 1. I-DEAS Properties

Components	Weight lbs	Volume ft ³	Surface Area ft ²	cg (x,y,z) ft
Body Frame	2092	15		0, 2, -35.24
Wing (2) Frame	450	2		0, 0, -41.24
V. Tail (2) Frame	168	1.5		0, 6.0, -31.59
Body Skin	3080	64	1370.78	0, 1.53, -33.87
Wing (2) Skin	188	2	240.11	0, 0, -42.93
V. Tail Skin	100	1.07	128.17	0, 6.12, -31.57
Scramjet	1330			0, -2.35, -42.57
Rocket Engine (3)	1140	8.85		0, 35.0, -592.54
O2 Fuel Tank	328	20		0, 1.85, -41.71
H2 Fuel Tank	1057	51		0, 1.41, -27.66
Nose Gear	165	5		0.16, -0.82, -29.83
Main Gear (2)	425	22		0.16, -0.82, -29.83
Payload	1000	35		0.16, -0.82, -29.83
Pressure System	1182			
Power Supply	491			
Avionics	407			
Empty Totals	13603			
Fuels:				
O2	28929	406		
H2	5241	1183		
Take-off	47,810	1728		

Figure 2.1. Weight Pie Chart

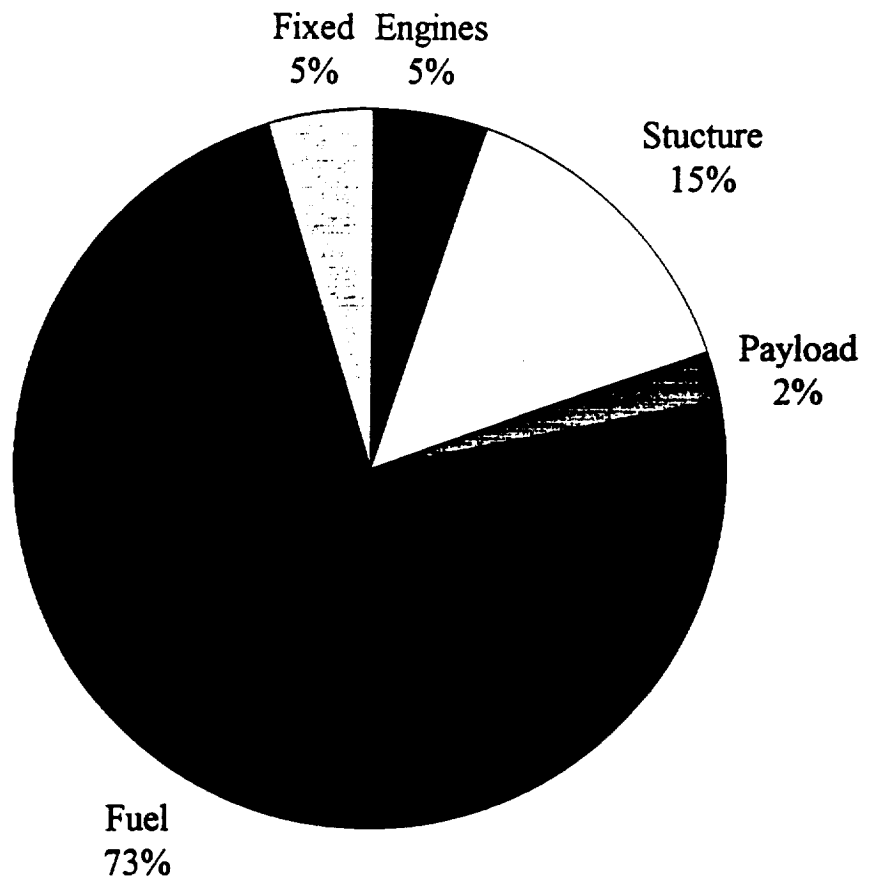


Figure 2.2. Volume Pie Chart

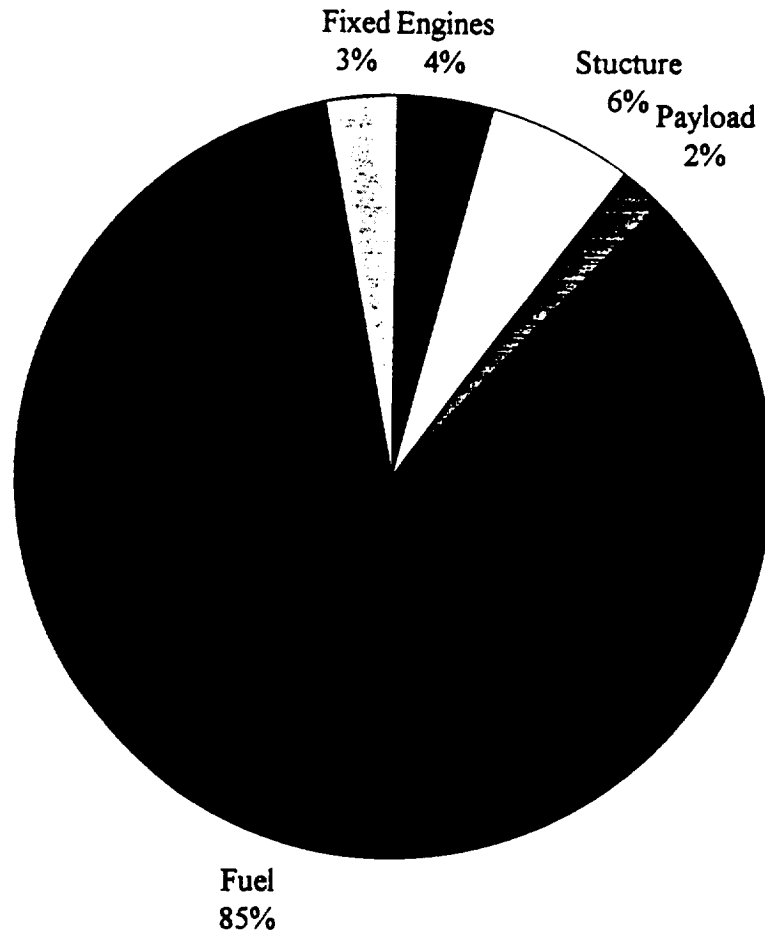
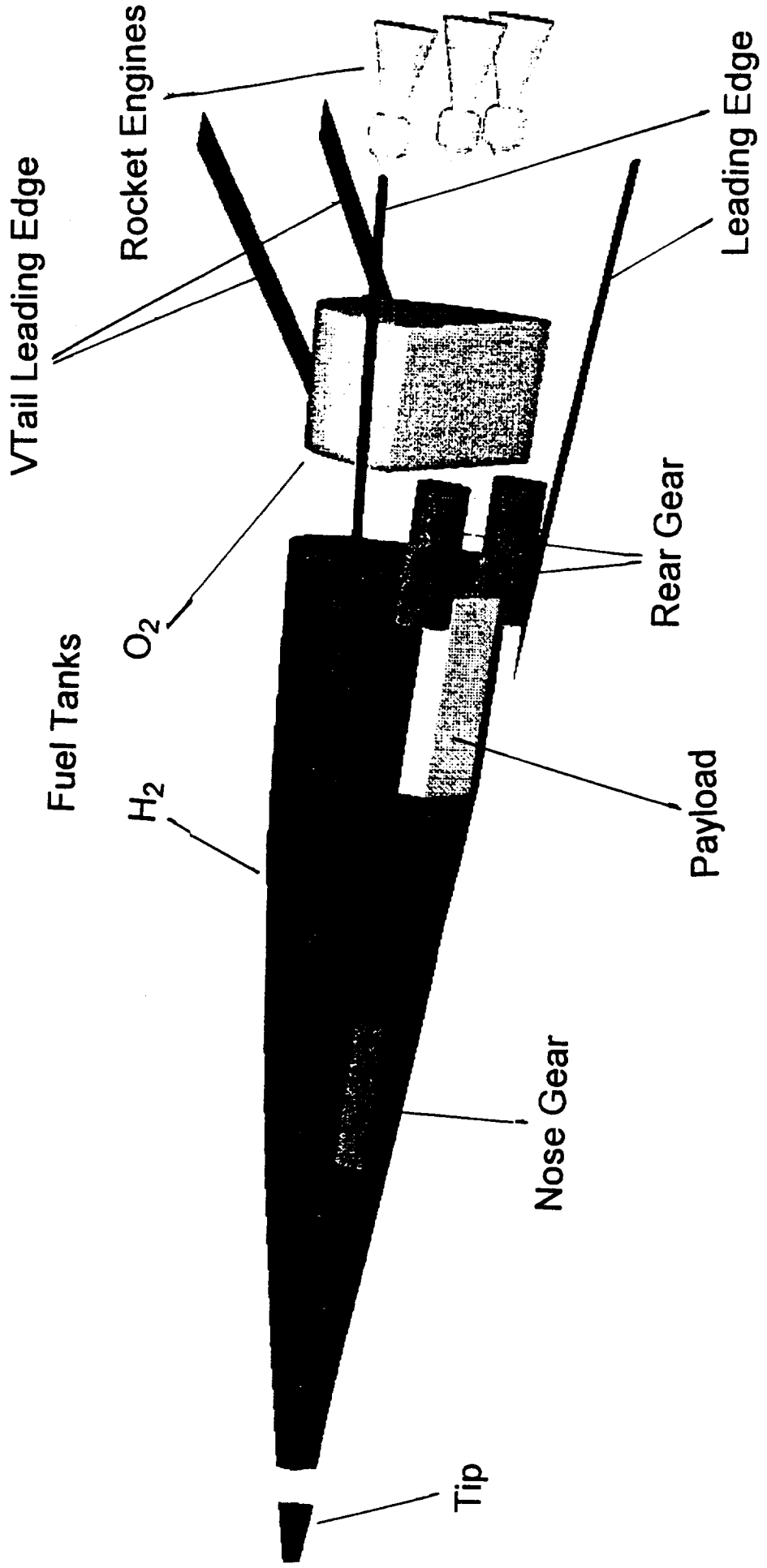


Table 2. I-DEAS vs. PDWAP Weight Comparison

	I-DEAS lbs	PDWAP lbs
Empty	13603	14564
Body	2092	2152
Wing	951	1952
Tail	540	992
Tanks	1385	1750
Pressure System		1182
Power		491
Avionics		407

4. Inboard platform



Appendix 3: Stress Contours

1. Configuration 1 (half)
- 1A. Configuration 1 (whole)
2. Configuration 2
3. Configuration 3
4. Configuration 4A
5. Configuration 4B
6. Configuration 5
7. Configuration 6
8. Configuration 7
9. Configuration 8
10. Configuration 9
11. Configuration 9 (close-up)

CAEDS V4R210: FE_Modeling_Analysis

11-MAR-93 21:47:31

abases: femrib
 w: none, none
 Task: Post Processing
 Model: 3-FBRIB1
 Display: none, none
 Model Bins: 1-MAIN
 Associated Wbrkset: 3-DRKING_SET3

LOAD SET: 1 - LOAD SET 1
 REF: GLOBAL
 STRESS - MAX PRIN MIN: -1.29E+06 MAX: 3.18E+06

femrib
 LOAD SET: 1 - LOAD SET 1
 REF: GLOBAL
 STRESS - MAX PRIN MIN: -1.29E+06 MAX: 3.18E+06

femrib
 LOAD SET: 1 - LOAD SET 1
 REF: GLOBAL
 STRESS - MAX PRIN MIN: -1.29E+06 MAX: 3.18E+06

3.18E+06

2.54E+06

1.90E+06

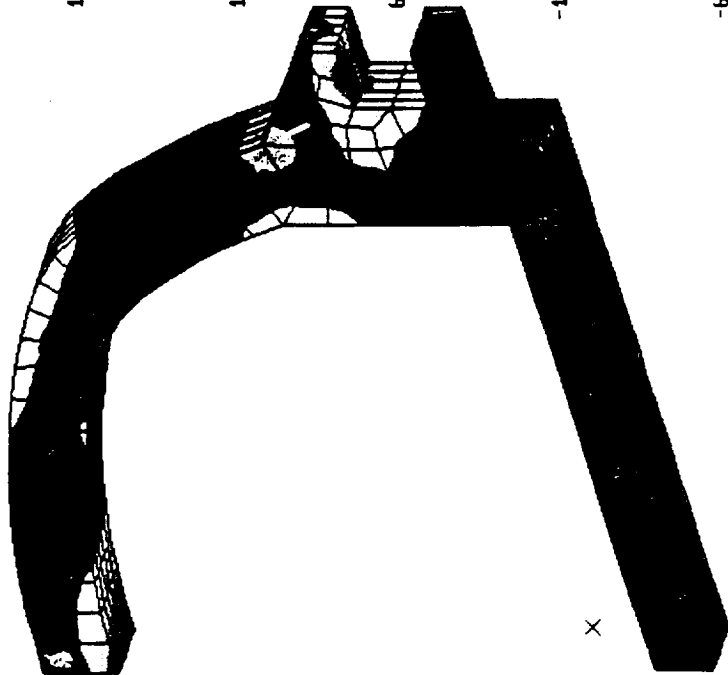
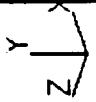
1.27E+06

6.27E+05

-12281.88

-6.51E+05

-1.29E+06



1. Configuration 1 (half)

3.18E+06

2.54E+06

1.90E+06

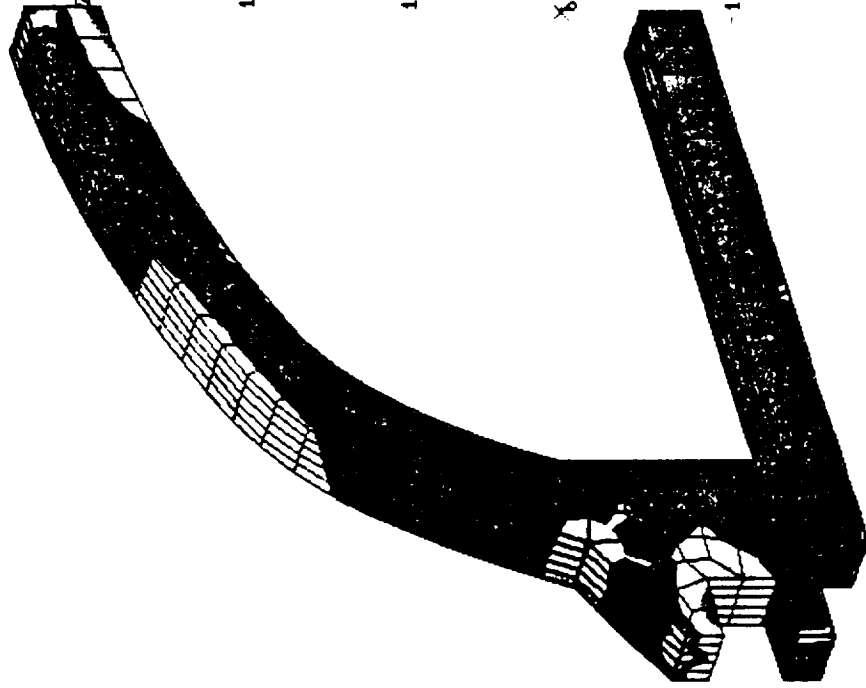
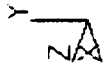
1.27E+06

6.27E+05

-12281.88

-6.51E+05

-1.29E+06



1A. Configuration 1 (whole)

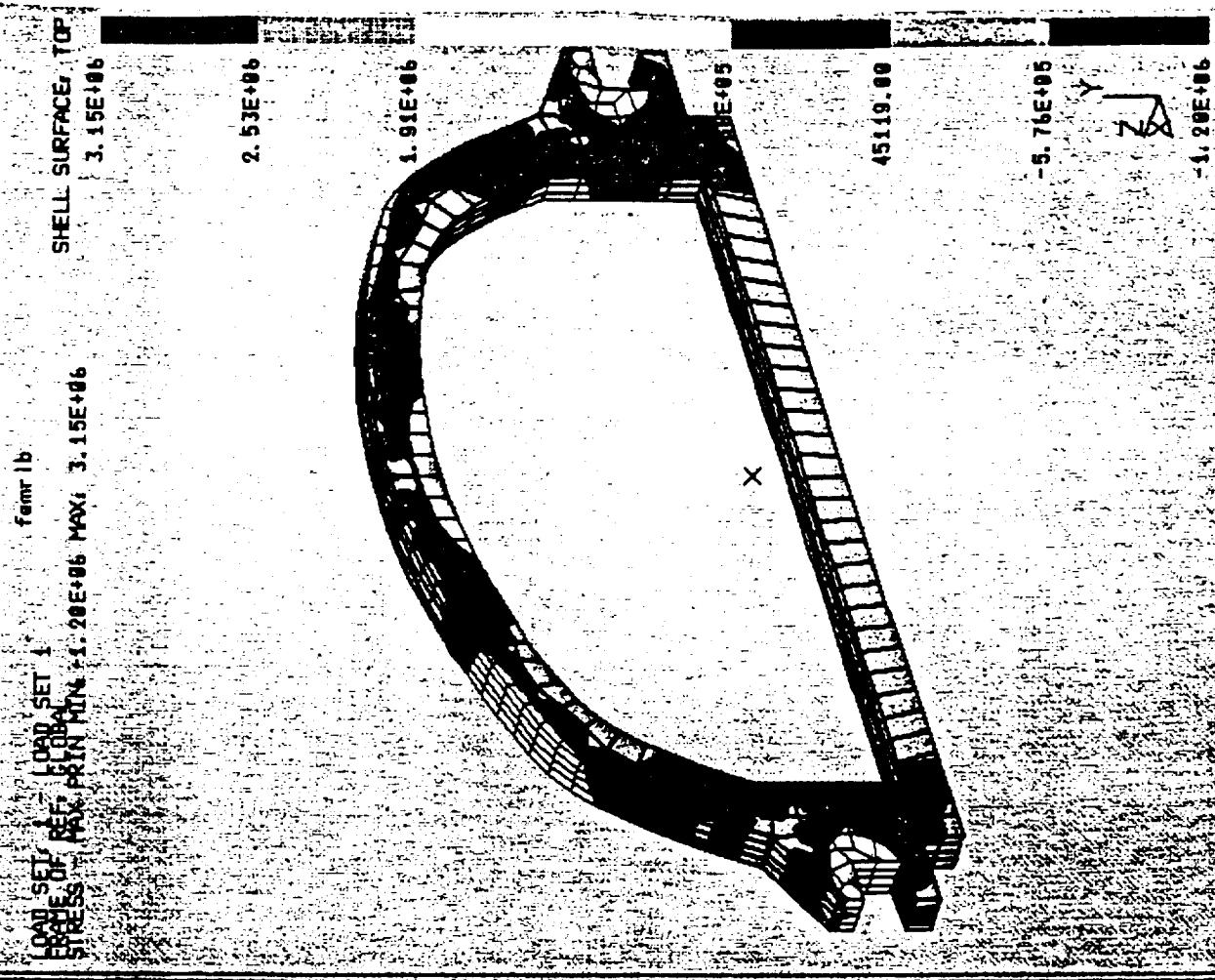
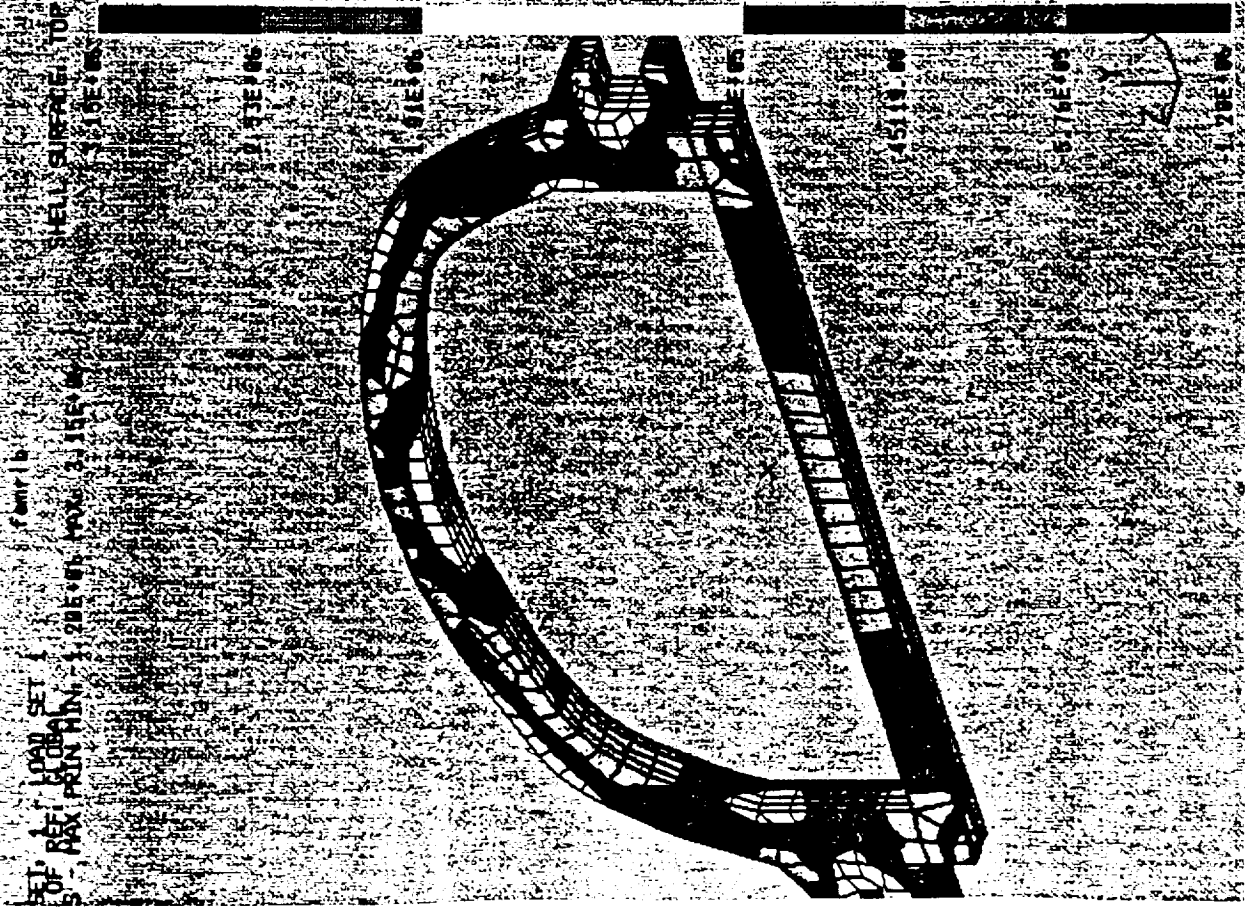
CAEDS VARZM0: FE_Modeling & Analysis

10-MAR-93

14:42:11

set femr1b
 none, none
 tasks Post Processing
 del: 2-WHOLE

Units : SI
 Display : none, none
 Model Bltn : 1-MAIN
 Associated lbrksets : 4-WORKING_SET4



CAEDS V4R2M0: FE_Modeling & Analysis

10-MAR-93 14:47:30

Units : SI
 Display : none, none
 Model Btry : 1-MAIN
 Associated wrkset: 9-WORKING_SET9

asea femr1b
 : none, none
 Task: Post Processing
 Model: 7-FBRIB3

SET, REF, LOAD SET 1
 OF GLOBAL
 SS - MAX PRIN MIN: -9.39E+06 MAX: 4.33E+07

femr1b
 LOAD SET, REF, LOAD SET 1
 OF GLOBAL
 SS - MAX PRIN MIN: -9.39E+06 MAX: 4.33E+07

4.33E+07

3.57E+07

2.82E+07

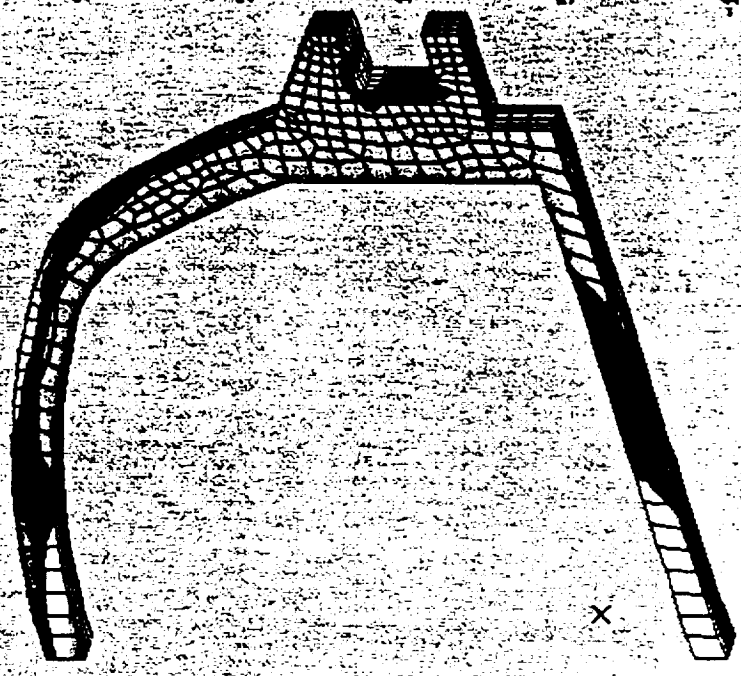
2.07E+07

1.32E+07

5.65E+06

-1.07E+06

-9.39E+06



4.33E+07

3.57E+07

2.82E+07

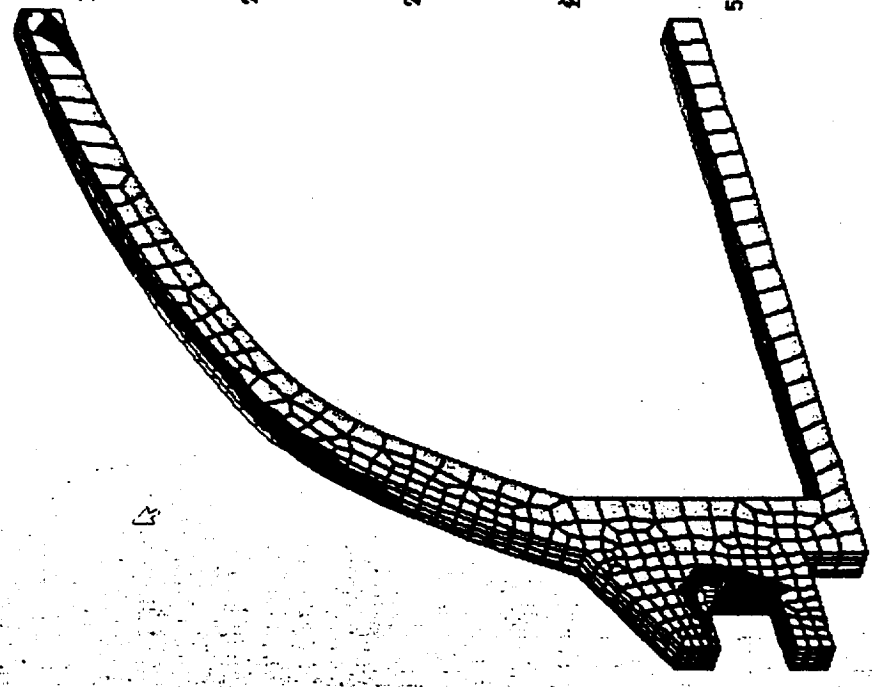
2.07E+07

1.32E+07

5.65E+06

-1.07E+06

-9.39E+06



2. Configuration 2

CAEDS V4R2M0: FE_Modeling & Analysis

10-MAR-93

15:03:42

bases femr1b

Units: none

Task: Post Processing

Model: 10-FBRIB5

Units: SI

Display: none, none

Model Base: 1-MAIN

Associated Worksets: 20-WORKING_SET28

LOAD SET 1

REF: GLOBAL

STRESS - MAX PRIN MIN: -4.60E+07 MAX: 1.42E+08

femr1b

LOAD SET 1

REF: GLOBAL

STRESS - MAX PRIN MIN: -4.60E+07 MAX: 1.42E+08

1.42E+08

1.15E+08

8.83E+07

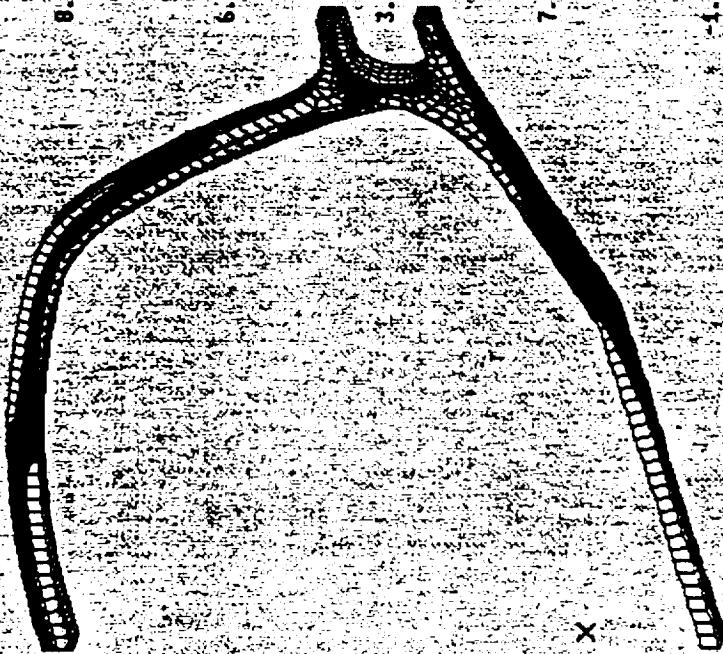
6.14E+07

3.46E+07

7.74E+06

-1.91E+07

-4.60E+07



1.42E+08

1.15E+08

8.83E+07

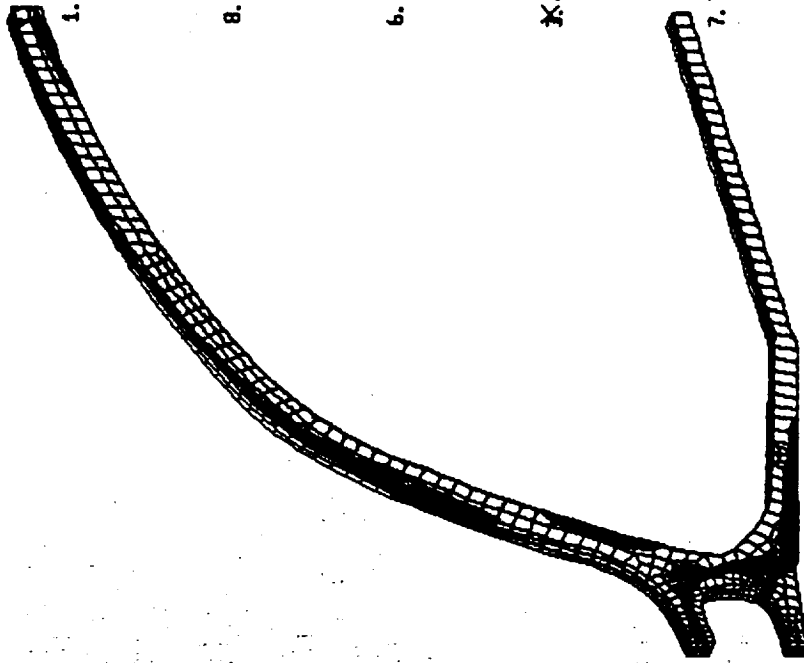
6.14E+07

3.46E+07

7.74E+06

-1.91E+07

-4.60E+07



4. Configuration 4A

5. Configuration 4B

CAEDS V4RZM0: FE Modeling & Analysis

10-MAR-93

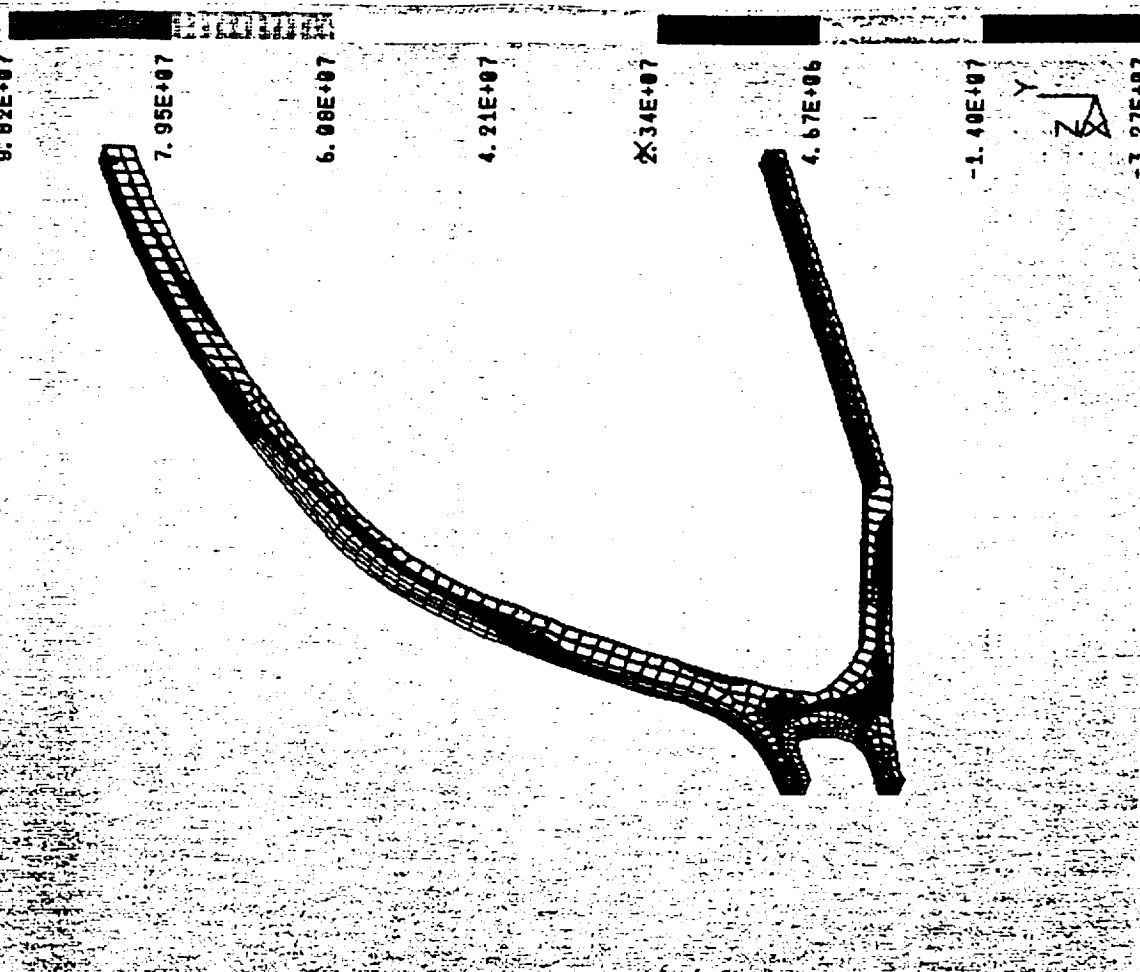
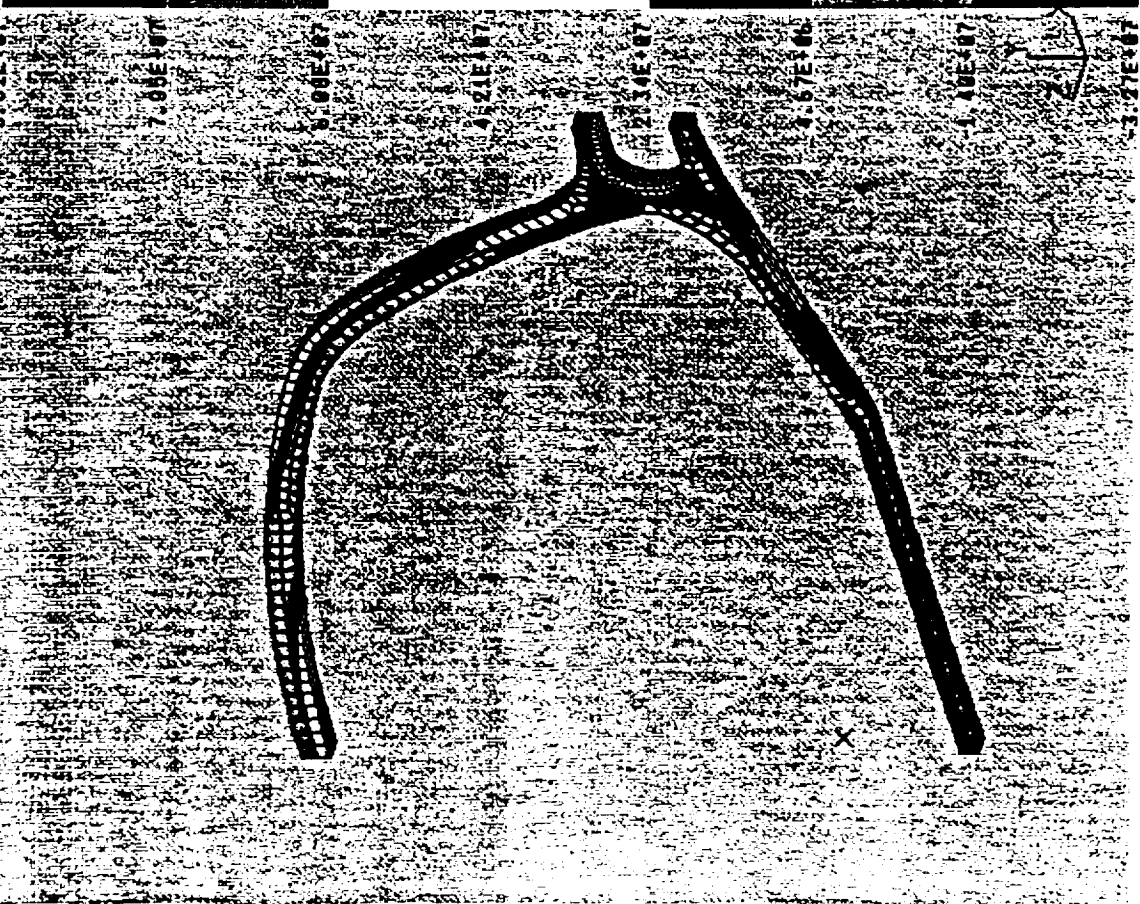
15:07:28

base: femr1b
 name: none
 Task: Post Processing
 Mode: 10-FBYRIB

Units: SI
 Display: none, none
 Model Bln: 1-MAIN
 Associated Workset: 20-WORKING_SET28

LOAD SET 1 - GLOBAL SET 1
 OF REF. COORD.
 STRESS - MAX PRIN. MIN. -3.27E+07 MAX. 9.82E+07

femr1b
 LOAD SET 1 - GLOBAL SET 1
 OF REF. COORD.
 STRESS - MAX PRIN. MIN. -3.27E+07 MAX. 9.82E+07



CAEDS V4R2M0: FE_Modeling & Analysis

base: femr1b
; none, none
Task: Post Processing
Model: 12-FB-RIB6

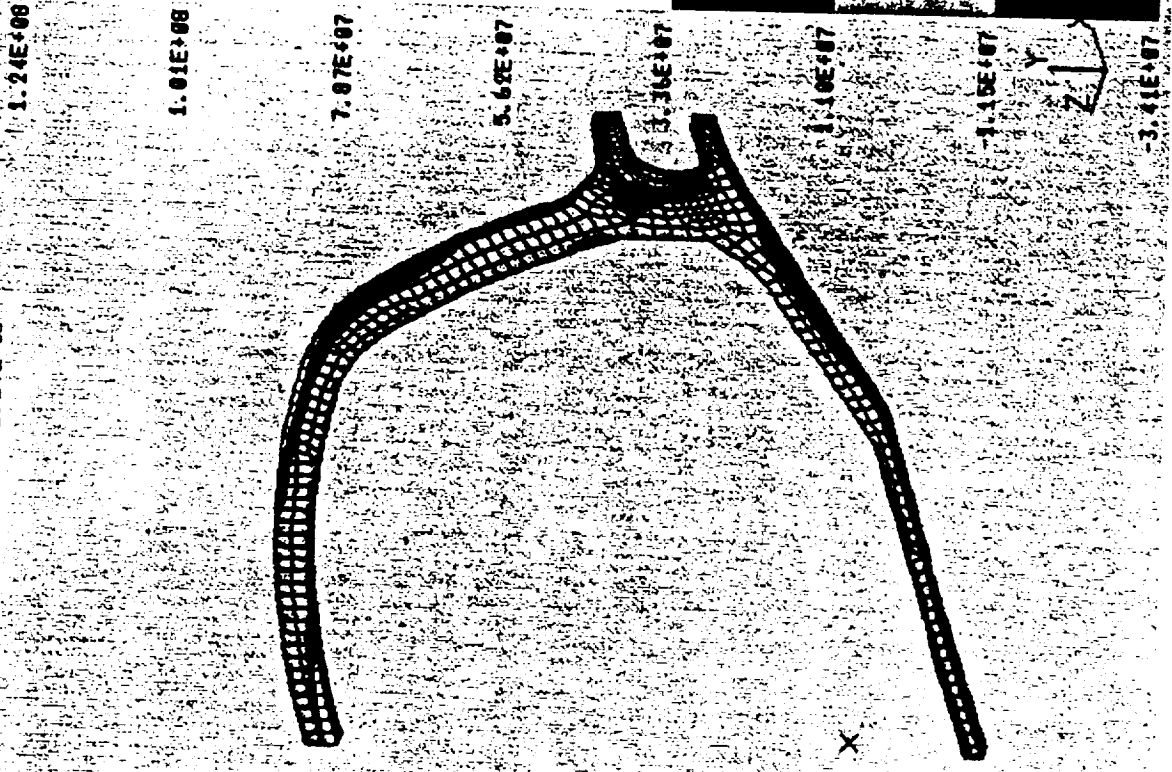
10-MAR-93

15:18:16

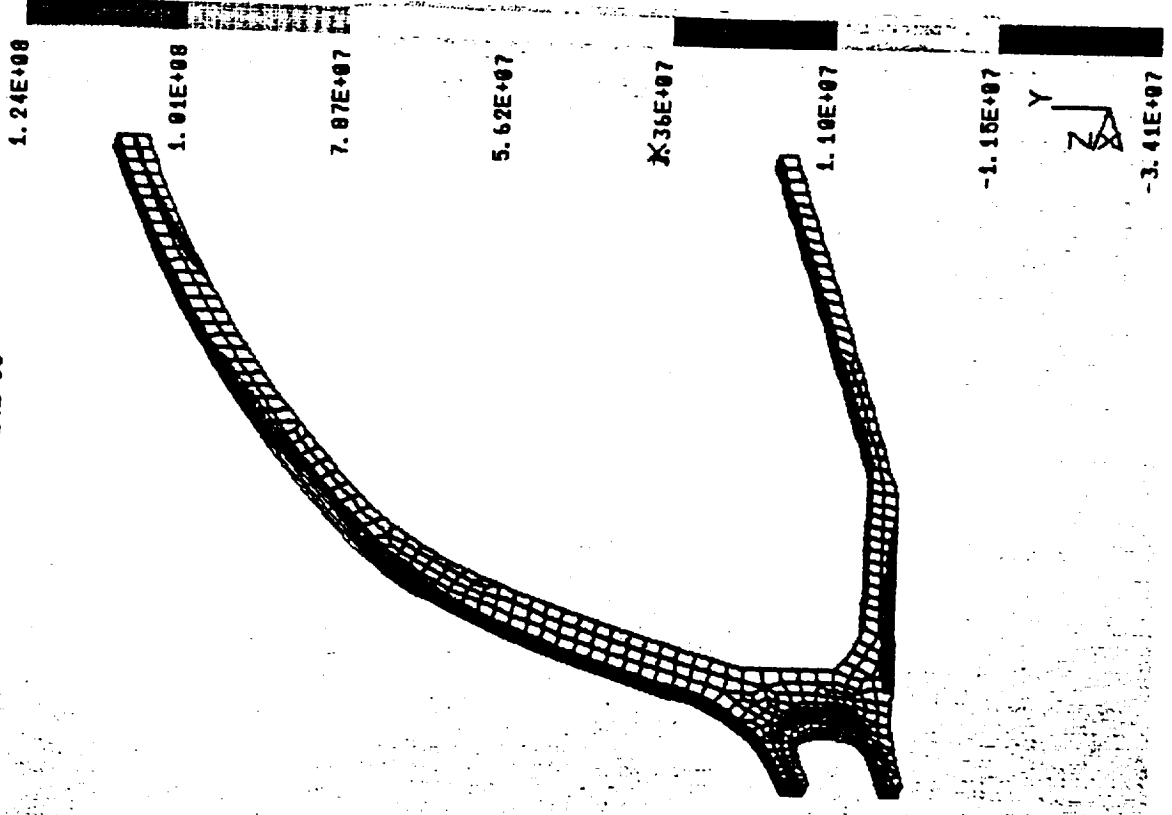
Units : SI
Display : none, none
Model Bldg : 1-MAIN
Associated wrkset: 35-WORKING_SET35

femr1b

LOAD SET 1 - LOAD SET 1
OF REF: GLOBAL
STRESS - MAX PRIN MIN: -3.41E+07 MAX: 1.24E+08



LOAD SET 1 - LOAD SET 1
OF REF: GLOBAL
STRESS - MAX PRIN MIN: -3.41E+07 MAX: 1.24E+08



6. Configuration 5

7. Configuration 6

CAEDS V4R210; FE Modeling & Analysis

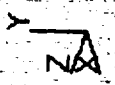
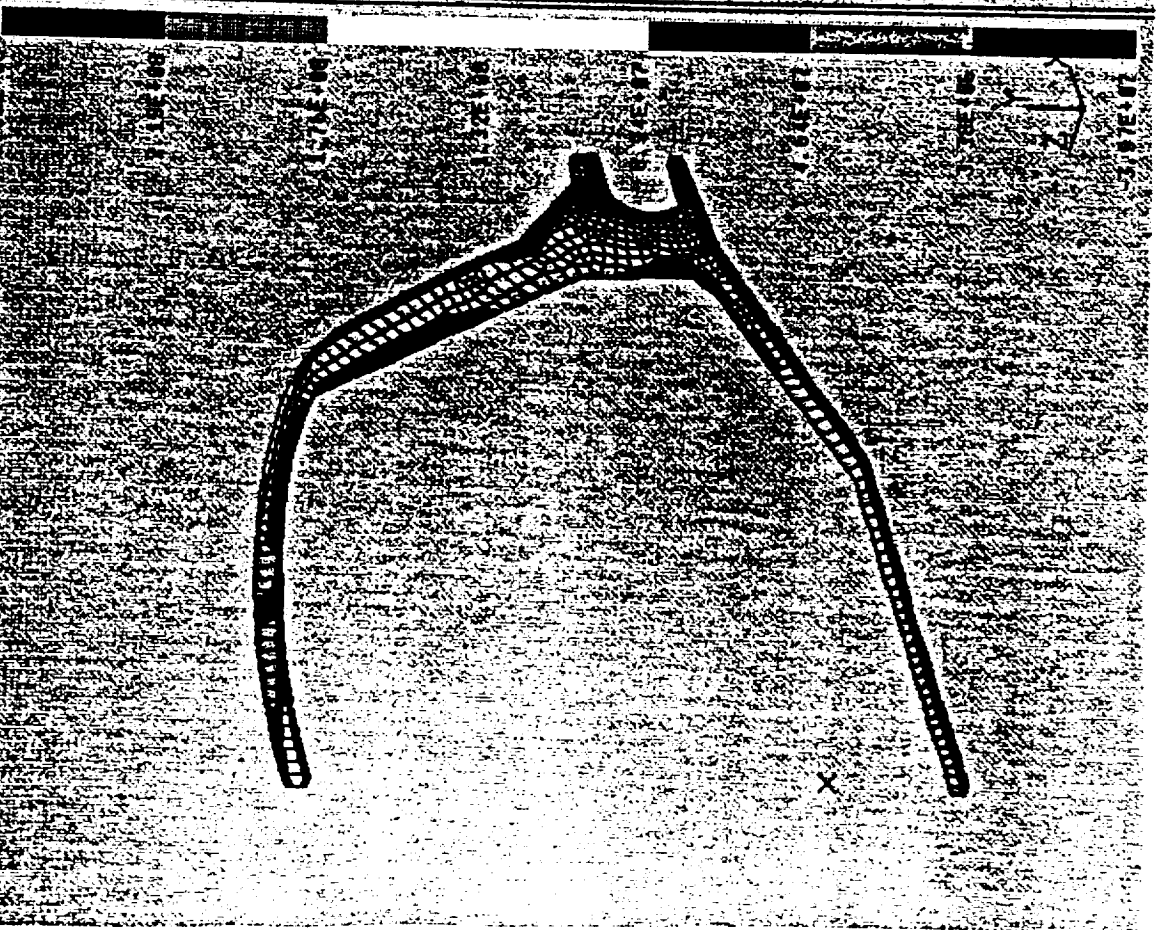
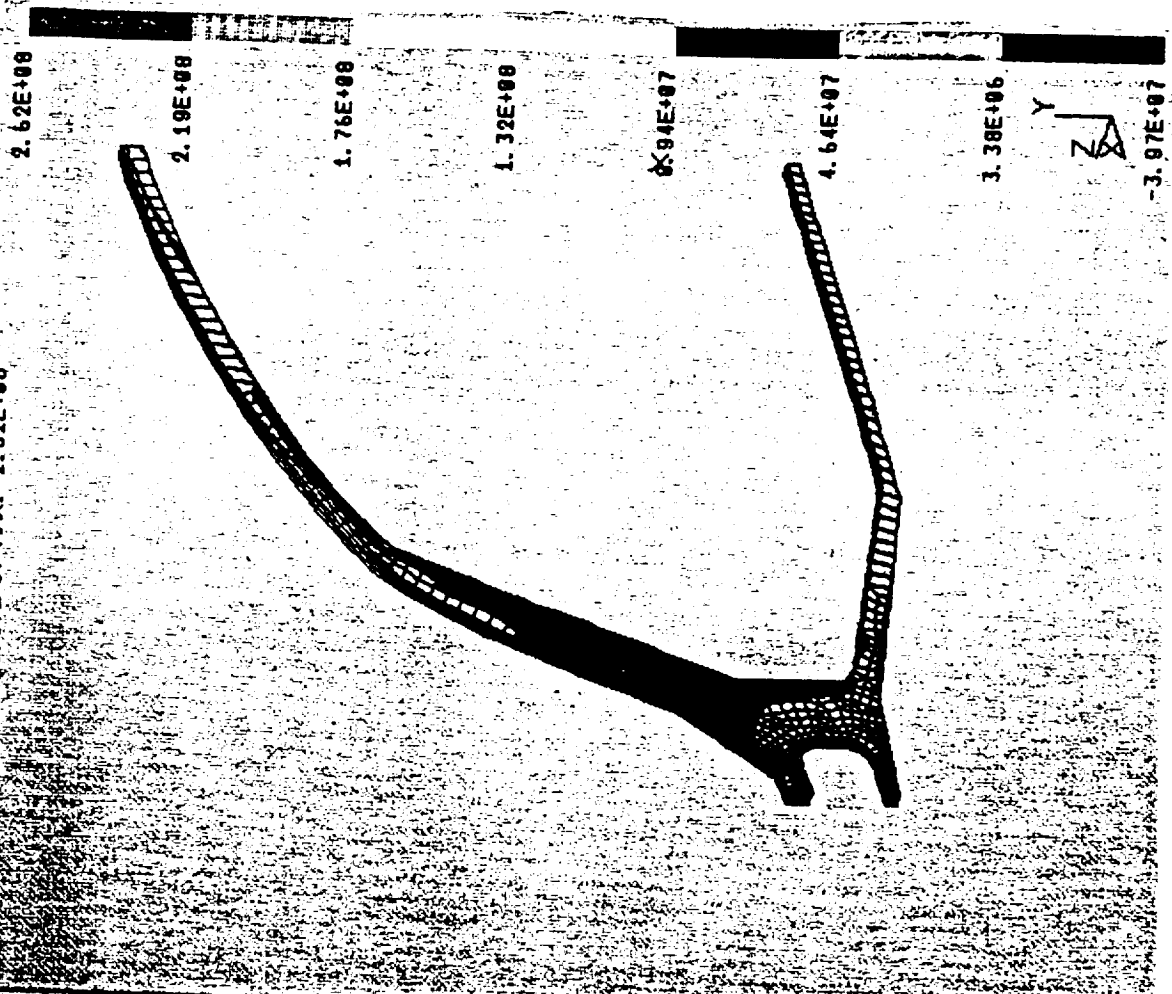
10-MAR-93 15:22:23

Units: SI
Display: none, none
Model Bln: 1-MAIN
Associated Wbrkset: 42-WORKING_SET42

base femr1b
none, none
Task: Post Processing
Model: 4-FEVALB7

LOAD SET 1 - LOAD SET 1
femr1b
STRESS DE MAX PRIN MIN 3.97E+07 MAX. 2.62E+08

LOAD SET 1 - LOAD SET 1
femr1b
STRESS DE MAX PRIN MIN 3.97E+07 MAX. 2.62E+08



8. Configuration 7

CAEDS V4RZM0: FE_Modeling & Analysis

user: femr1b
task: Post Processing
date: 6-FB-R1B8

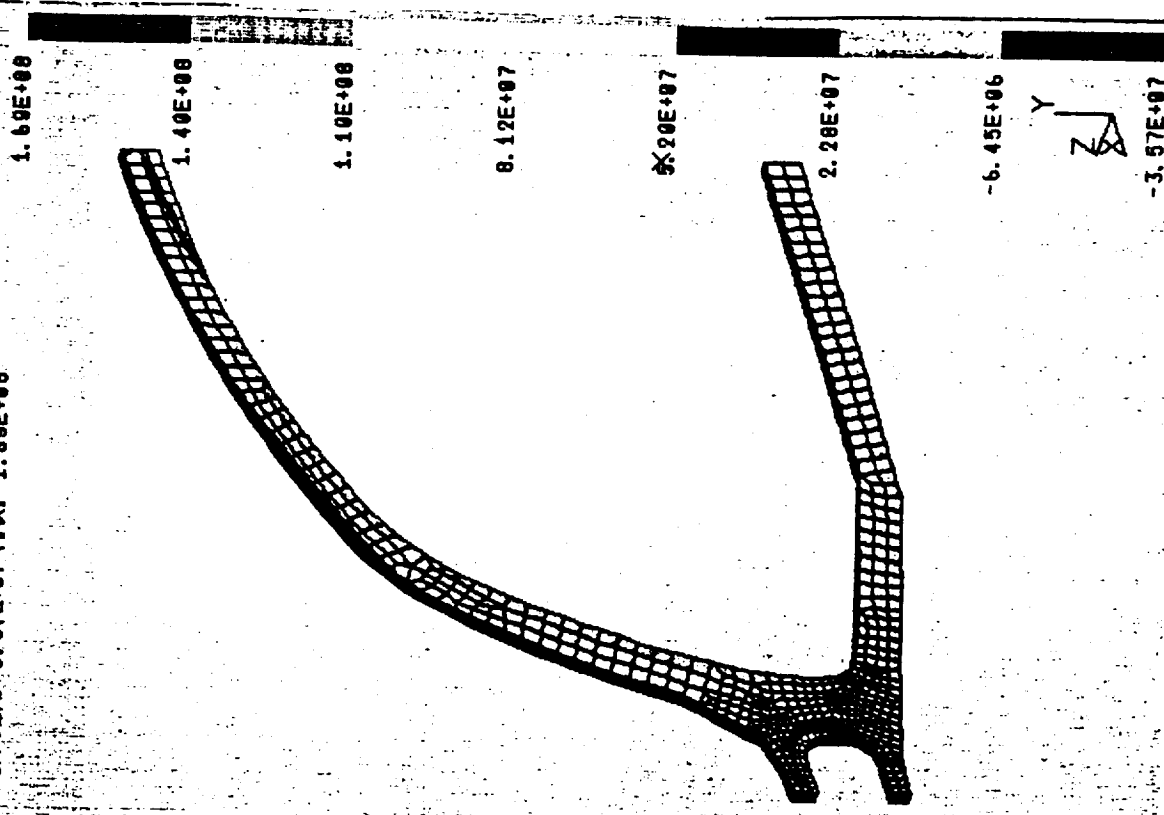
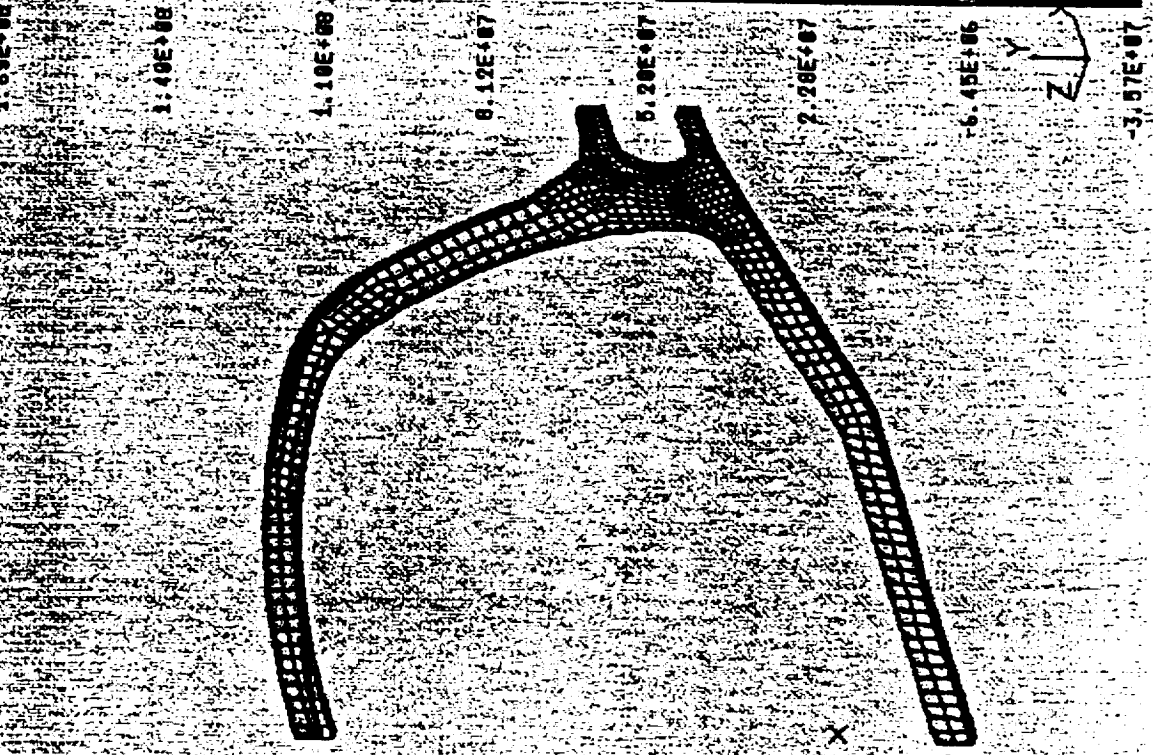
10-MAR-93

15:29:36

Units: SI
Display: none, none
Model Bltn: 1-MAIN
Associated lbrkset: 45-WORKING_SET45

SET: REF. LOAD SET 1
OF: GLOBAL
IS: MAX PRIN MIN: -3.57E+07 MAX: 1.69E+08

femr1b
LOAD SET 1 - LOAD SET 1
FRAME OF REF. PRIN MIN: -3.57E+07 MAX: 1.69E+08



9. Configuration 8

CAEDS V4R2M01 FE Modeling & Analysis

10-MAR-93

16:38:38

base: ferr1b
units: none, none
Task: Post Processing
Model: 1-FERR1B

Display: none, none
Model Bld: 1-MAIN
Associated Workset: 54-WORKING_SET54

SET: 1 - LOAD SET 1

LOAD SET 1 - LOAD SET 1
NODES OF SET: 1000
STRESS - MAX PRIN MIN = 3.70E+07 MAX: 1.44E+08

ferr1b

1.44E+08

1.10E+08

9.25E+07

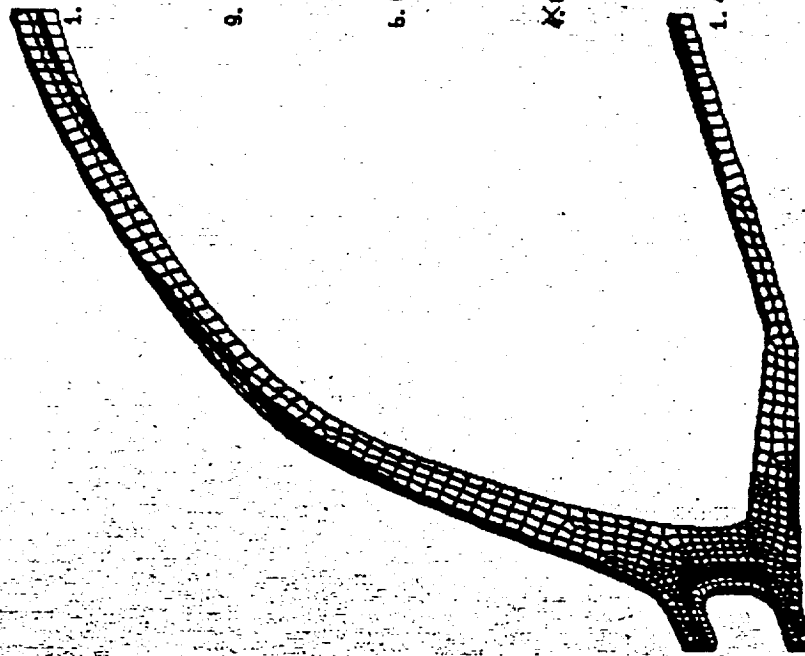
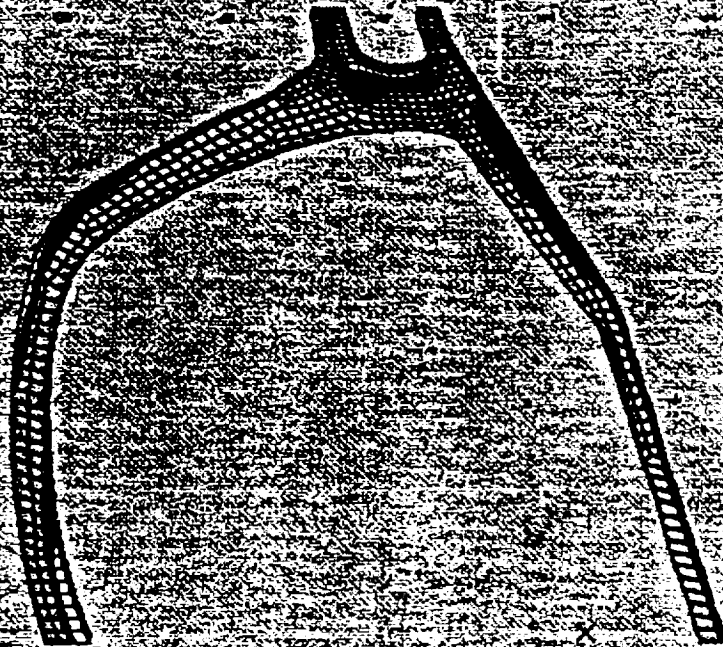
6.66E+07

3.97E+07

1.48E+07

-1.11E+07

-3.70E+07



CAEDS V4R2M0: FE_Modeling_&_Analysis

ase: ferrib

: none, none

Tasks: Post Processing

odel: 13-FBRIB10

11-MAR-93

22:46:05

Units: SI

Display: none, none

Model Bins: 1-TAIN

Associated Wbrkset: 56-WORKING_SET156

ferrib

SET: 1 - LOAD SET 1

OF REF: GLOBAL

55 - MAX PRIN MIN: -3.63E+07 MAX: 1.18E+08

LOAD SET: 1 - LOAD SET 1

FRAME OF REF: GLOBAL

STRESS - MAX: PRIN MIN: -3.63E+07 MAX: 1.18E+08

ferrib

1.18E+08

9.61E+07

7.40E+07

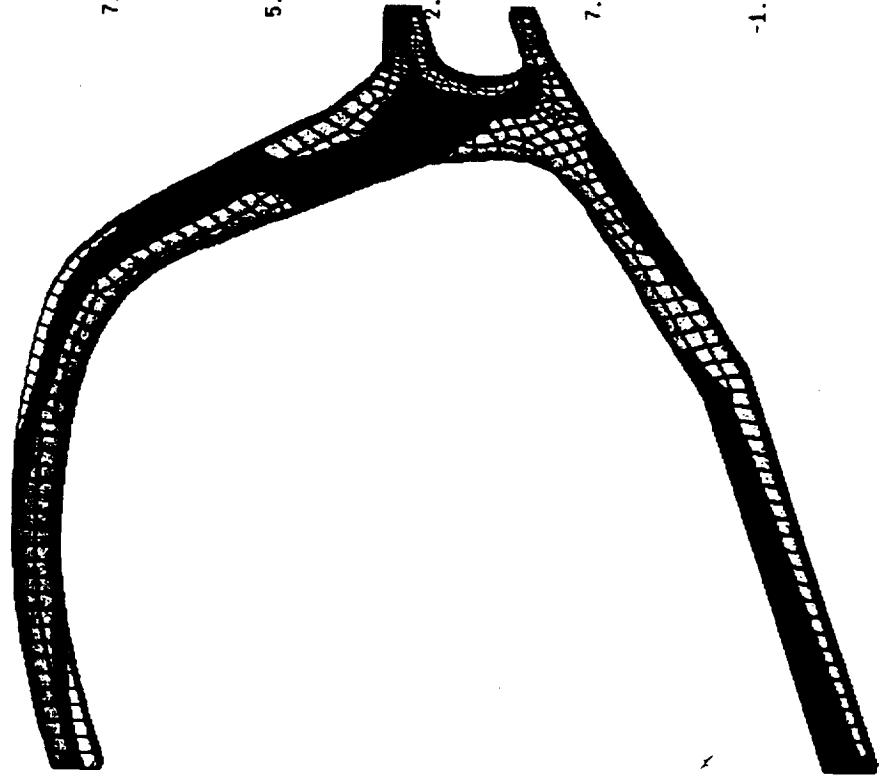
5.19E+07

2.99E+07

7.80E+06

-1.43E+07

-3.63E+07



1.18E+08

9.61E+07

7.40E+07

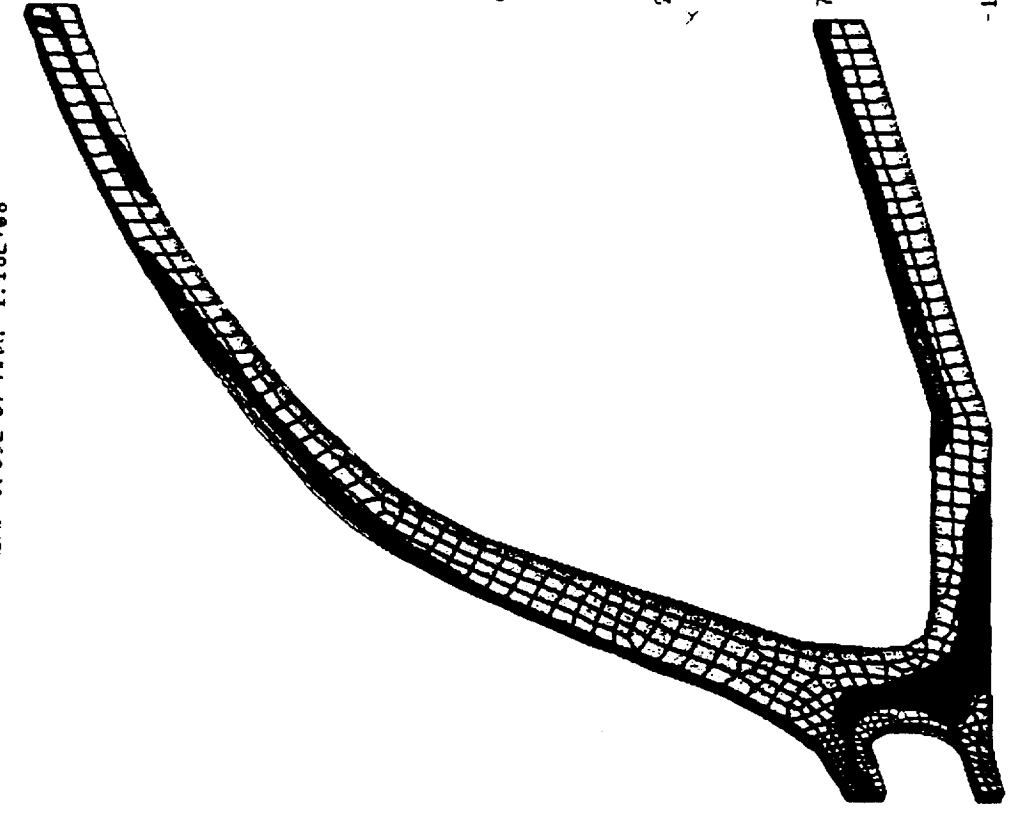
5.19E+07

2.99E+07

7.80E+06

-1.43E+07

-3.63E+07



CAEDS V4R210: FE_Modeling_&_Analysis

11-MAR-93

22:54:11

cases femrib

units none, none

Tasks: Post Processing

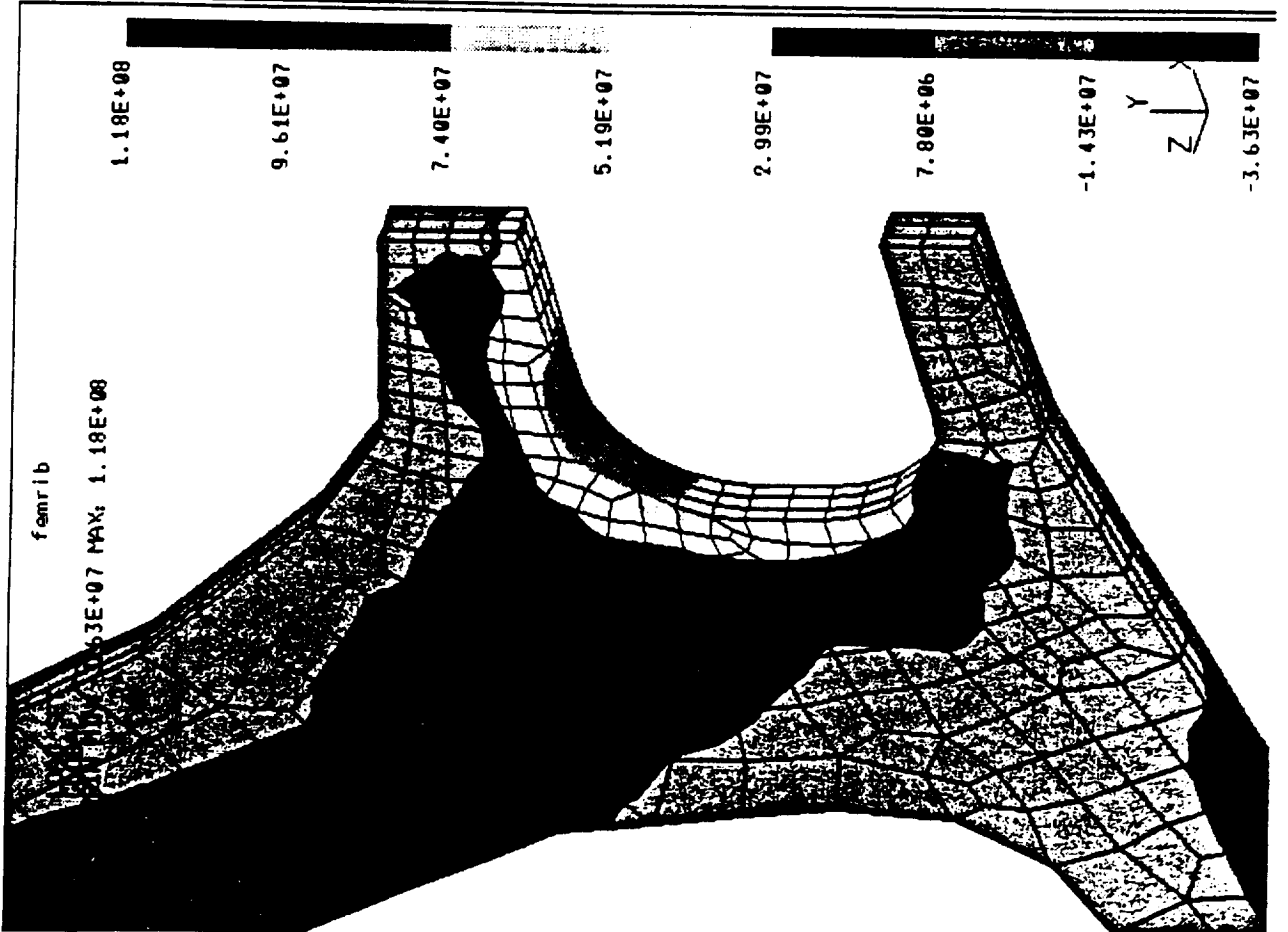
Model: 13-FB-RIB10

Units: SI

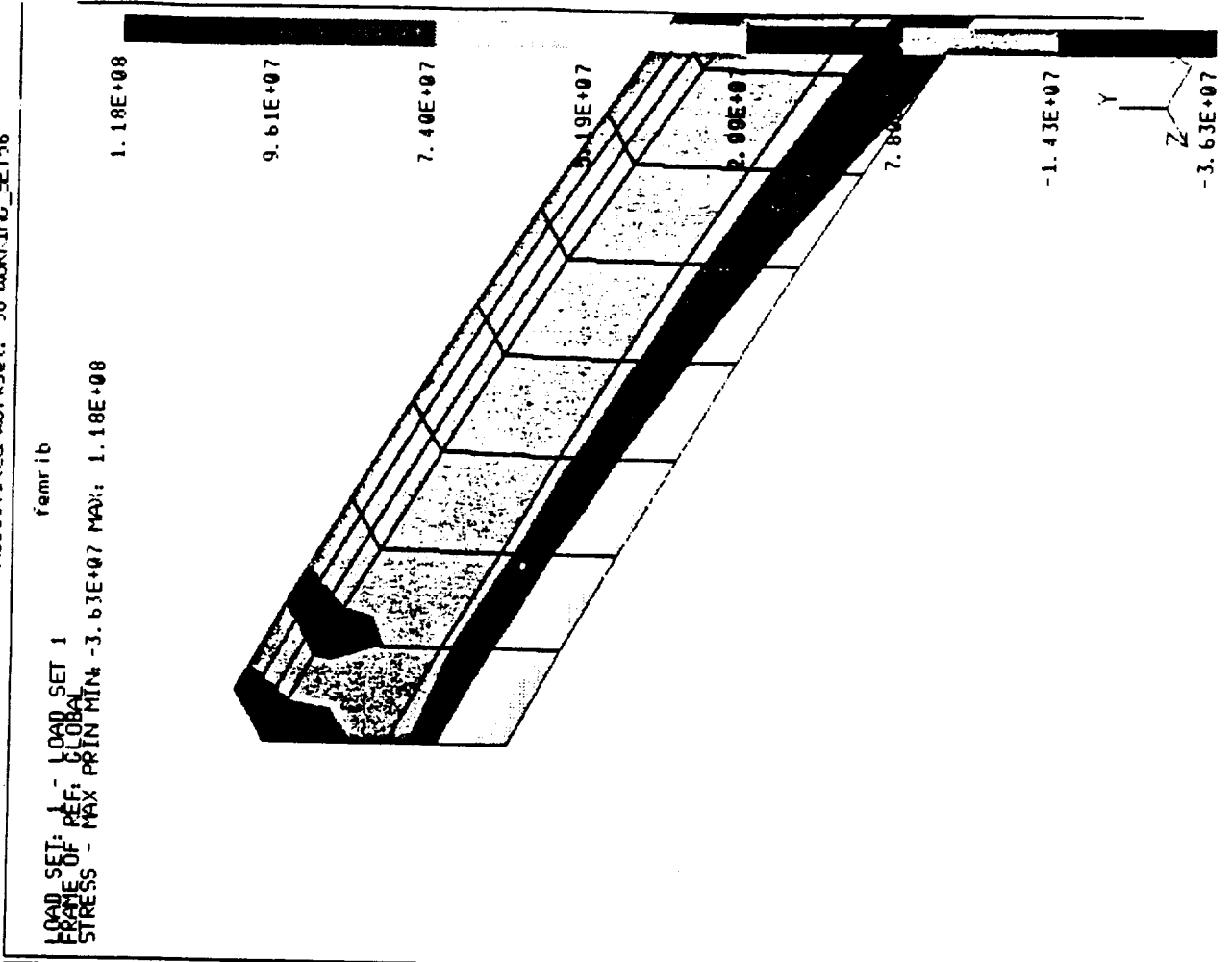
Display: none, none

Model Bire: 1-MAIN

Associated wrkset: 56-WORKING_SET56



11. Configuration 9 (close-up)



Appendix 4: Deflections

1. Configuration 1 (half)
- 1A. Configuration 1 (whole)
2. Configuration 2
3. Configuration 3
4. Configuration 4A
5. Configuration 4B
6. Configuration 5
7. Configuration 6
8. Configuration 7
9. Configuration 8
10. Configuration 9
11. Configuration 9 (close-up)

CAEDS V4R2M0: FE_Modeling_6_Analysis

08-MAR-93

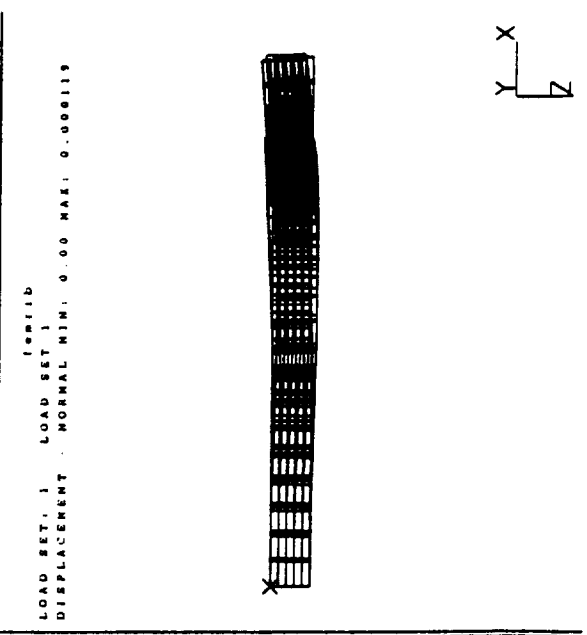
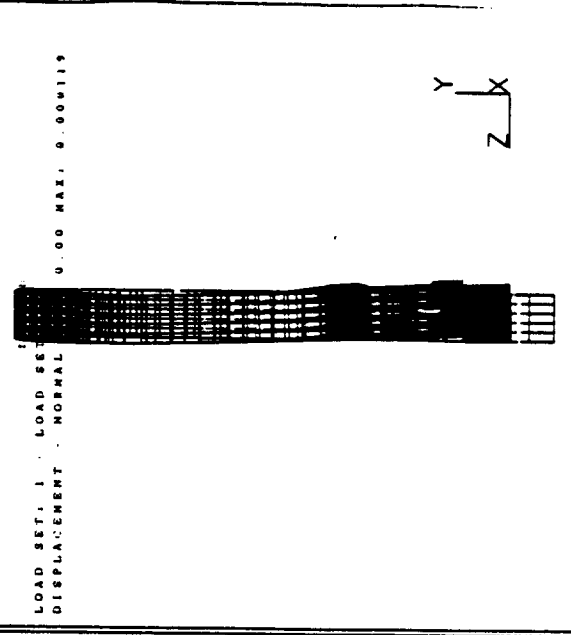
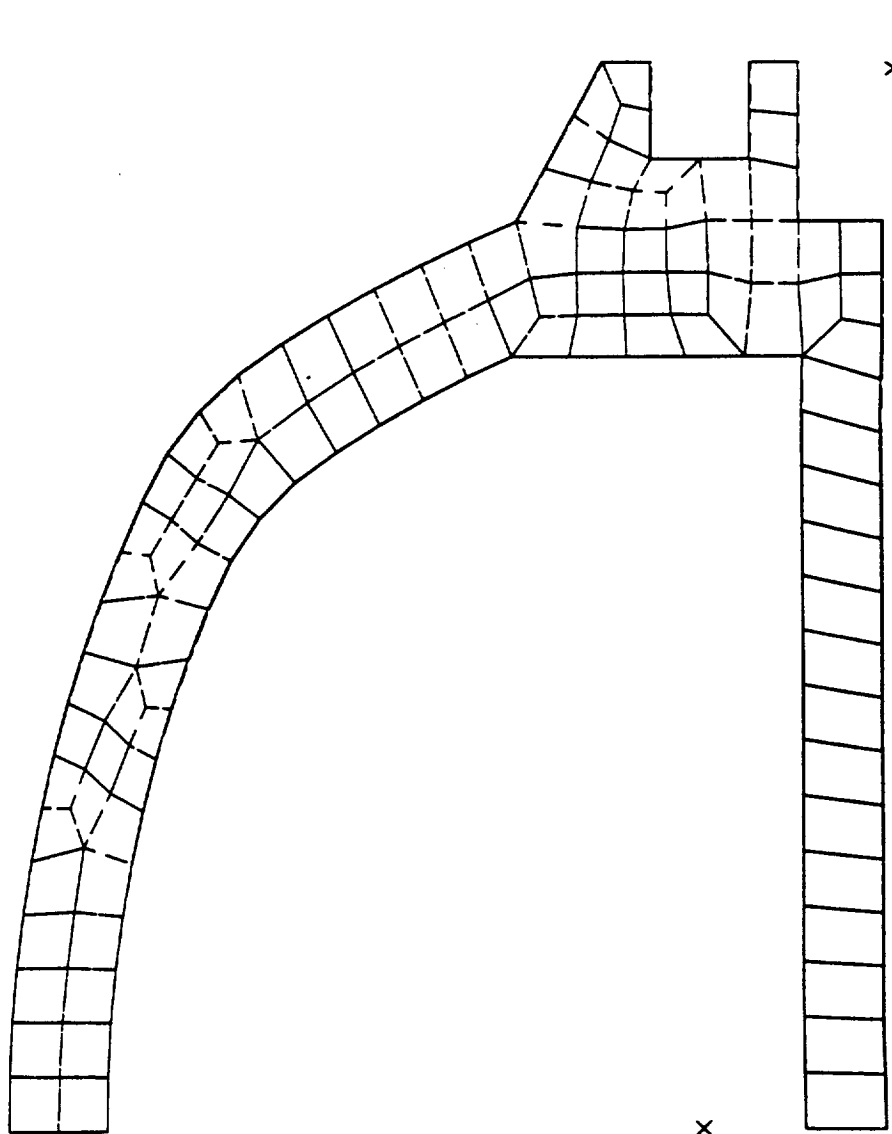
21:29:54

Database: fmr1b
View: none, none, none
Task: Post Processing
Model: 3: FMR1B1

Display: none, none, none
Units: SI
Model Bin: 1: MAIN
Associated Model Sets: 3: WORKING_SET1

fmr1b
LOAD SET: 1 - LOAD SET 1
DISPLACEMENT - NORMAL MIN: 0.00 MAX: 0.000119

fmr1b
LOAD SET: 1 - LOAD SET 1
DISPLACEMENT - NORMAL
0.00 MAX: 0.000119



CAEDS VAR2ND: FE_Modeling_&_Analysis

08-MAR-93

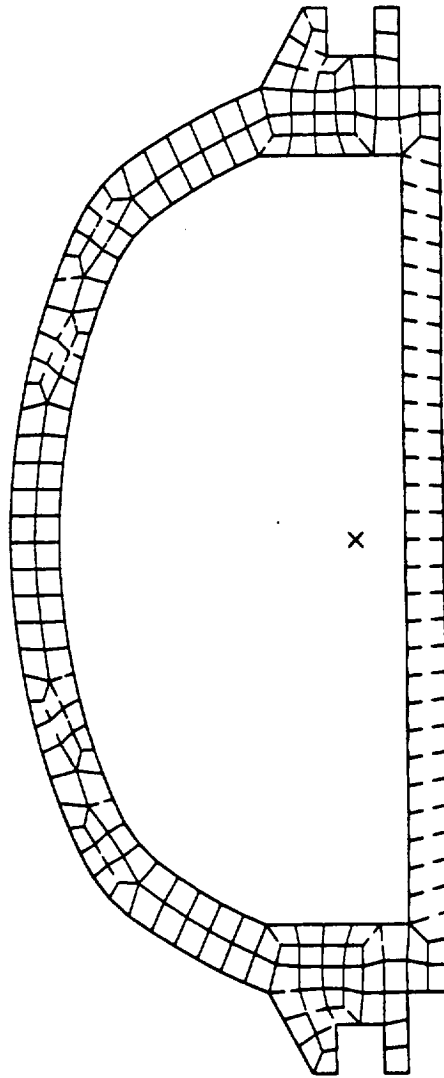
21:32:22

Database: femrib
/view : none, none, none
Task: Post Processing
Model: 2.MOUL

Display : none, none, none
Model Size: 1 MAIN
Associated Workset: 4 WORKIP_3FTE
Units : SI

femrib
LOAD SET: 1 - LOAD SET 1
DISPLACEMENT - NORMAL MIN: 0.00 MAX: 0.000119

femrib
LOAD SET: 1 - LOAD SET 1
DISPLACEMENT - NORMAL
0.00 MAX: 0.000119



femrib
LOAD SET: 1 - LOAD SET 1
DISPLACEMENT - NORMAL MIN: 0.00 MAX: 0.000119



2. Configuration 2

CAEDS V4R2M0: FE_Modeling_6_Analysis

08-MAR-93

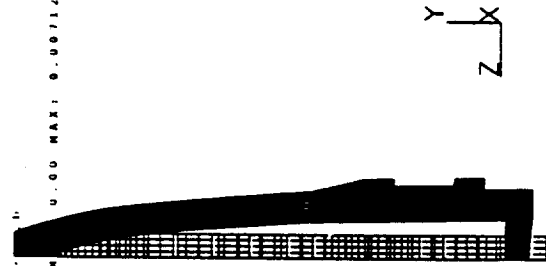
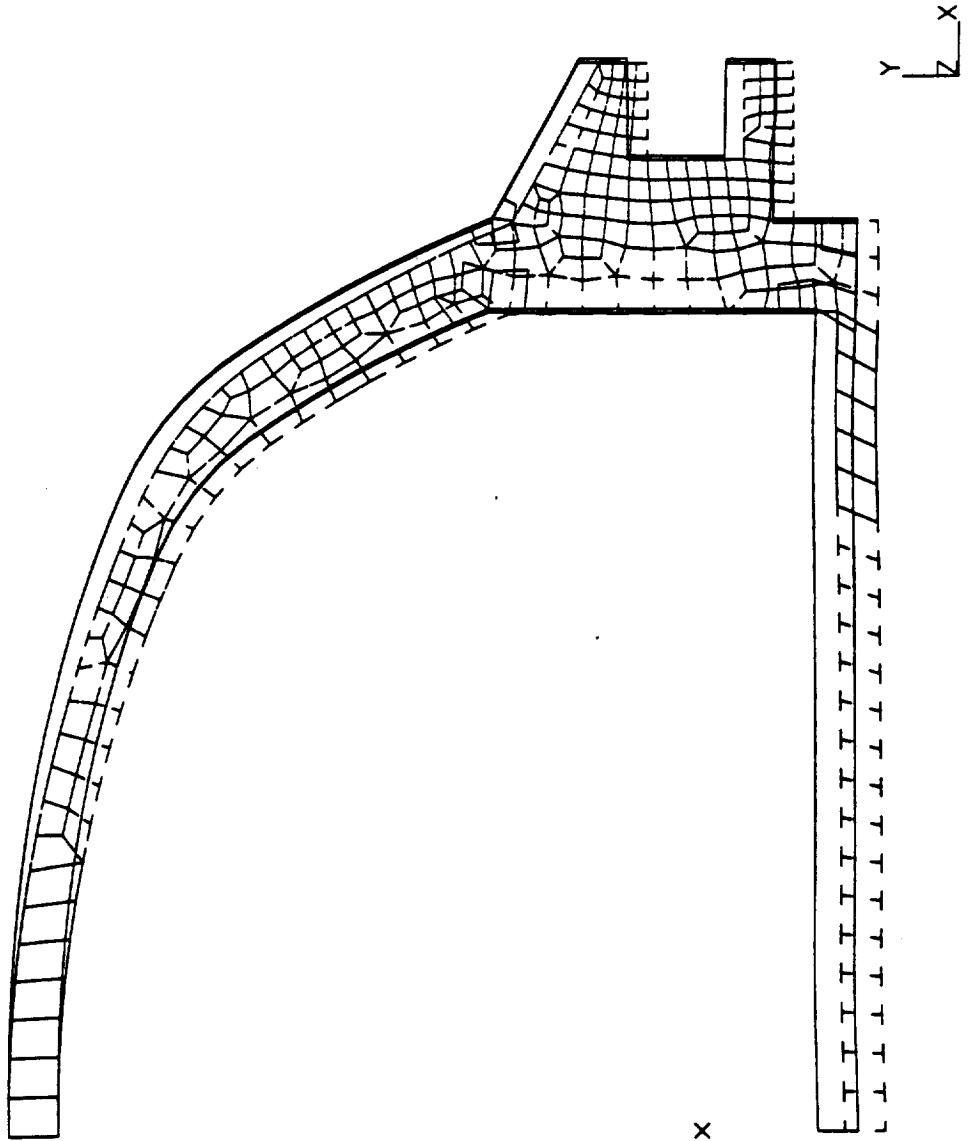
21:34:24

Database: femrib
View: none, none, none
Task: Post Processing
Model: 7-FEMRIB

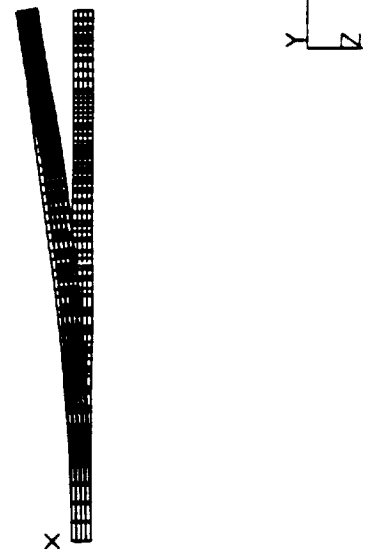
Units: SI
Display: none, none, none
Model Min: 1 MAIN
Associated Models: 9 MWEING_SET*

femrib
LOAD SET: 1 LOAD SET 1
DISPLACEMENT - NORMAL MIN: 0.00 MAX: 0.007129

femrib
LOAD SET: 1 LOAD SET 1
DISPLACEMENT - NORMAL MIN: 0.00 MAX: 0.007129



femrib
LOAD SET: 1 LOAD SET 1
DISPLACEMENT - NORMAL MIN: 0.00 MAX: 0.007129



3. Configuration 3

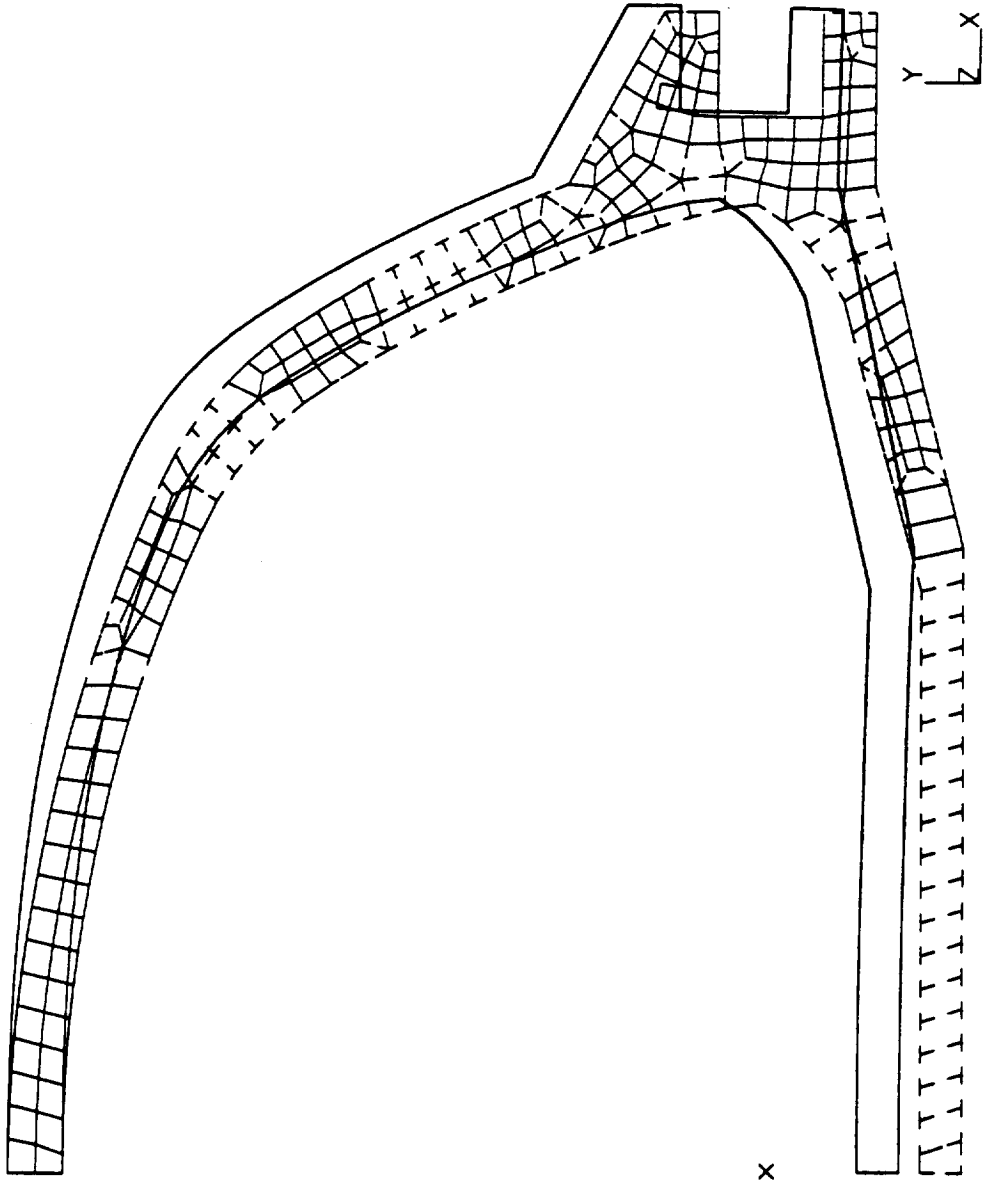
CAEDS V4R2H0: FE_Modeling_6_Analysis

08-MAR-93 17:28:24

Meshes: femr1b
/view : none, none, none
Task: Post Processing
Model: 9 FEMR1B

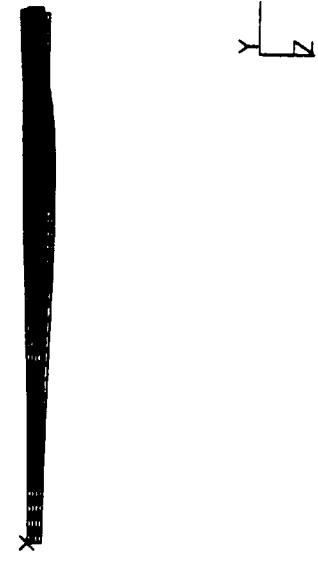
Display : none, none, none
Model Bin: 1-MAIN
Associated Meshes: 1: WORKING_SET15

femr1b
LOAD SET: 1 - LOAD SET 1
DISPLACEMENT - NORMAL MIN: 0.00 MAX: 0.004712



femr1b
LOAD SET: 1 - LOAD SET 1
DISPLACEMENT - NORMAL MIN: 0.00 MAX: 0.004712

femr1b
LOAD SET: 1 - LOAD SET 1
DISPLACEMENT - NORMAL MIN: 0.00 MAX: 0.004712



4. Configuration 4A

08-MAR-93 17:24:04

CARDS V4R2M0: FE_Modeling_&_Analysis

Database: fecrib

View: none, none, none

Task: Post Processing

Model: 10-FEM185

Units: SI

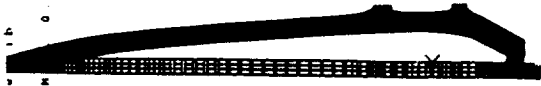
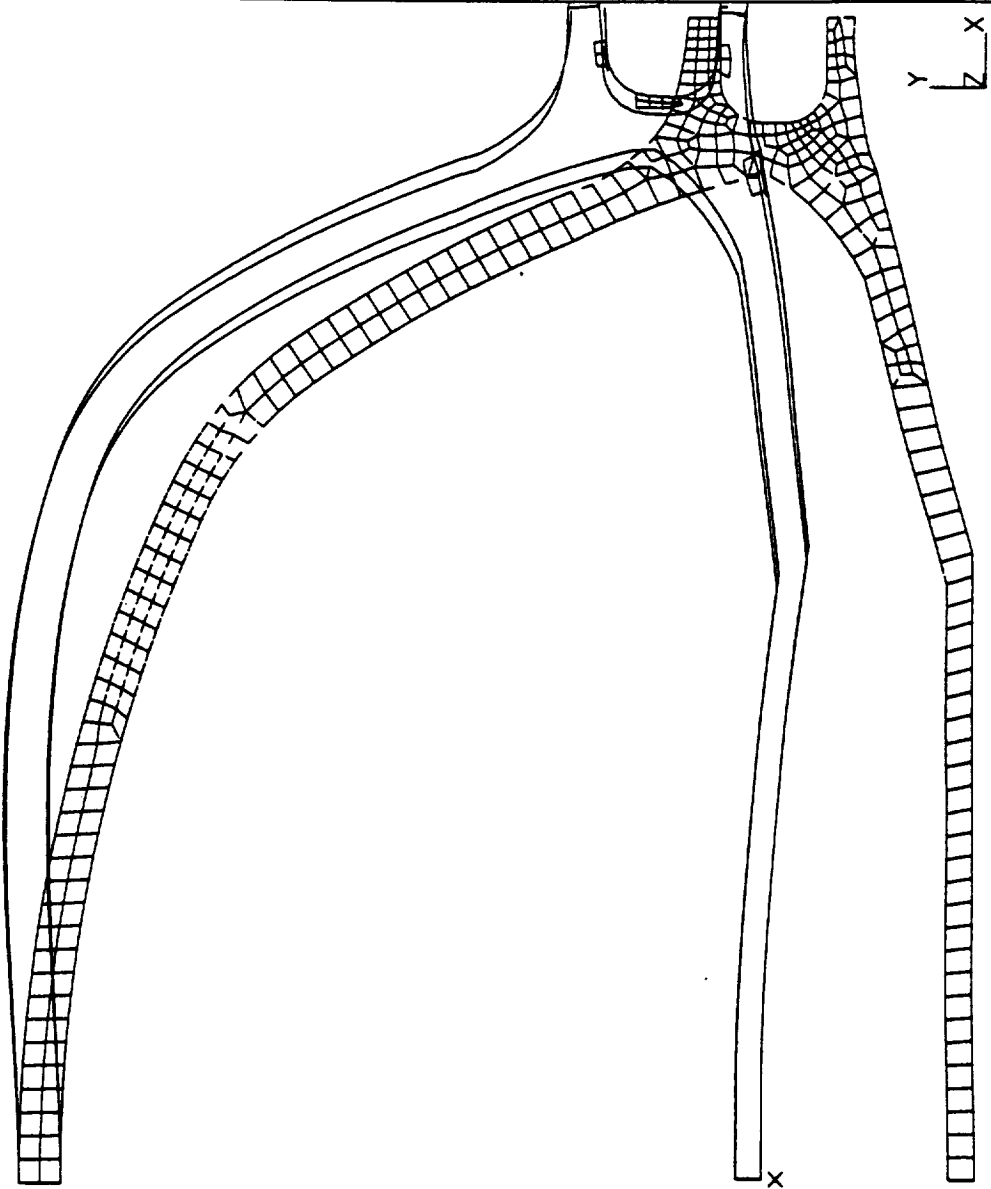
Display: none, none, none

Model: Bin: 1 MAIN

Associated Model: 20 MAPPING_SET28

fecrib
LOAD SET: 1 - LOAD SET 1
DISPLACEMENT: NORMAL MIN: 0.00 MAX: 0.045170

fecrib
LOAD SET: 1 - LOAD SET 1
DISPLACEMENT: NORMAL MIN: 0.00 MAX: 0.045170



fecrib
LOAD SET: 1 - LOAD SET 1
DISPLACEMENT: NORMAL MIN: 0.00 MAX: 0.045170



5. Configuration 4B

08-MAR-93 17:26:30

CAEDS V4R2M0: FE_Modeling_4_Analysis

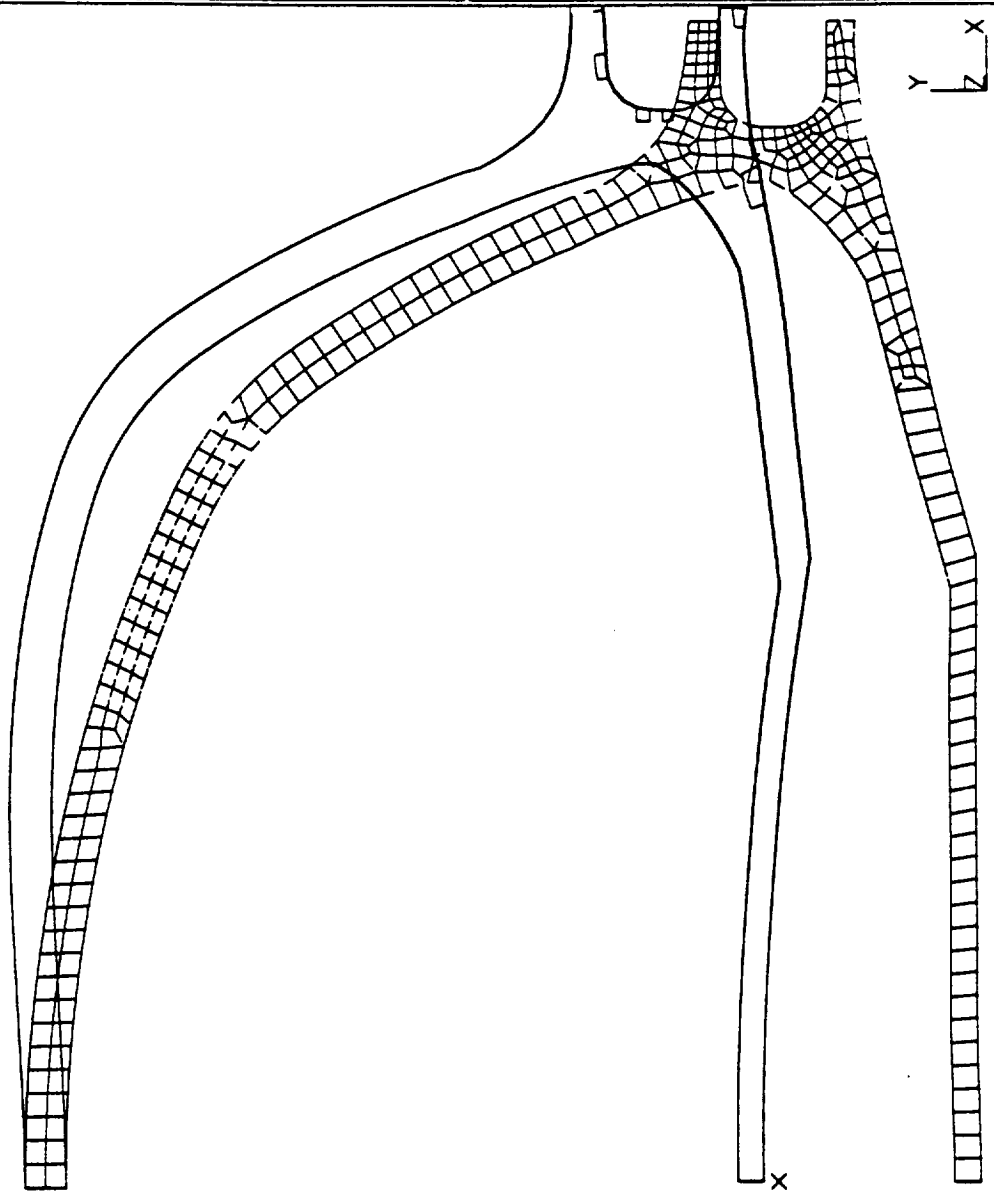
Database: fcarib
View: none, none, none
Task: Post Processing
Model: 10 FEMRIB5

Display: none, none, none
Model Bin: 1 MAIN
Associated Worksets: 28 MARKING_SET28

Units: SI

fcarib
LOAD SET: 1 - LOAD SET 1
DISPLACEMENT . NORMAL MIN: 0.00 MAX: 0.016062

fcarib
LOAD SET: 1 - LOAD SET 1
DISPLACEMENT . NORMAL MIN: 0.00 MAX: 0.016062



fcarib
LOAD SET: 1 - LOAD SET 1
DISPLACEMENT . NORMAL MIN: 0.00 MAX: 0.016062



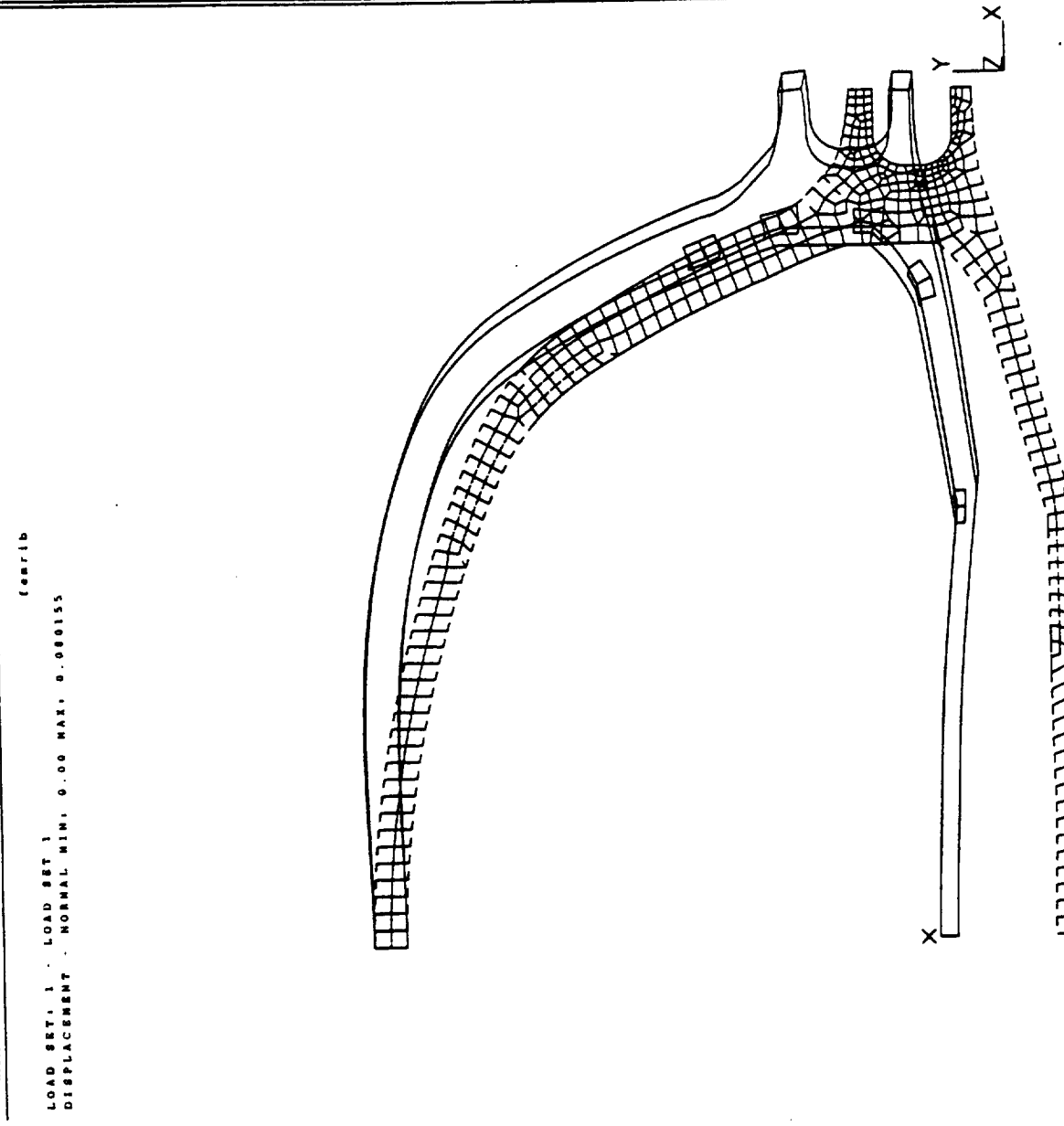
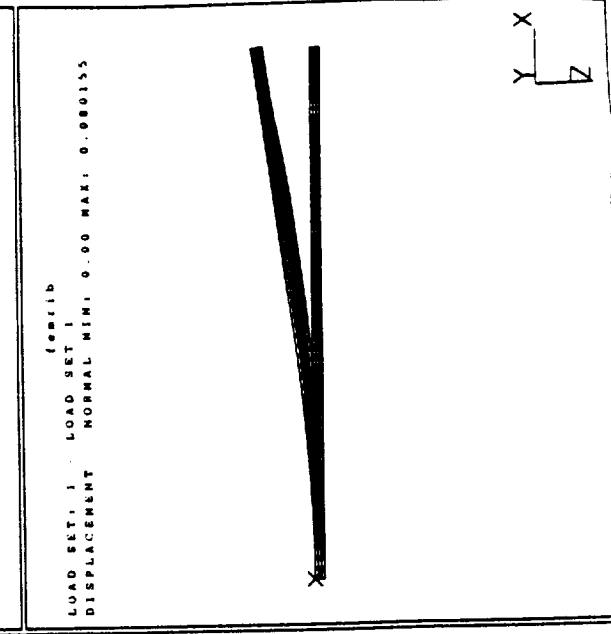
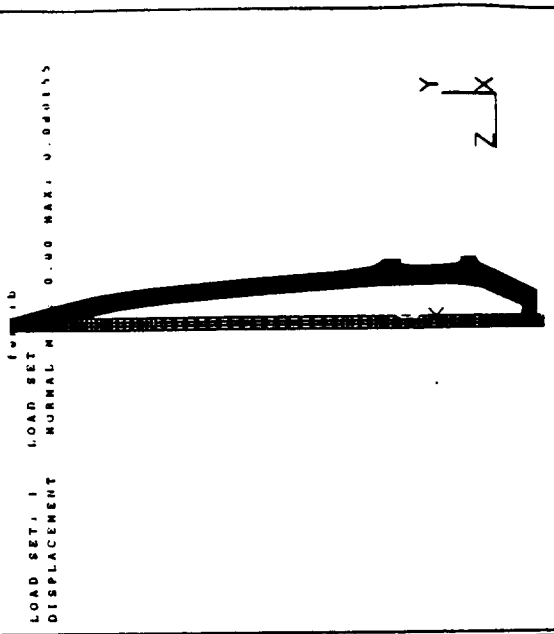
08-MAR-93 17:19:52

CAEDS VAR2M0: FE_Modeling_&Analysis

Units : SI

Jobname: fcarib
/view : none, none, none
Task: Post Processing
Model: 12-fcarib6

Display : none, none, none
Model Min: 1 MAIN
Associated Meshes: 35-MESH16.SET15



7. Configuration 6

08-MAR-93 17:14:56

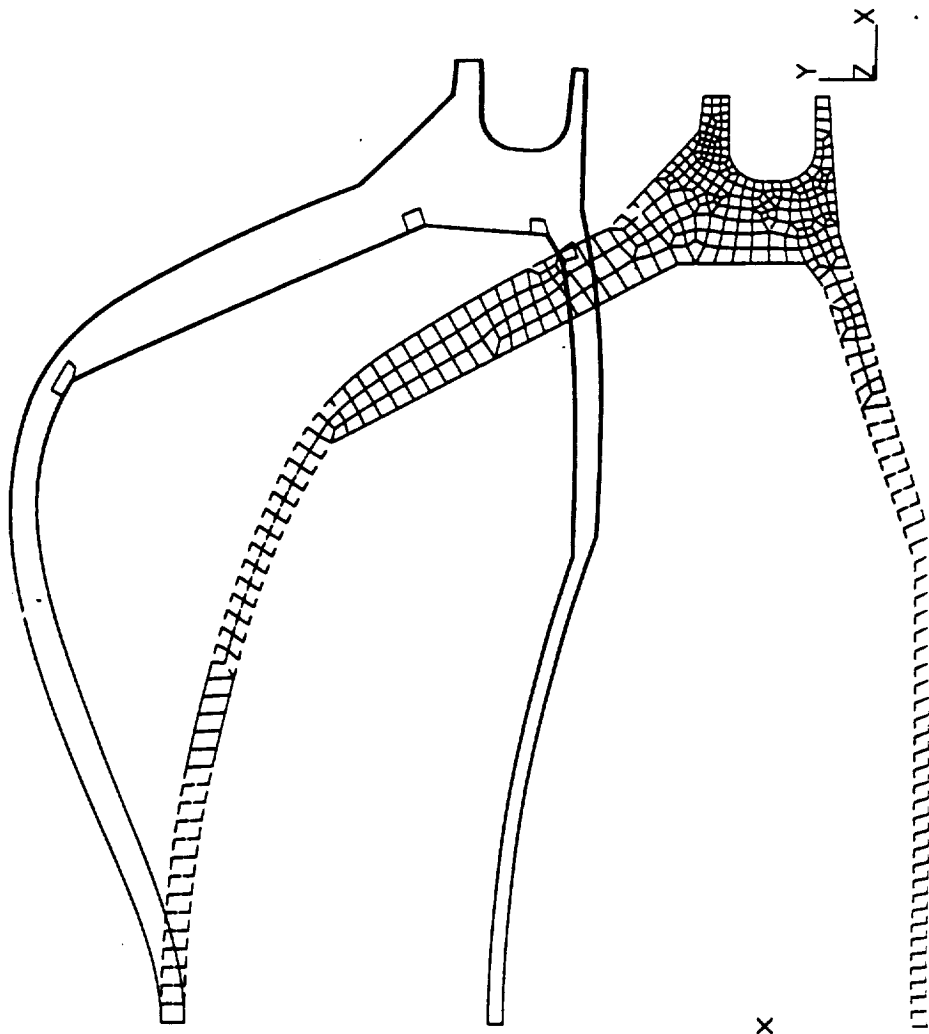
CAEDS VAR2H0: FE_Modeling_6_Analysis

Database: feorib
View: none, none, none
Task: Post Processing
Model: 4 FEORIB7

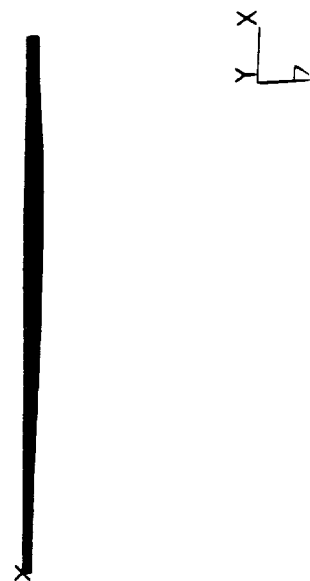
Display: none, none, none
Model Size: 1 MBIN
Associated Worksheet: 42: MORNING_DET42

feorib
LOAD SET: 1 - LOAD SET 1
DISPLACEMENT - NORMAL MIN: 0.00 MAX: 0.039991

feorib
LOAD SET: 1 - LOAD SET 1
DISPLACEMENT - NORMAL MIN: 0.00 MAX: 0.039991



feorib
LOAD SET: 1 - LOAD SET 1
DISPLACEMENT - NORMAL MIN: 0.00 MAX: 0.039991



ORIGINAL FILE IN
OF POOR QUALITY

8. Configuration 7

08-MAR-93

17:10:18

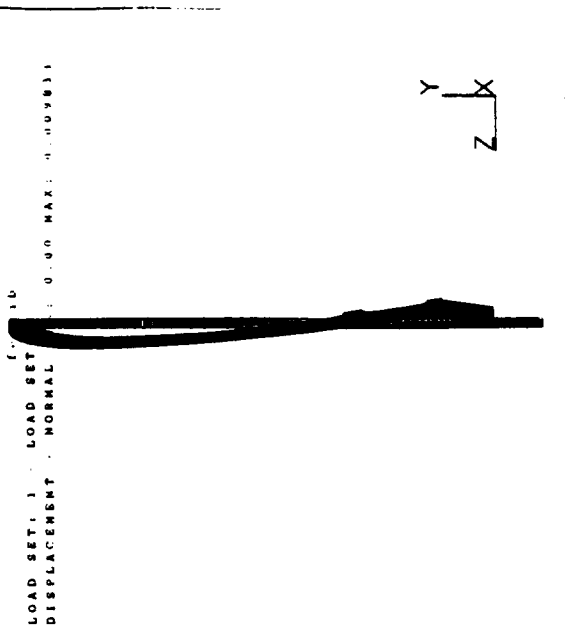
Units: 1.51
Display: none, none, none
Model Bin: 1 MAIN
Associated Worksheet: 45 WORKING_SETS

CAEDS VAR240: FE_Modeling_6_Analysis

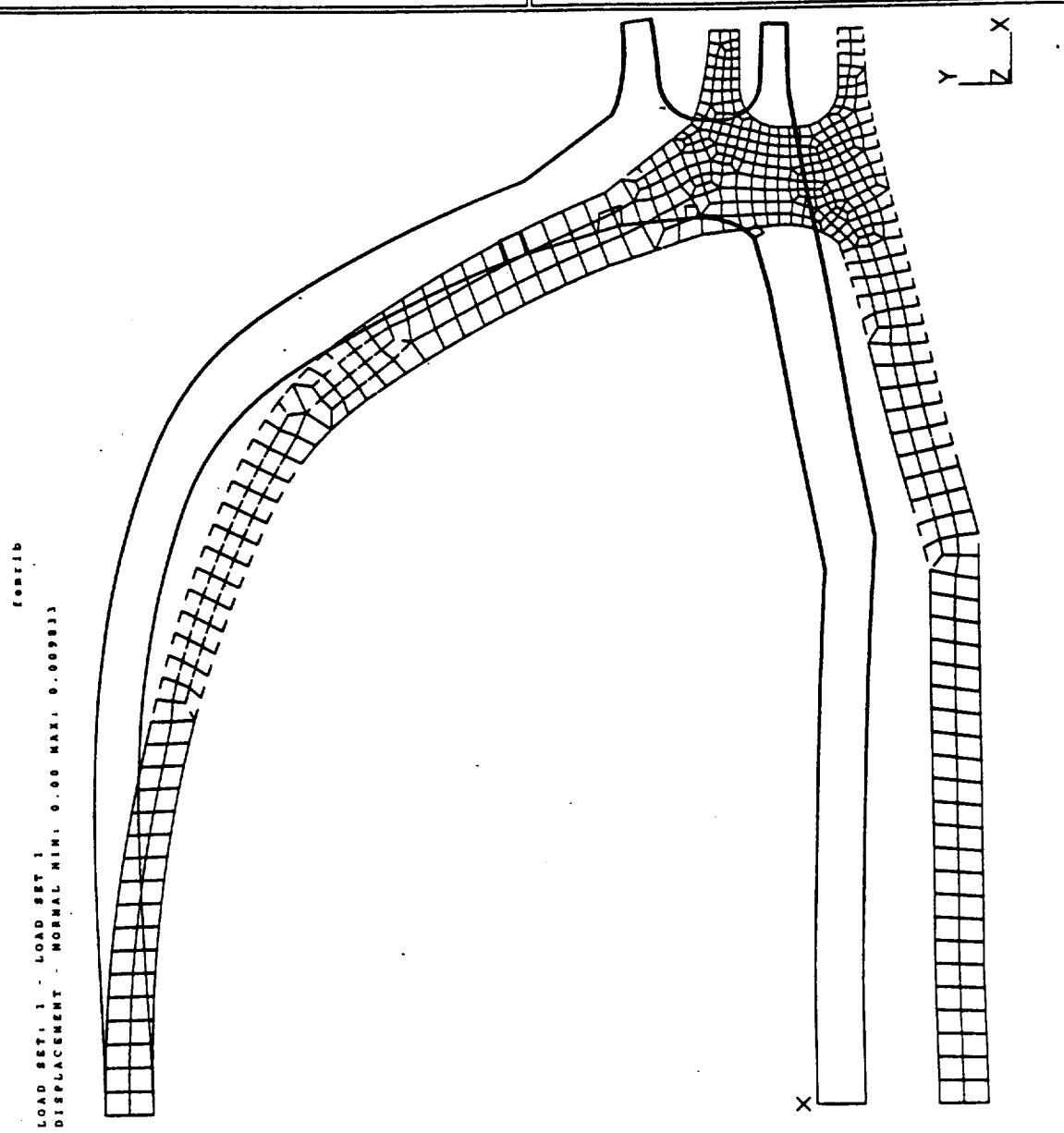
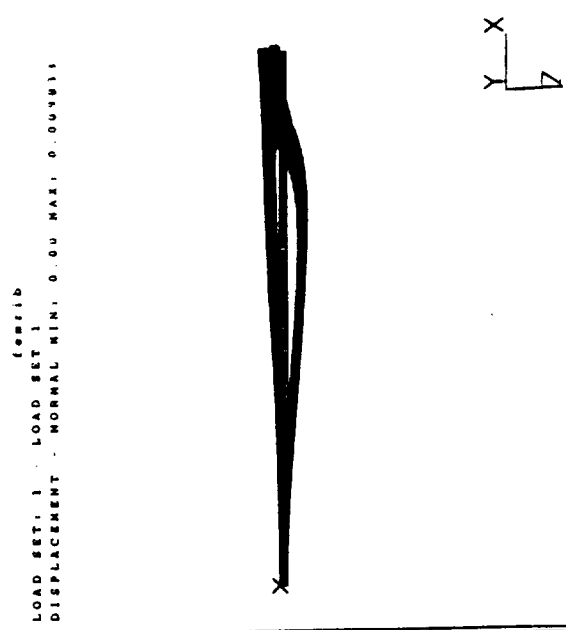
Jobbase: feobj
/view none, none, none
Task: Post Processing
Model: 6-FEMR188

[feobj]
LOAD SET: 1 - LOAD SET 1
DISPLACEMENT - NORMAL MIN: 0.00 MAX: 0.009833

[feobj]
LOAD SET: 1 - LOAD SET 1
DISPLACEMENT - NORMAL MIN: 0.00 MAX: 0.009833



[feobj]
LOAD SET: 1 - LOAD SET 1
DISPLACEMENT - NORMAL MIN: 0.00 MAX: 0.009833



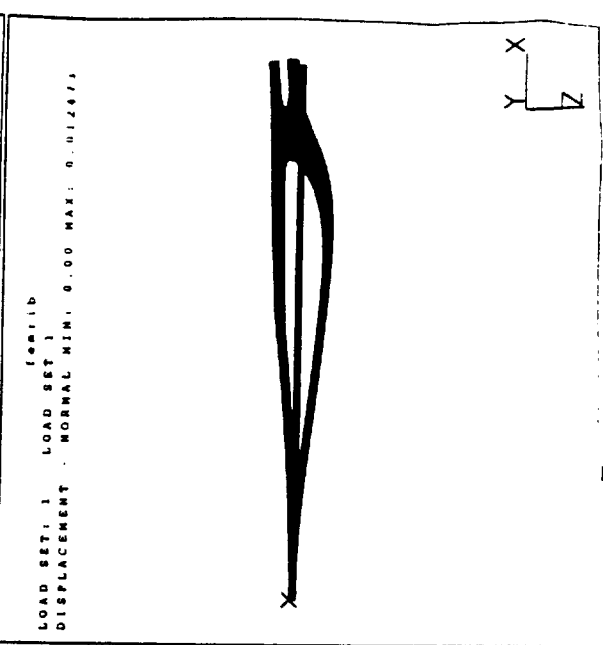
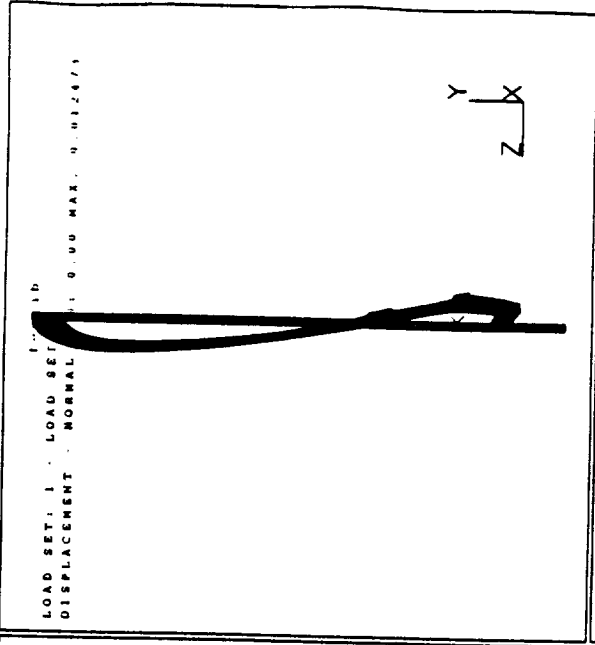
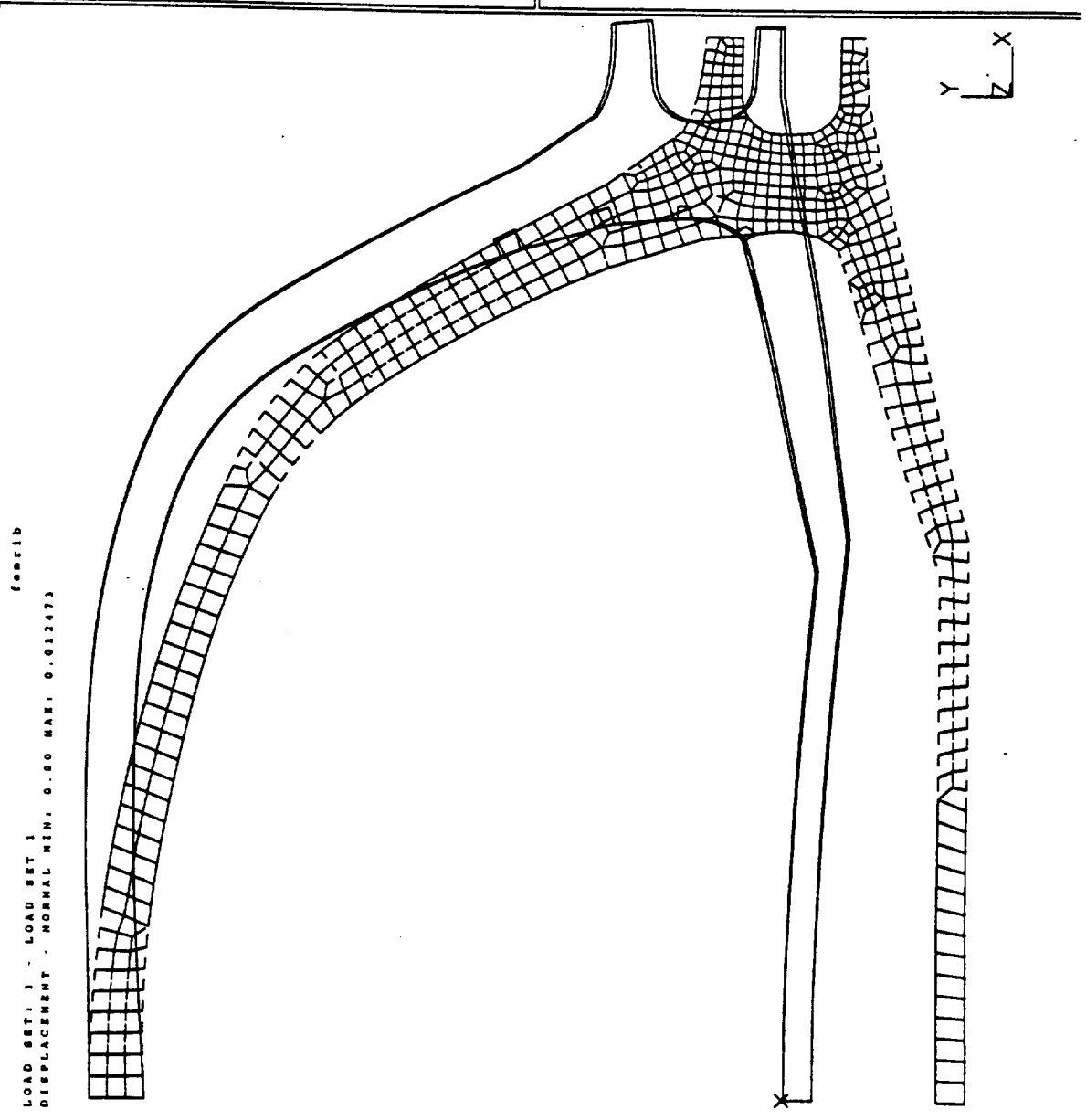
9. Configuration 8

CAEDS VAR2M0: FE_Modeling_&Analysis

08-MAR-93 17:07:30

!database: fearib
/new i none, none, none
Task: Post Processing
Model: 1-FEMIB9

Display: 1 none, none, none
Model Bin: 1 MAIN
Associated Worksheet: 54 WORKBKS_SETS4



10. Configuration 9

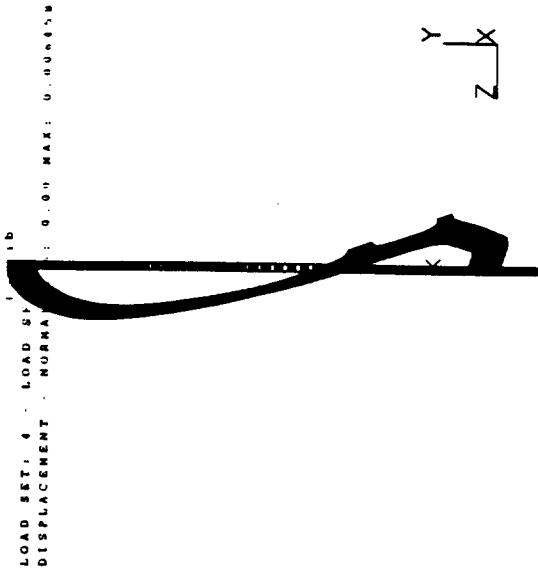
CAEDS V4R2M0: FE_Modeling_&_Analysis

08-MAR-93 17:02:58

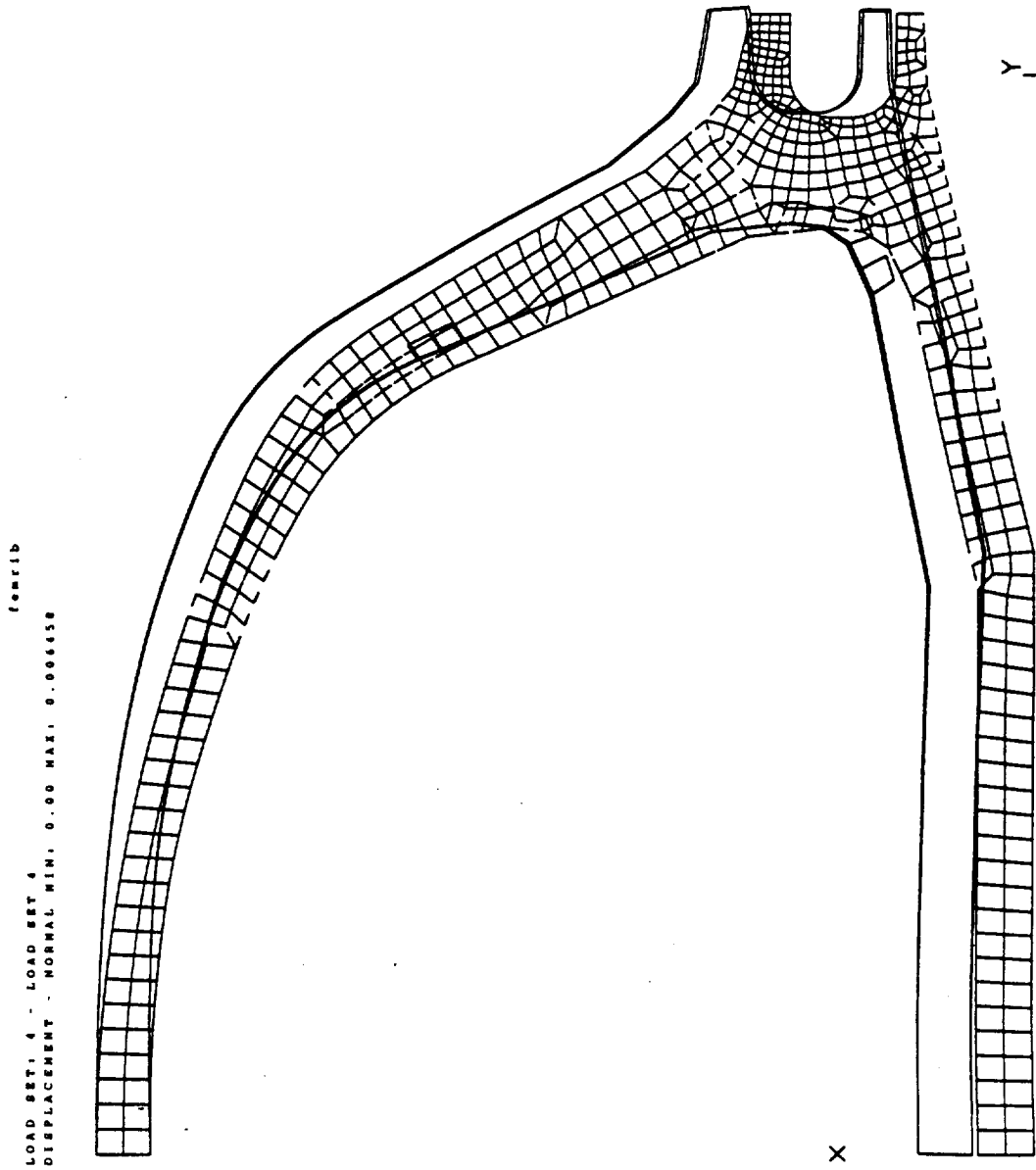
Database: femrib
View : none, none, none
Task: Post Processing
Model: 13-FEMRIB10

Display : trim, inner, none
Units : SI
Model Min: 1 MAX: 1
Associated Workset: % WORKING.SET's

femrib
LOAD SET: 4 - LOAD SET 4
DISPLACEMENT - NORMAL MIN: 0.00 MAX: 0.006658



femrib
LOAD SET: 4 - LOAD SET 4
DISPLACEMENT - NORMAL MIN: 0.00 MAX: 0.006658

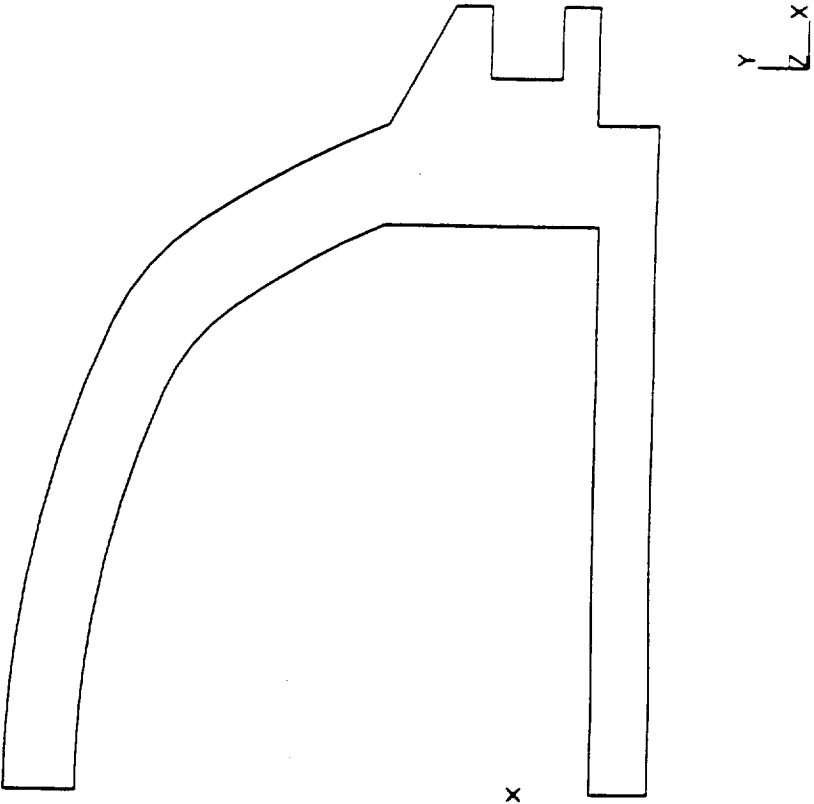


APPENDIX 5: Engineering Analysis of Fuselage Wing Bulkhead

1. Figure 1: Initial bulkhead configuration and weight
2. Figure 2: Bulkhead configurations and weights for 2-5
3. Figure 3: Bulkhead configurations and weights for 3-5
4. Figure 4: Final bulkhead configuration and weight
5. Figure 5: Fuselage and wing bulkhead connection
6. Figure 6: Loads on wing clamp
7. Figure 7: Restraints on fuselage wing bulkhead

Figure 1 : Initial Bulkhead Configuration and Weight

1700 lb



3400 lb

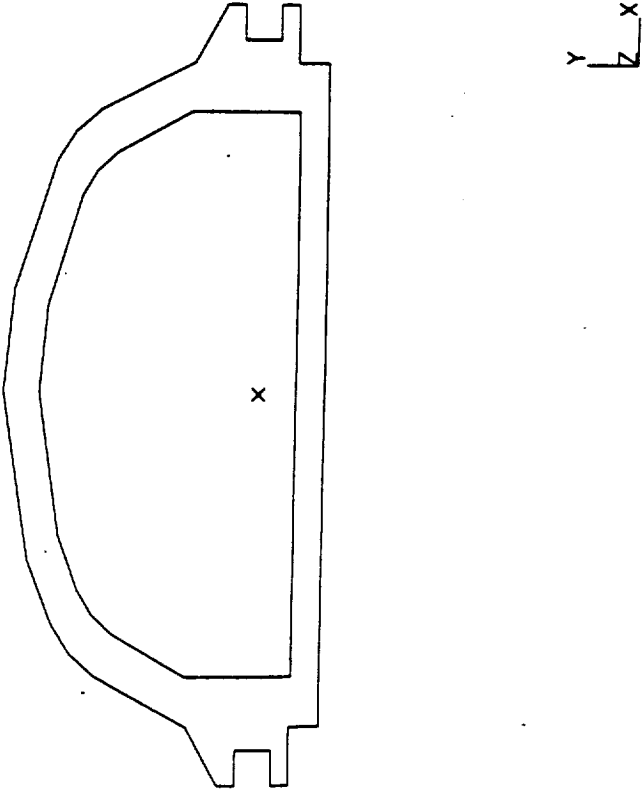


Figure 2 : Bulkhead Configurations and Weights for 2-5

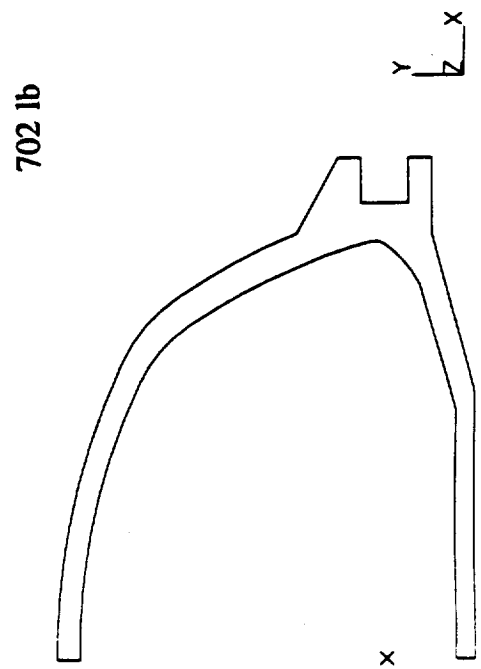
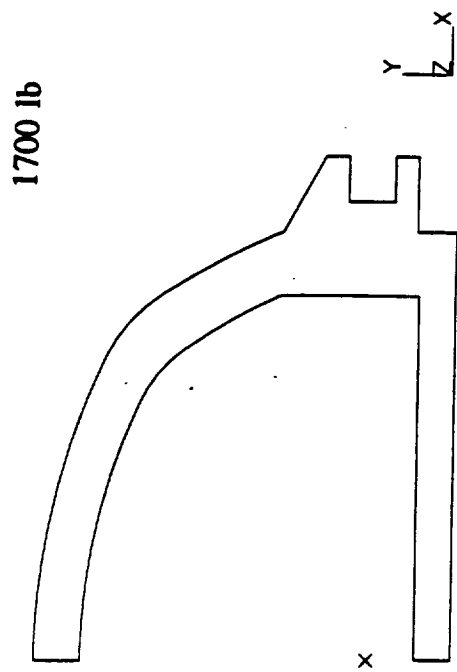
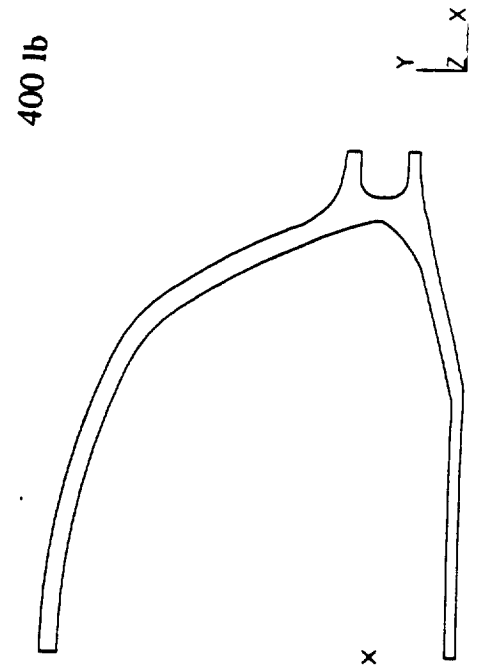
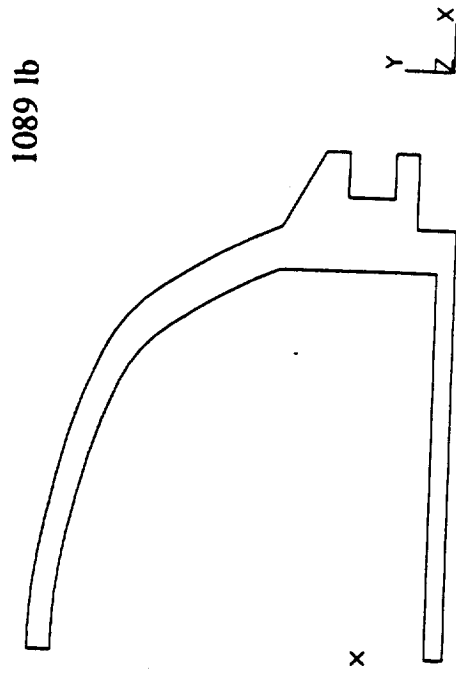


Figure 3 : Bulkhead Configurations and Weights for 5-9

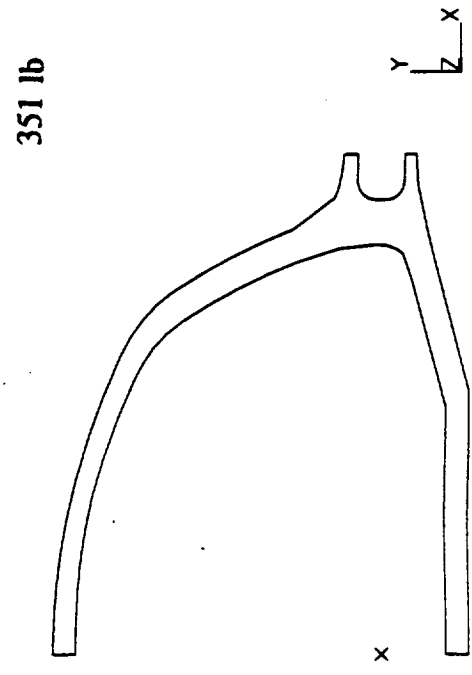
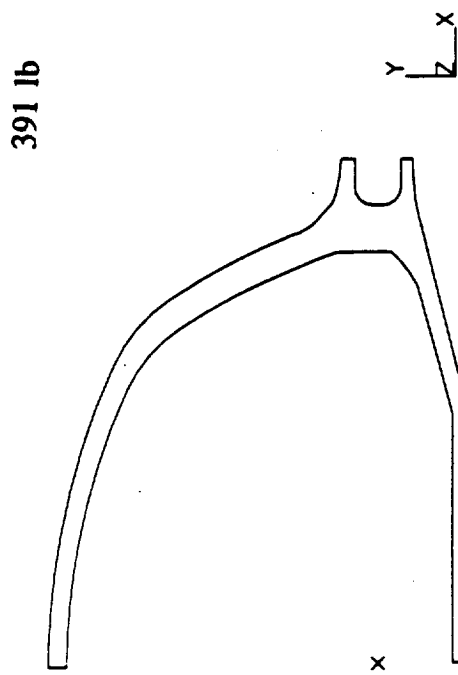
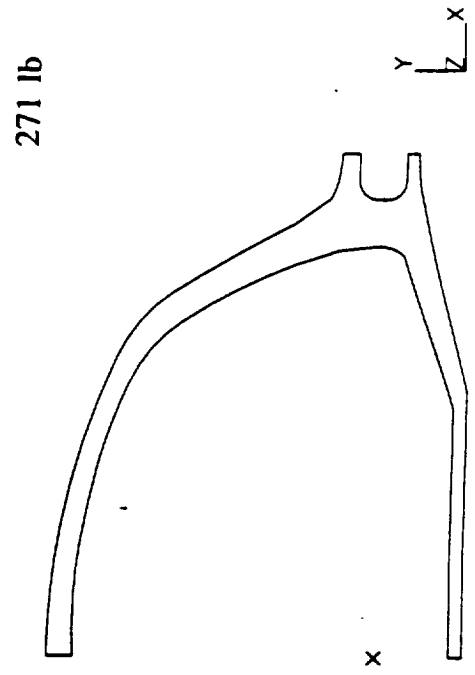
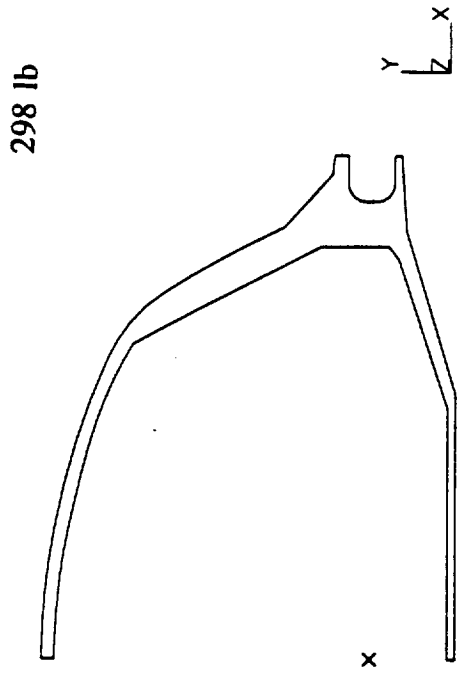


Figure 4 : Final Bulkhead Configuration and Weight

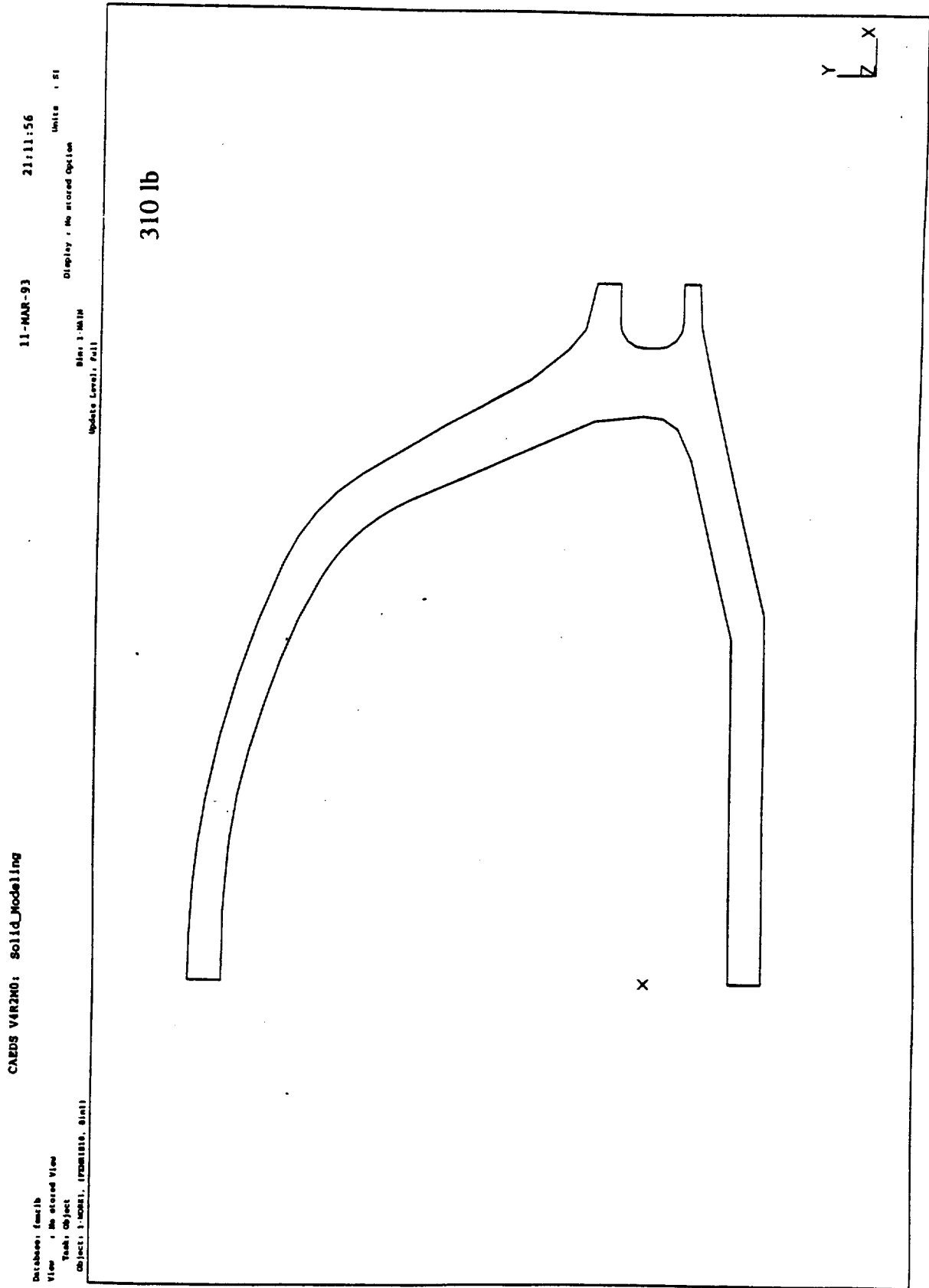


Figure 5 : Fuselage and Wing Bulkhead Connection

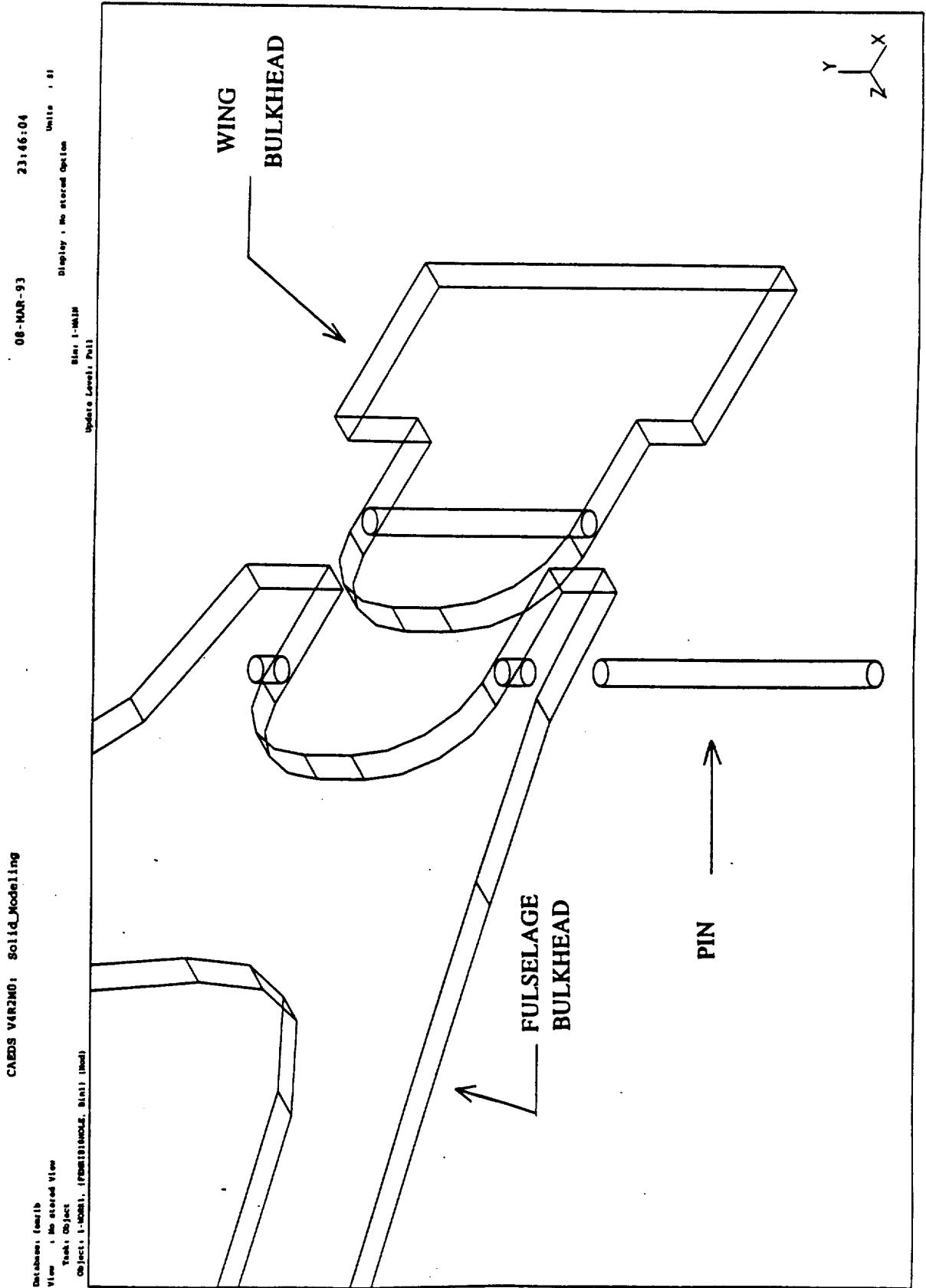
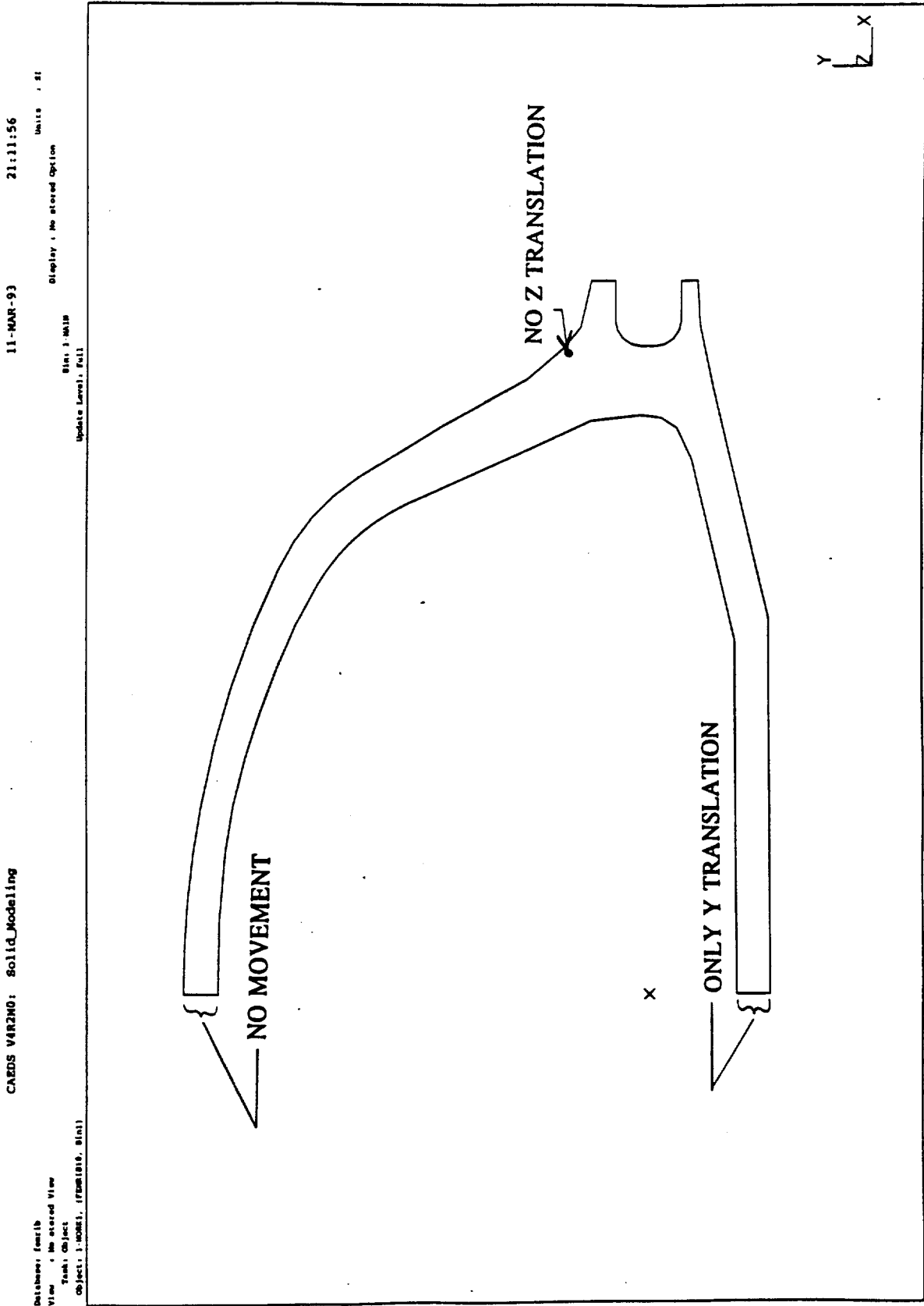


Figure 7: Restraints on Fuselage Wing Bulkhead



Appendix 6: Force Calculations

Lift, Drag, and Moment Determination

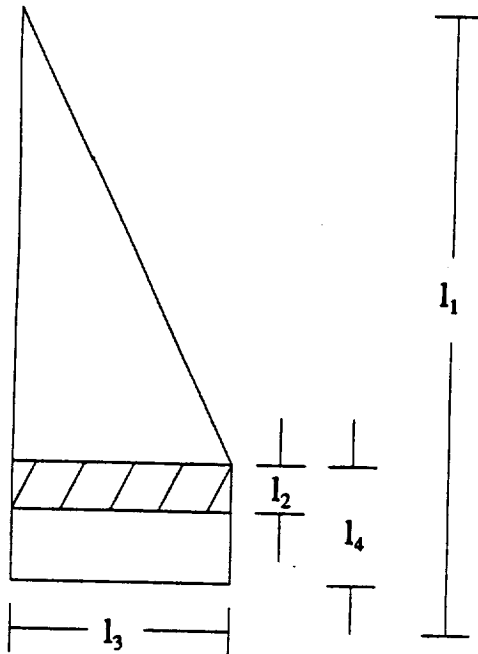
The lift over a wing is not evenly distributed, and it was hoped that the actual lift and drag distributions over the wing could be obtained from a computer program. However, this program was not available soon enough to be of any use. This meant that for the sake of simplicity the lift force is assumed to be evenly distributed over the wing. A ramp distribution over a spanwise cross section is also assumed. With these simplification, the determination of the forces and moments follows:

Equilibrium Equations at Cruise:

$$L = W_{\text{cruise}} = 66,723.3 \text{ N}$$

$$D = T = 18,682.524 \text{ N}$$

$$L_{\text{wings}} = 1/4 * L = 16,680.83 \quad (\text{this is due to the lifting-body configuration})$$



$$L_w = L_{\text{wings}} / 2 = 8,340.4 \text{ (lift on one wing)}$$

$$l_1 = 6.4008 \text{ m} \quad l_4 = 0.9144 \text{ m}$$

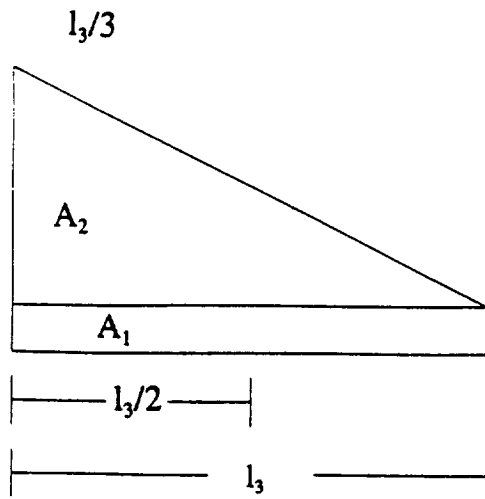
$$l_2 = 0.6096 \text{ m}$$

$$l_3 = 1.524 \text{ m}$$

L' is the lift contribution due to the shaded region

$$L' = L_w * l_2 * l_3 / (l_3 * l_4 + l_3 * (l_1 - l_4) / 2)$$

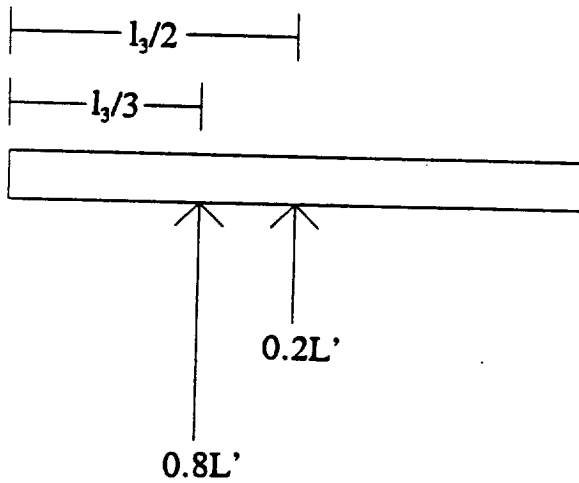
$$L' = 1,390.1 \text{ N}$$



Lift force L' is distributed as follows:

$A_1 = 80\%$ of the lift

$A_2 = 20\%$ of the lift



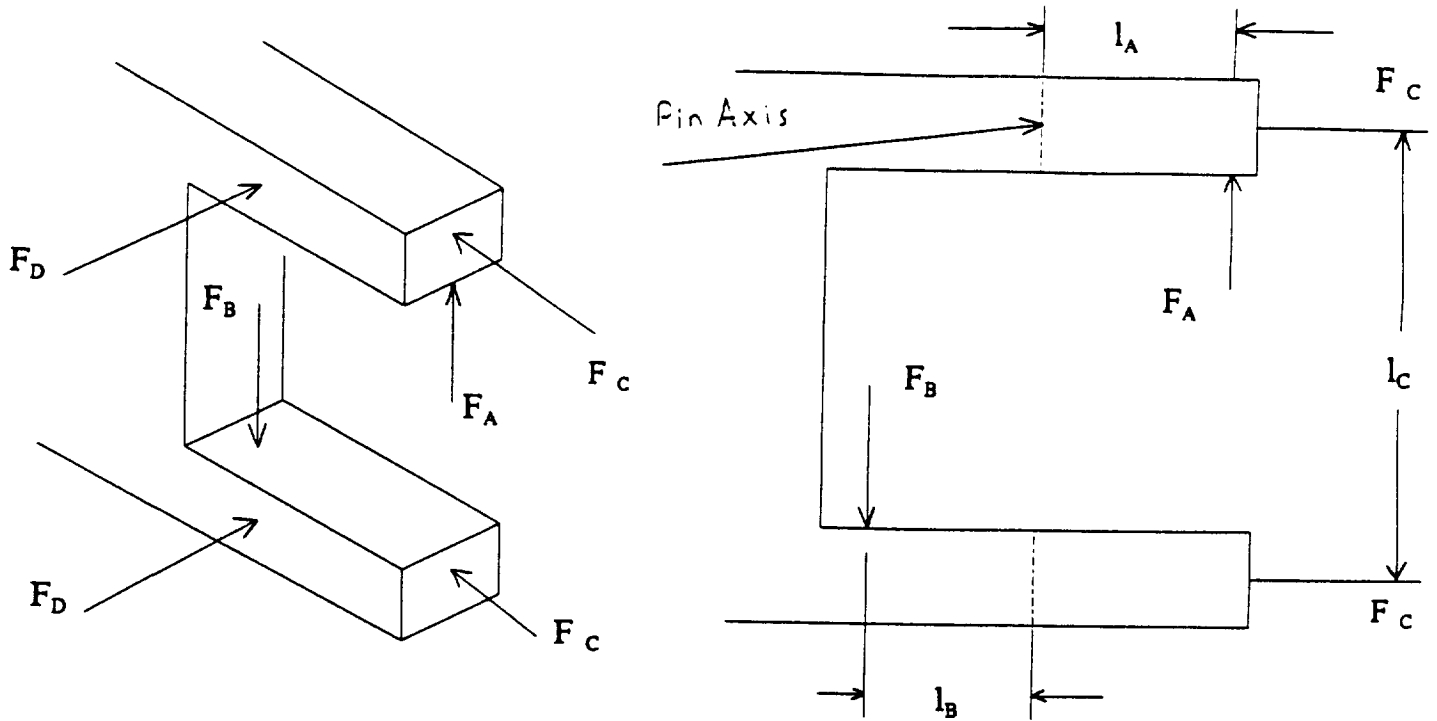
Determination of Equivalent concentrated loading.

$$l_4 = l_3 / 3 * 8L' / 10 + l_3 / 2 * 2L' / 10$$

$$l_4 = 8/30 l_3 + 1/10 l_3$$

$$l_4 = 11/30 l_3$$

$$l_4 = 0.5588 m$$



All the forces shown are directly carried by the wing clamp. F_C represents the force carried by the pin, which in turn is transmitted to the clamp. All of the moment is assumed to be carried by the clamp. The resulting equations follow:

$$F_C = 0$$

$$F_A - F_B = L_{\text{limit}}$$

$$l_A F_A + l_B F_B = M_{\text{limit}}$$

The drag force is represented by distributing a force on the upper and lower front sides of the clamp along the axis of the pin. Hence,

$$F_D = D_{\text{limit}} / 2$$

In the actual application of the forces in I-DEAS, F_A , F_B , and F_D are distributed along a line. If F_C was finite it would be distributed over an area. The loading condition for all the configurations is as follows:

$$l_A = 0.08 \text{ m}$$

$$l_B = 0.055 \text{ m}$$

$$l_C = 0.1905 \text{ m}$$

With a load factor of 9,

$$L_{\text{limit}} = n * L' = 9*(1,390.1) = 12,510.9 \text{ N}$$

The maximum moment is

$$M_{\text{limit}} = I_4 * L_{\text{limit}} = 0.5588*(12,510.9) = 6,991.1 \text{ N-m}$$

The drag force is calculated using the ratio of the wing area over the total area

$$S_{\text{tot}} = 297.29 \text{ m}$$

$$S_w = 20.3 \text{ m} \quad (\text{area of one wing})$$

$$D_w = S_w / S_{\text{tot}} * T \quad (\text{drag on one wing})$$

$$D_w = 1,401.2 \text{ N}$$

The drag on the wing is evenly distributed between the 6 rear fuselage bulkheads

$$D' = D_w / 6 = 233.53 \text{ N}$$

$$D_{\text{limit}} = n * D' = 9*(233.53) = 2,101.8 \text{ N}$$

solving the equations,

$$F_A = 56,857.36 \text{ N}$$

$$F_B = 44,346.74 \text{ N}$$

$$F_C = 0 \text{ N}$$

$$F_D = 1,050.9 \text{ N}$$

Appendix 7. Aerodynamic Characteristics

1. Figure 7.1. Configuration Trade Studies - L/D vs α (Config 1,2,3,4,5)
2. Figure 7.2. Configuration Trade Studies - L/D vs α (Config 1,6,7,8)
3. Figure 7.3. Configuration Trade Studies - C_m vs α (Config 1,2,3,4,5)
4. Figure 7.4. Configuration Trade Studies - C_m vs α (Config 1,6,7,8)
5. Figure 7.5. C_m vs α ($M = 4, 6, 12$)
6. Figure 7.6. C_l vs α ($M = 0.3, 0.6, 0.9$)
7. Figure 7.7. C_l vs α ($M = 4, 6, 12$)
8. Figure 7.8. C_l vs C_d ($M = 0.3, 0.6, 0.9$)
9. Figure 7.9. C_l vs C_d ($M = 4, 6, 12$)
10. Figure 7.10. L/D vs α ($M = 4, 6, 12$)
11. Figure 7.11. C_{do} vs Mach Number
12. Figure 7.12 dC_m/dC_l vs Mach Number
13. Conformal Temperature Map

Figure 7.1. Configuration Trade studies - L/D vs alpha

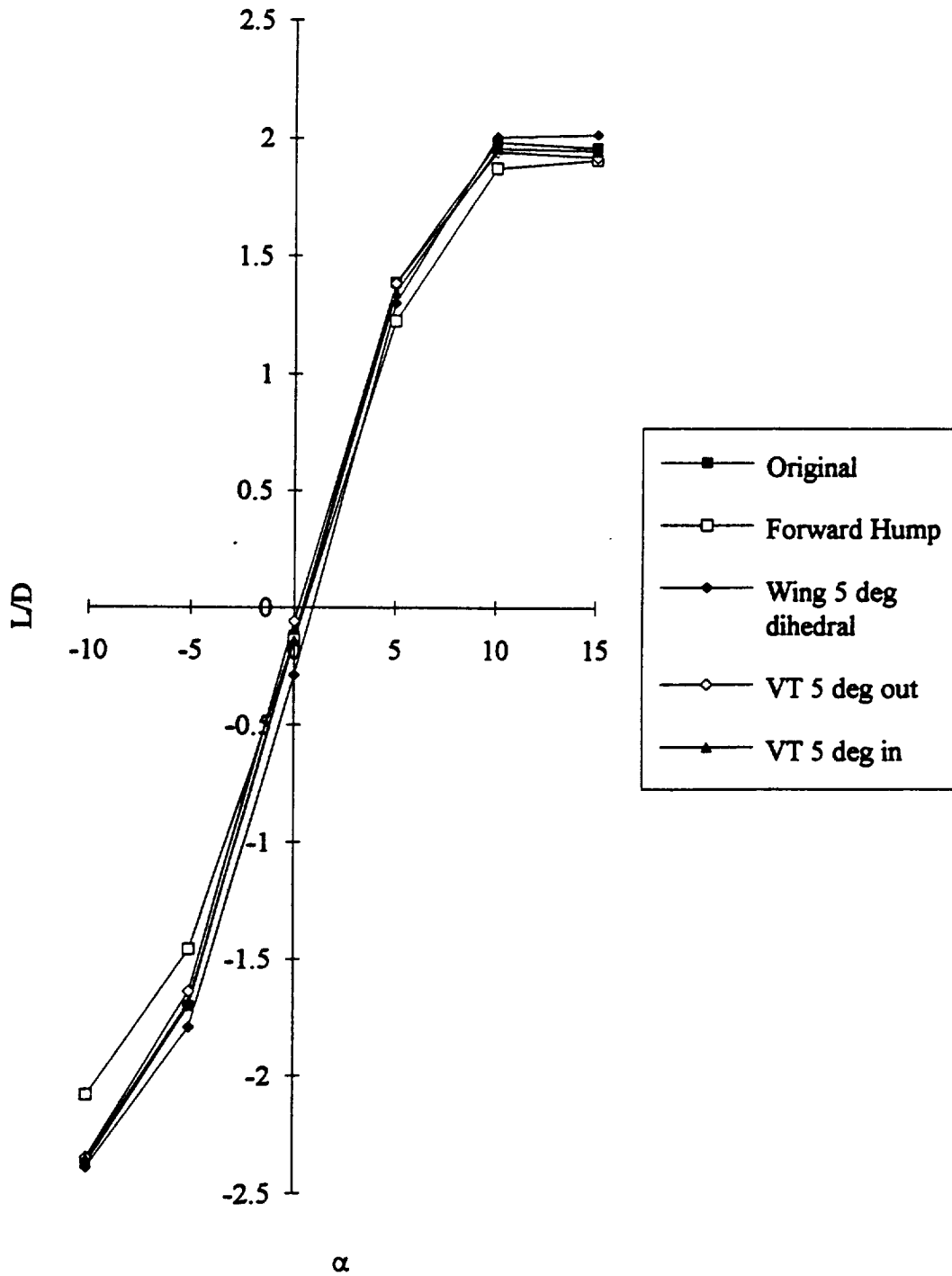


Figure 7.2. Configuration Trade Studies : L/D vs alpha

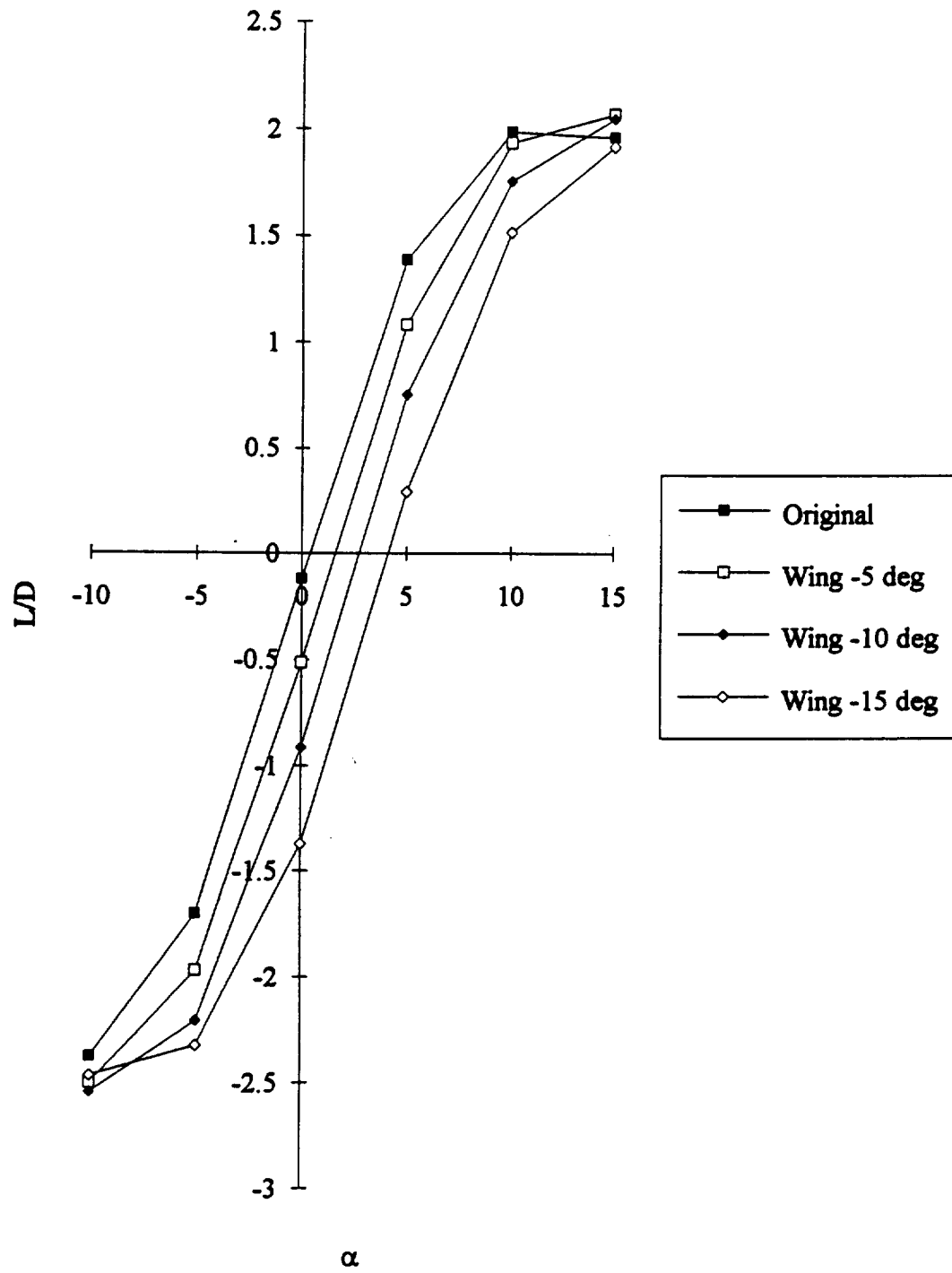


Figure 7.3. Configuration Trade Studies : C_m vs α

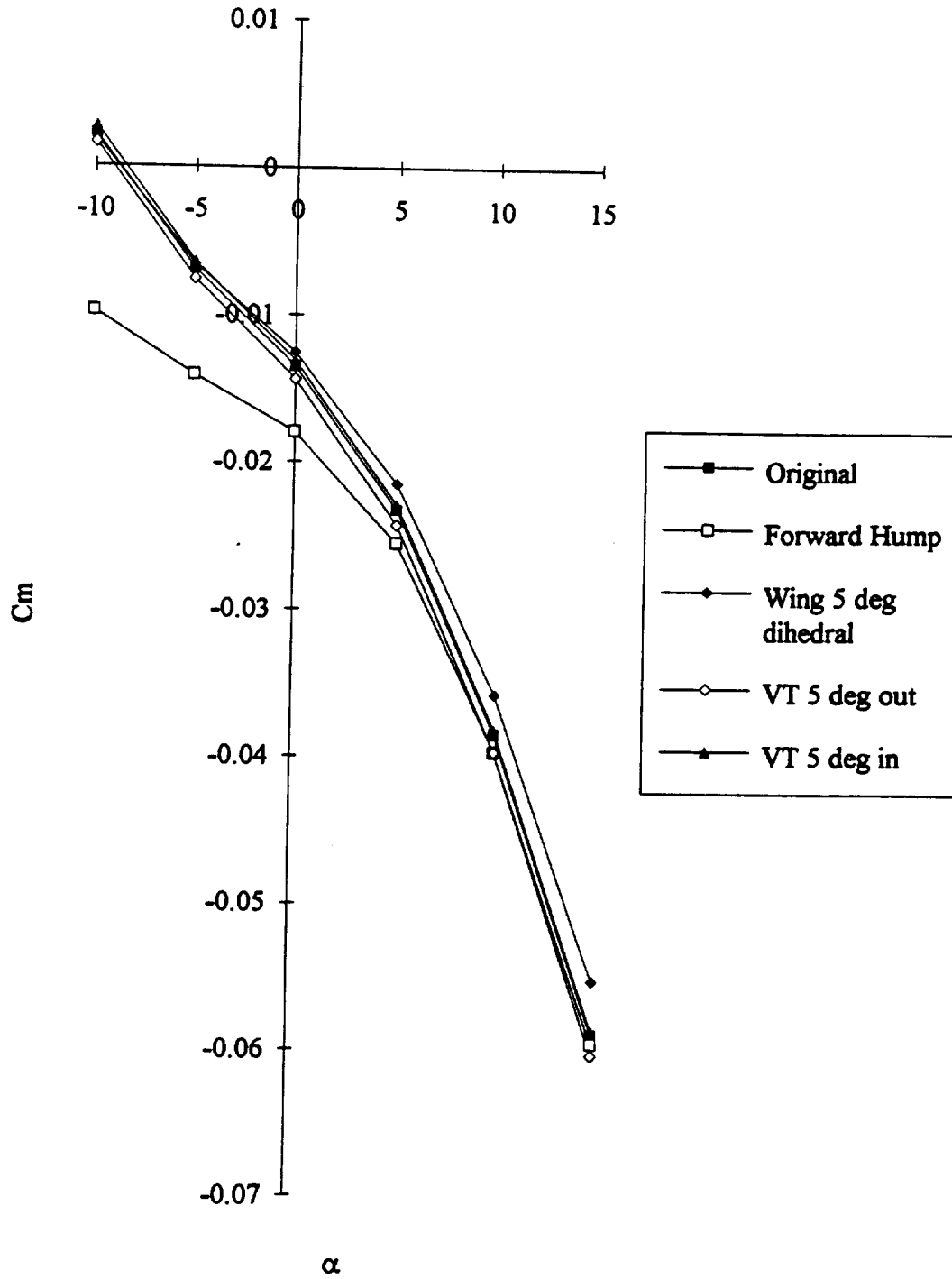


Figure 7.4. Configuration Trade Studies : Cm vs alpha

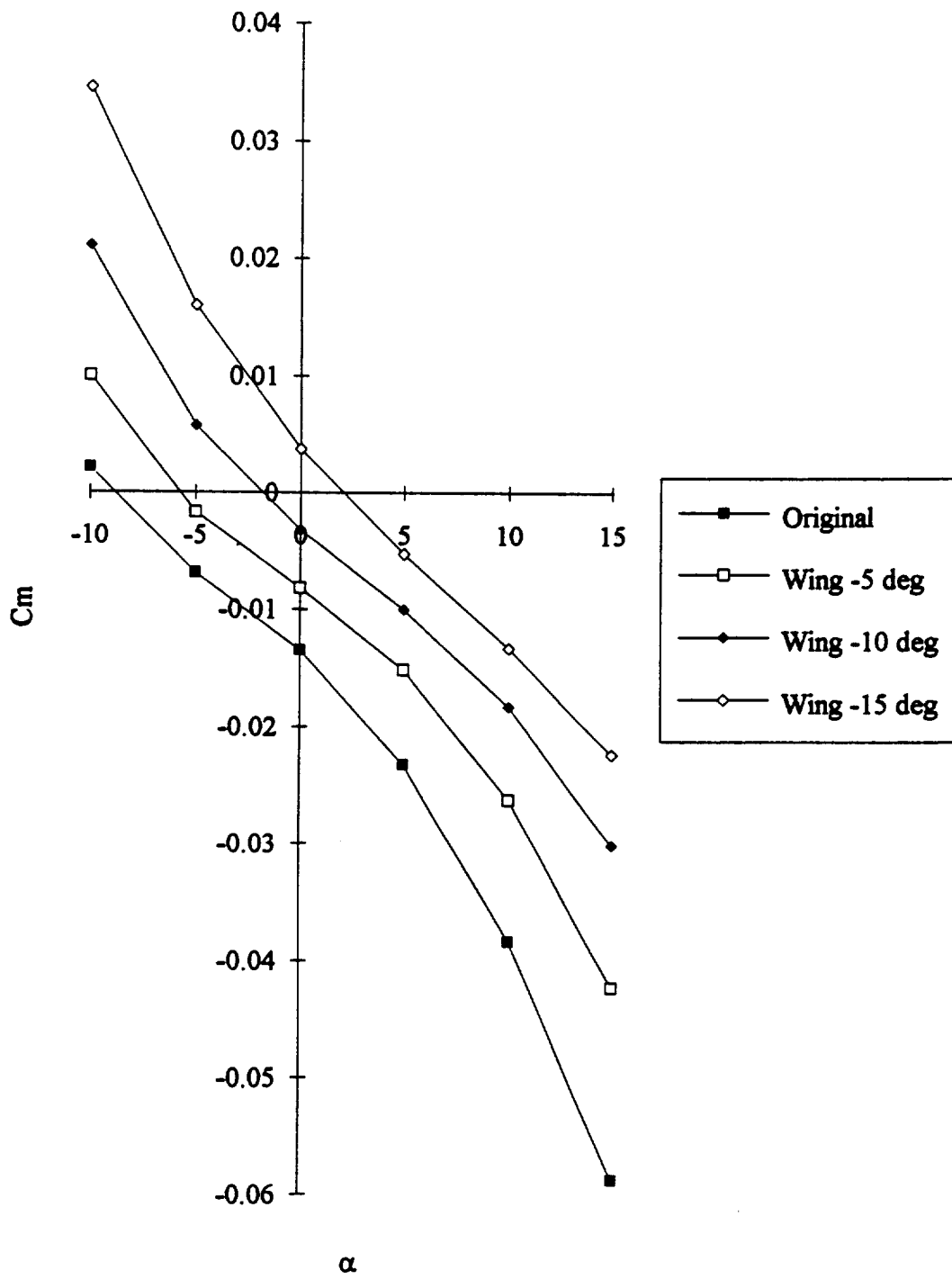


Figure 7.5. C_m vs α

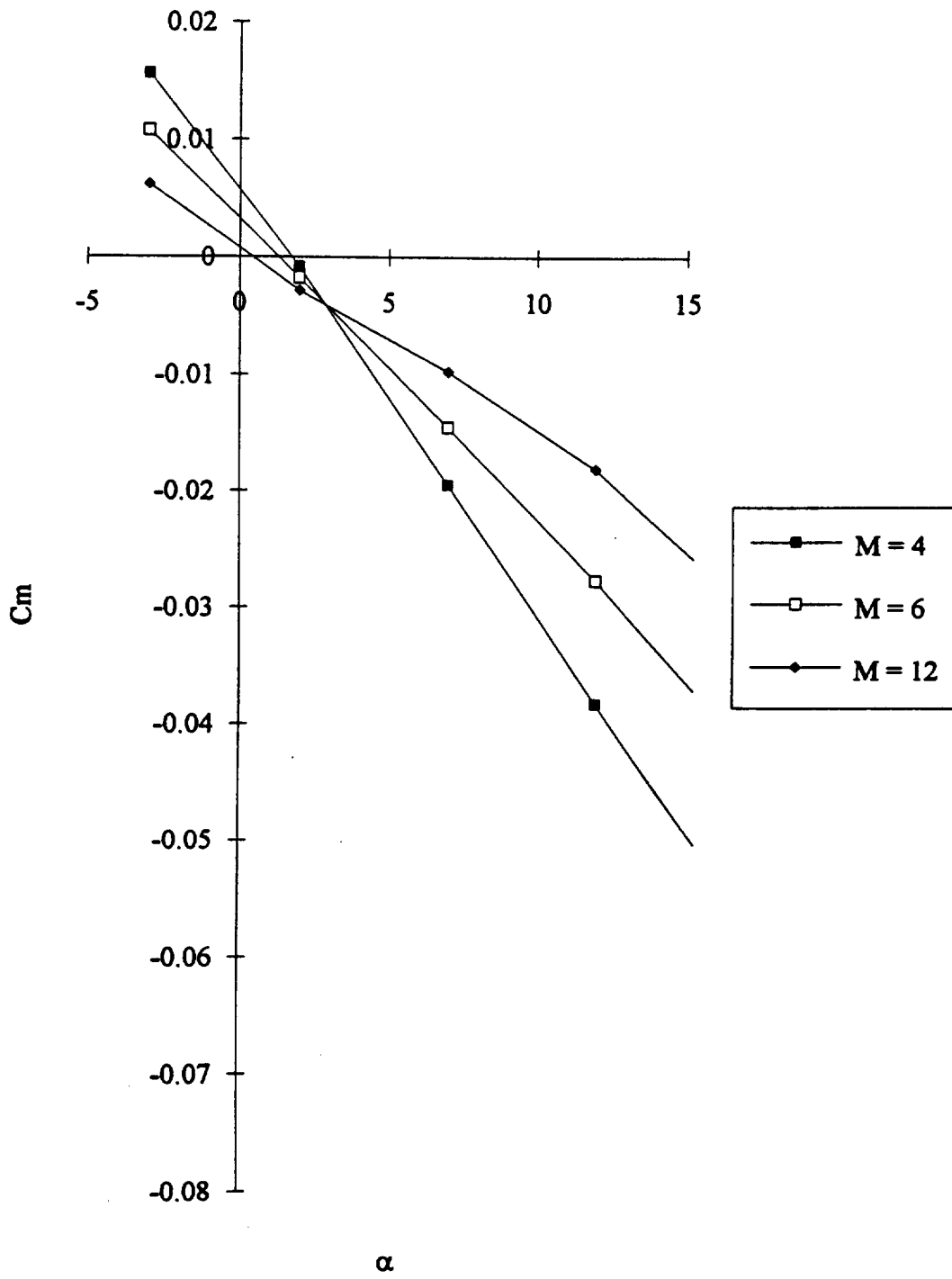


Figure 7.6. Cl vs alpha

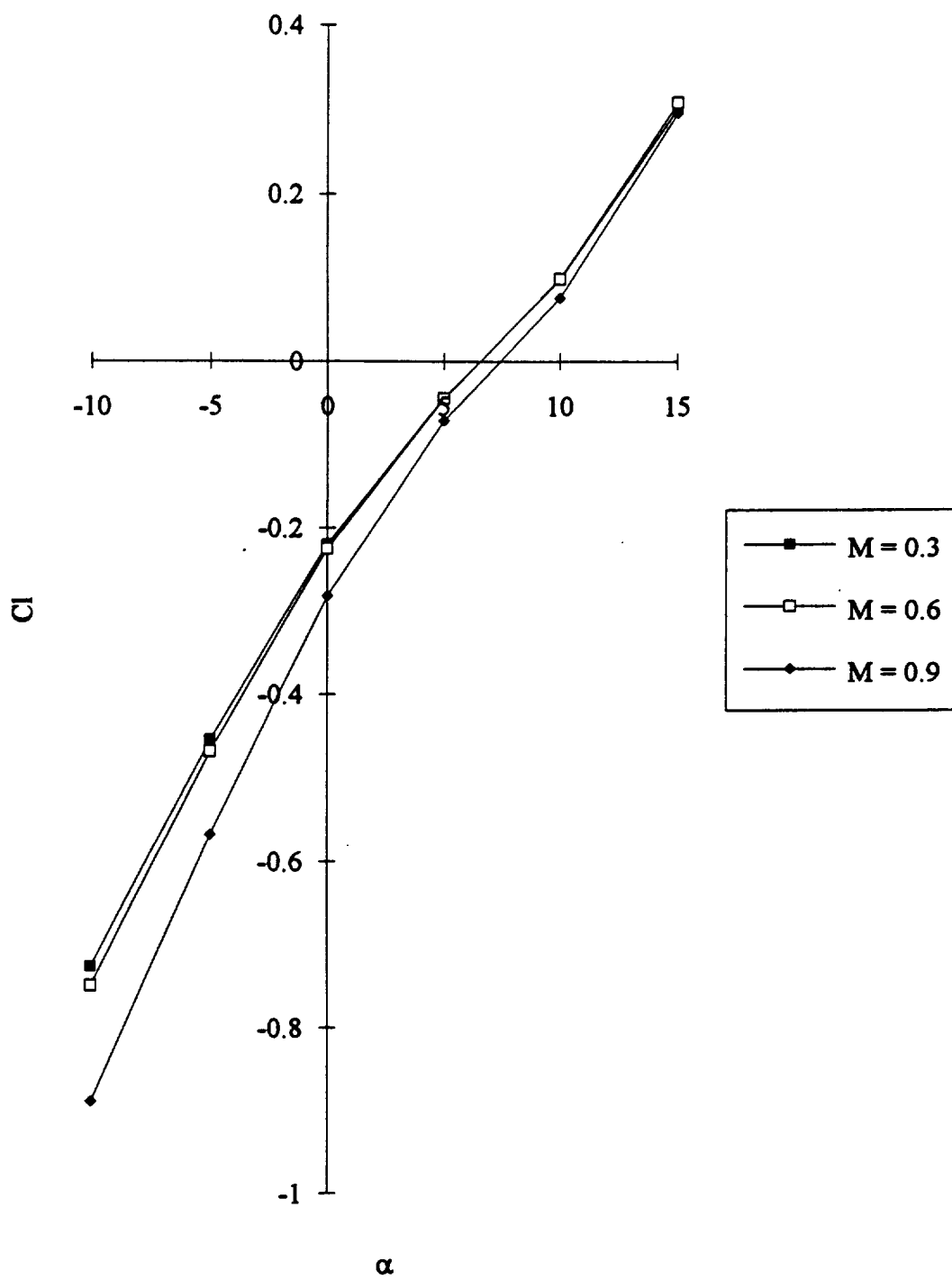


Figure 7.7. CI vs alpha

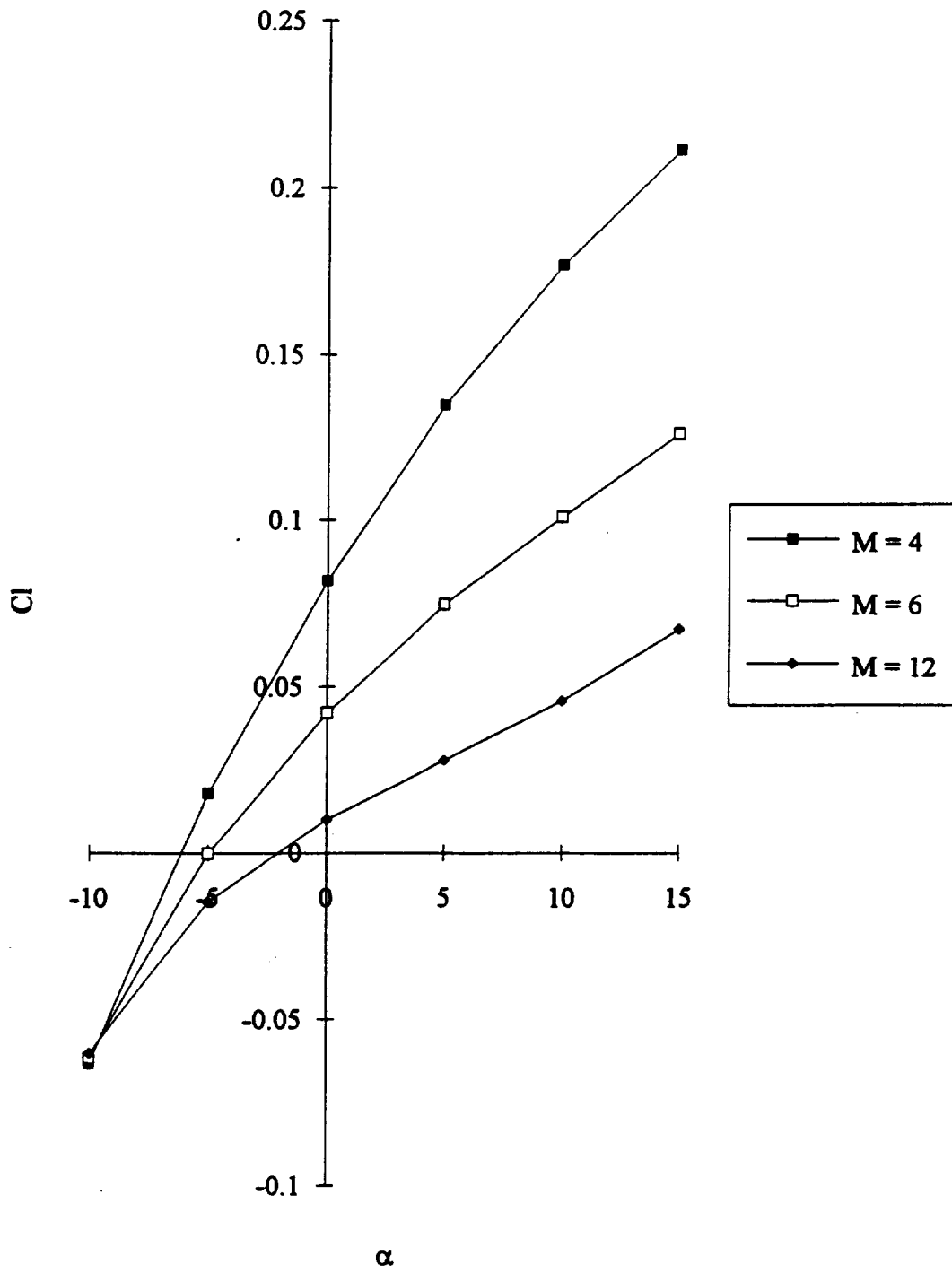


Figure 7.8. Cl vs Cd

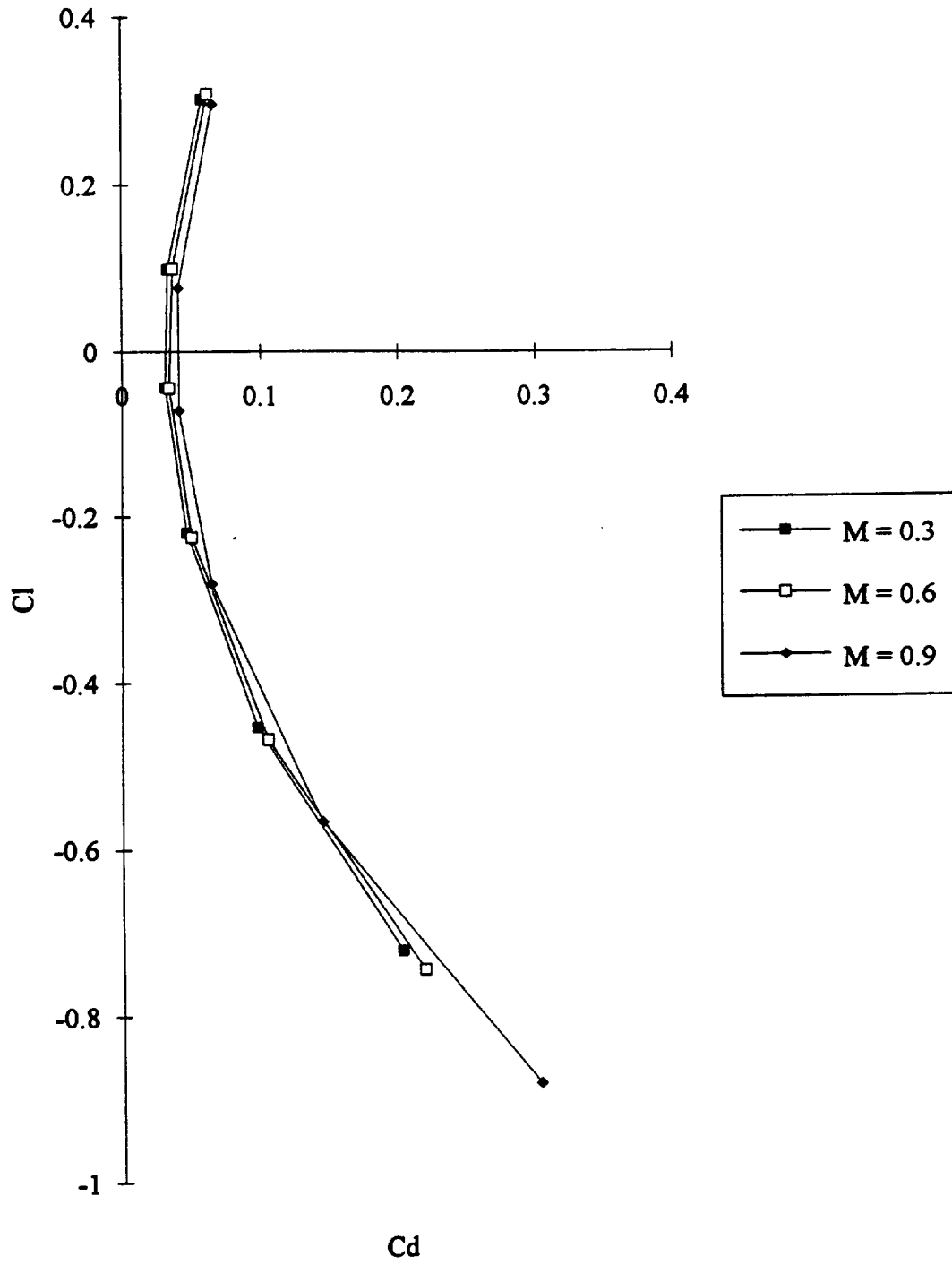


Figure 7.9. Cl vs Cd

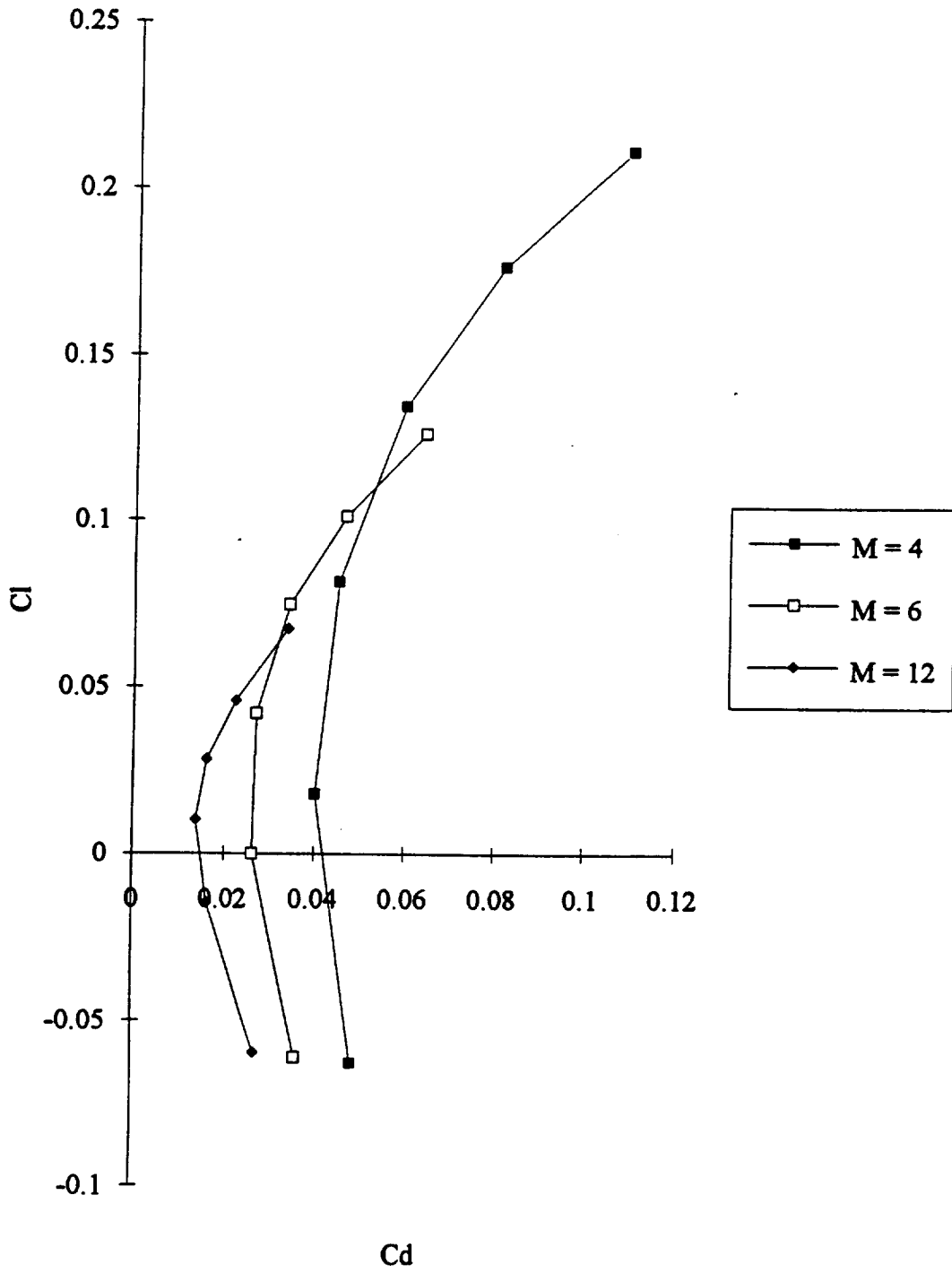


Figure 7.10. L/D vs alpha

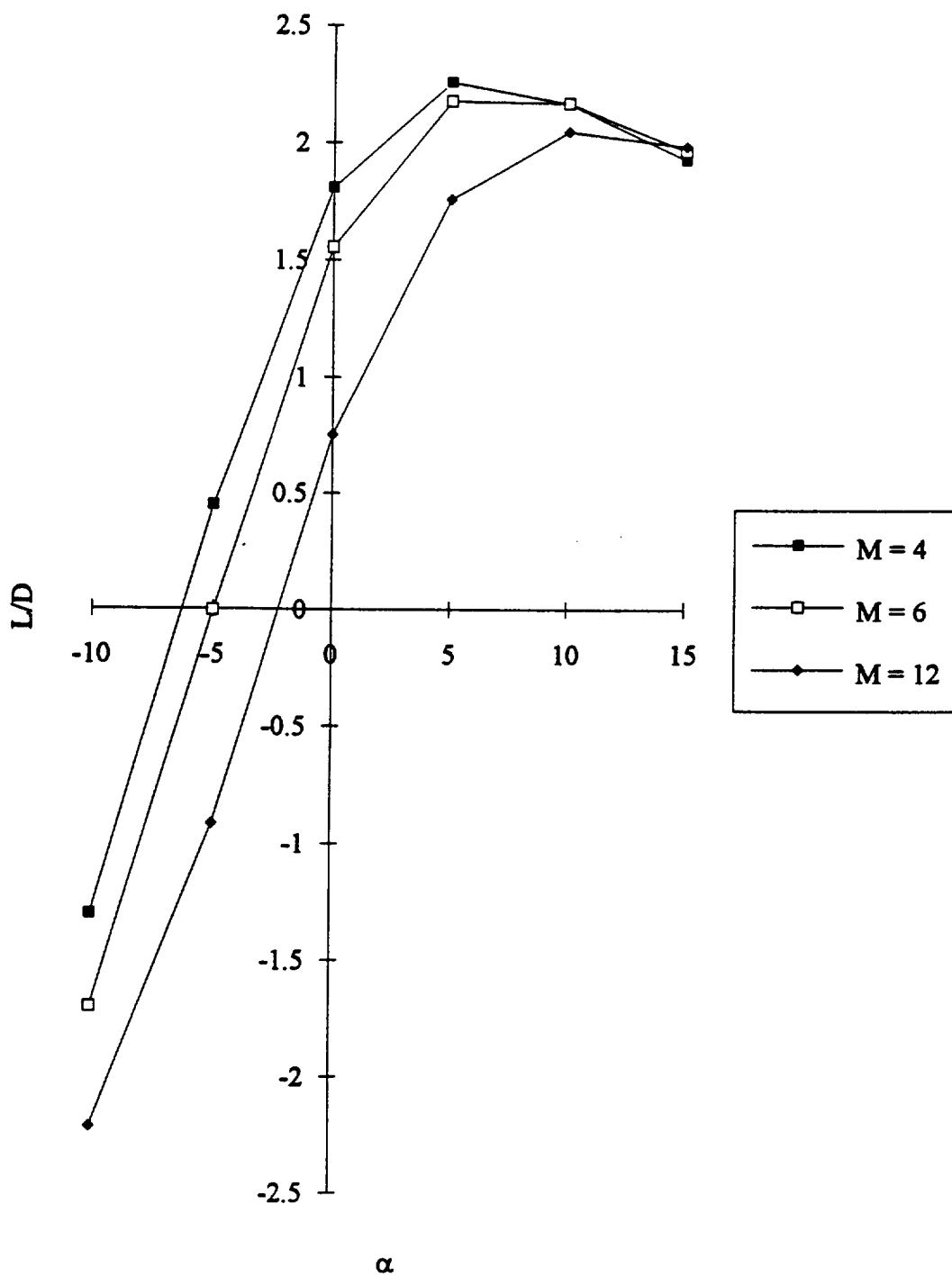


Figure 7.11. C_{do} vs Mach Number

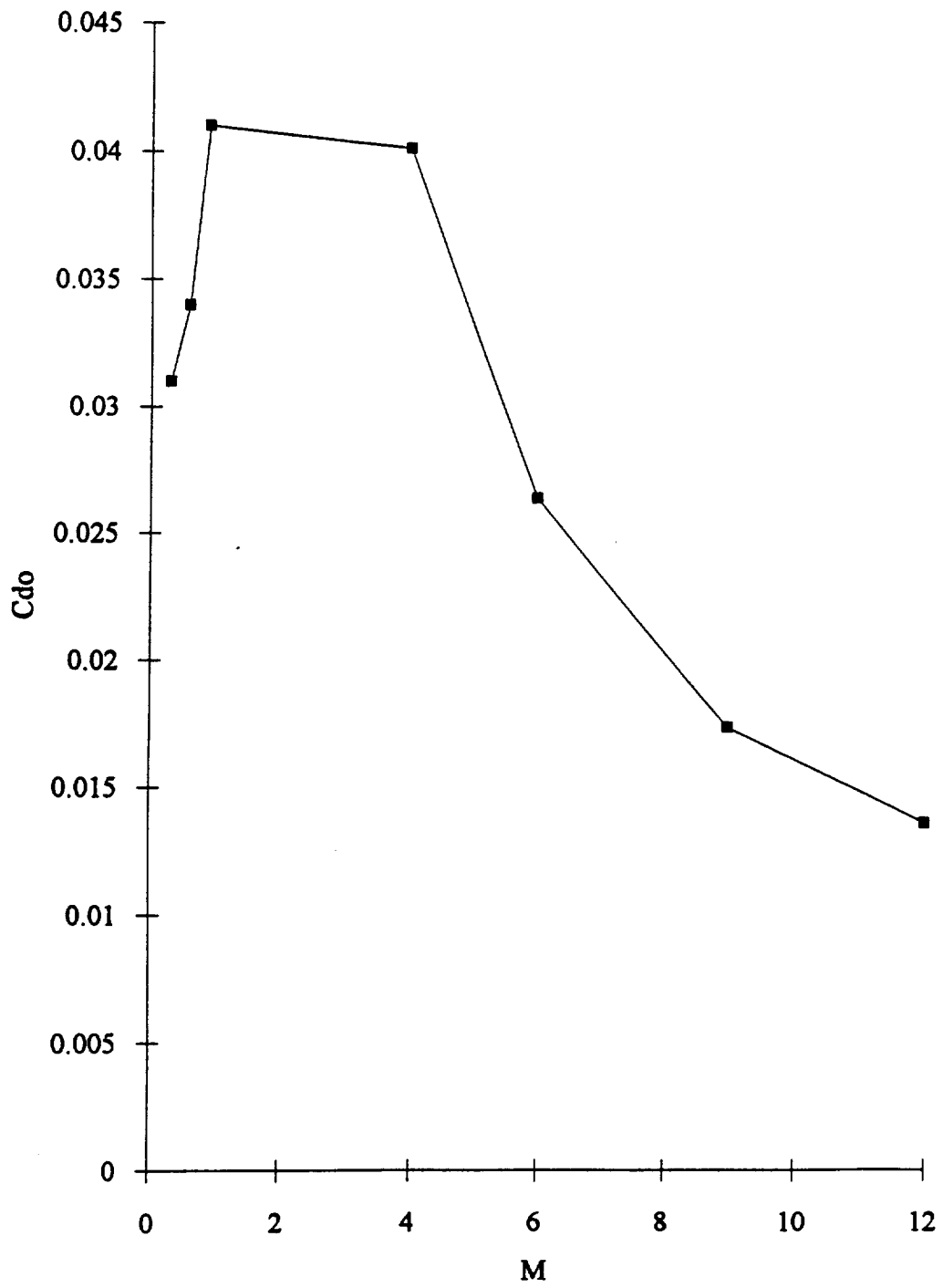
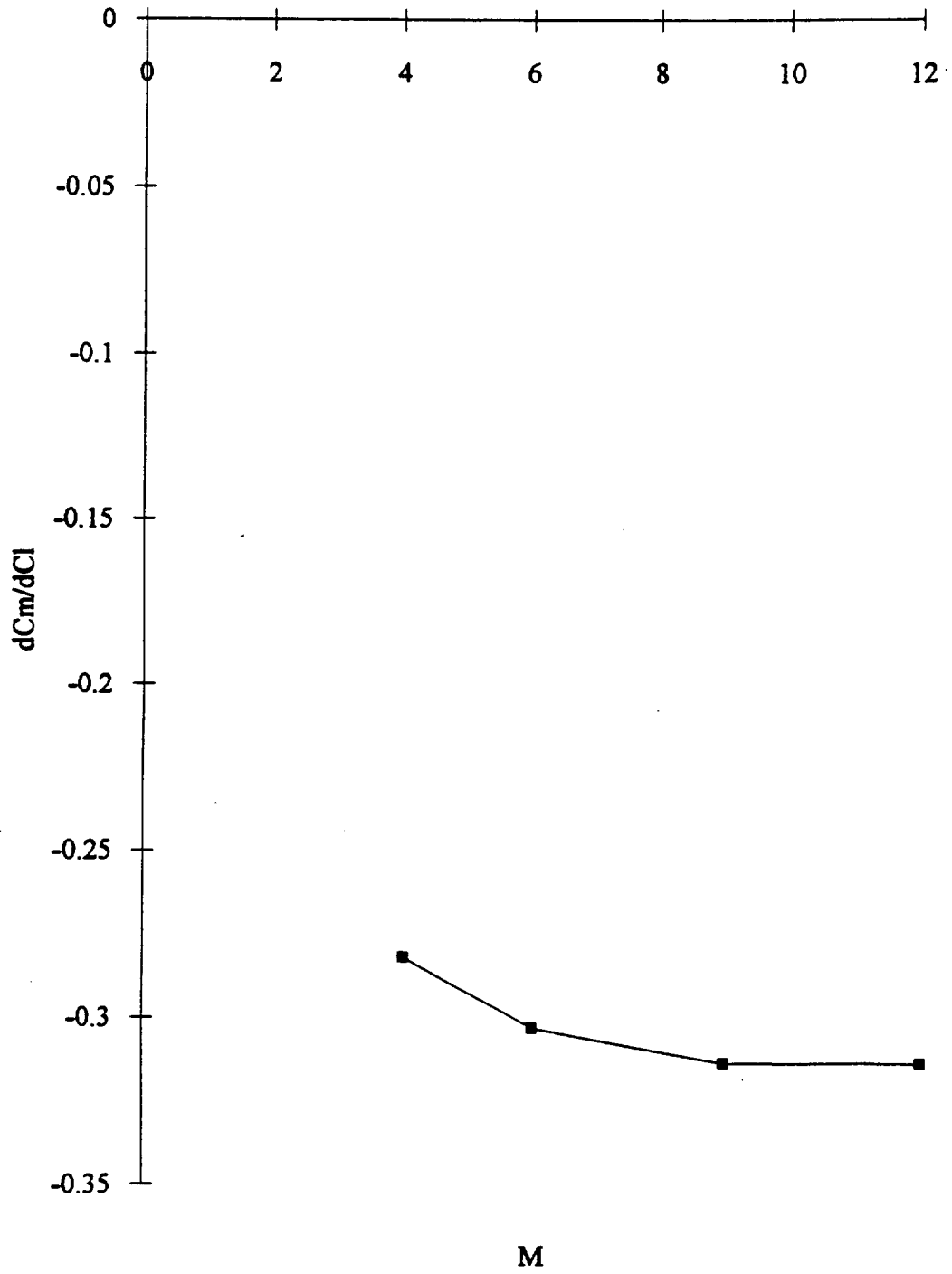
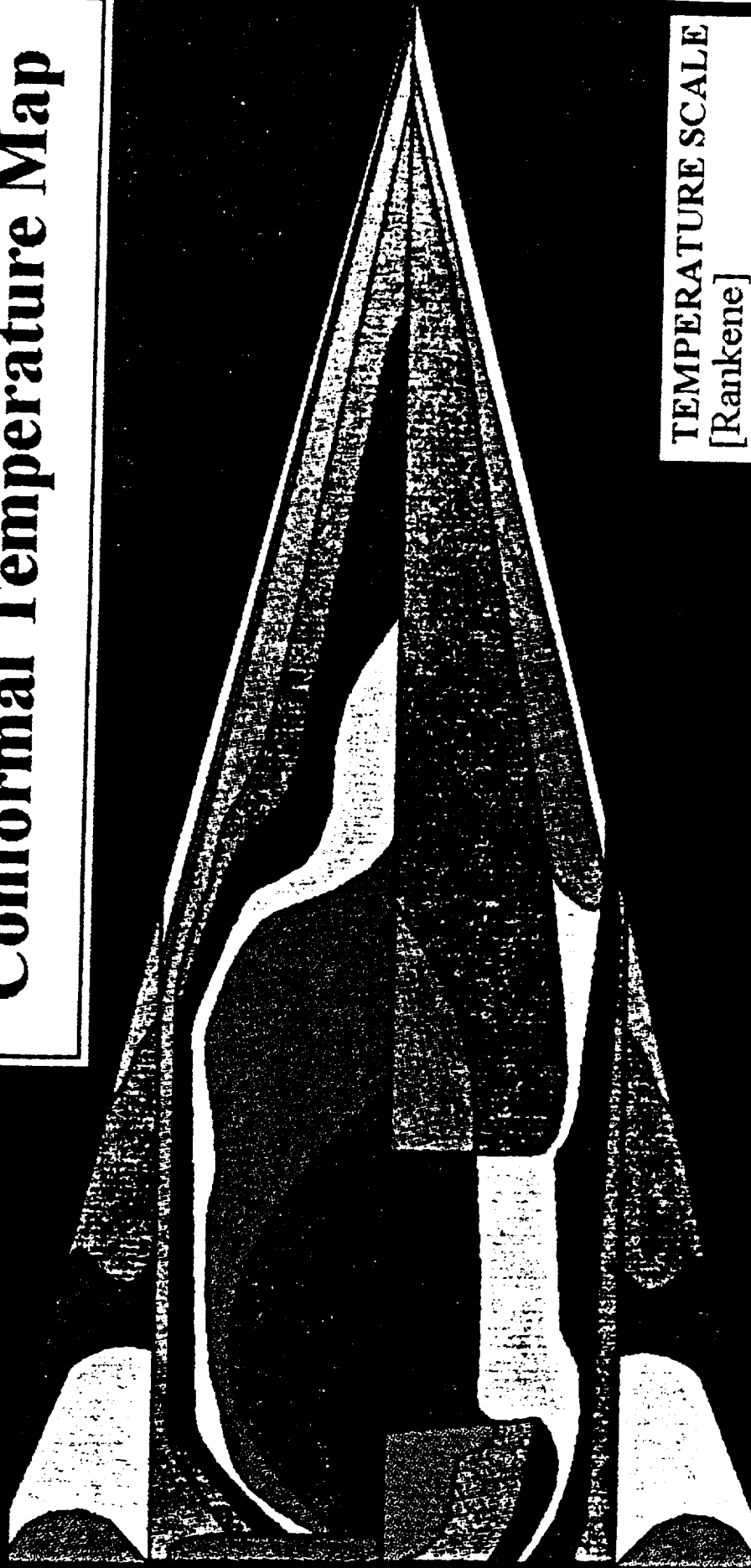


Figure 7.12. dC_m/dC_l vs Mach Number



Conformal Temperature Map



TEMPERATURE SCALE [Rankene]

[Solid Black]	500 - 750
[Stippled]	750 - 1000
[Horizontal Lines]	1000 - 1250
[White]	1250 - 1500
[Solid Black]	1500 - 1750
[Horizontal Lines]	1750 - 2000
[Stippled]	2000 - 2500
[Horizontal Lines]	2500 - 3000
[White]	3000 - 3500

Appendix 8. Trajectory

1. **Figure 8.1. Weight vs Time**
2. **Figure 8.2. Rate of Climb vs Mach Number**
3. **Figure 8.3. Altitude vs Distance**
4. **Figure 8.4. Thrust Available and REquired vs Mach Number**
5. **Figure 8.5. Altitude vs Mach Number**
6. **Figure 8.6. Thrust Available vs Altitude**
7. **ETO Input Listing**

Figure 8.1. Weight vs Time

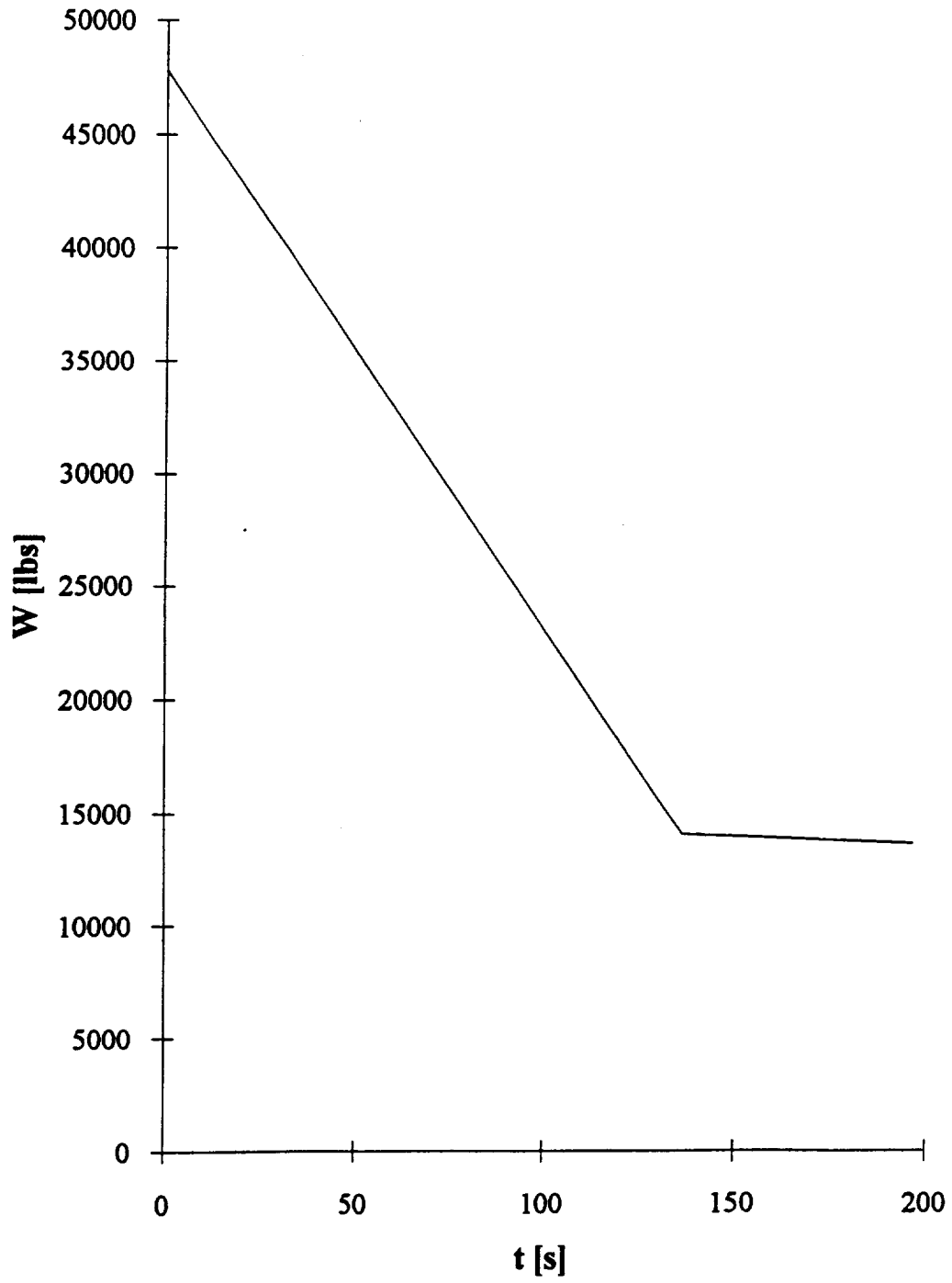


Figure 8.2. Rate of Climb vs Mach Number

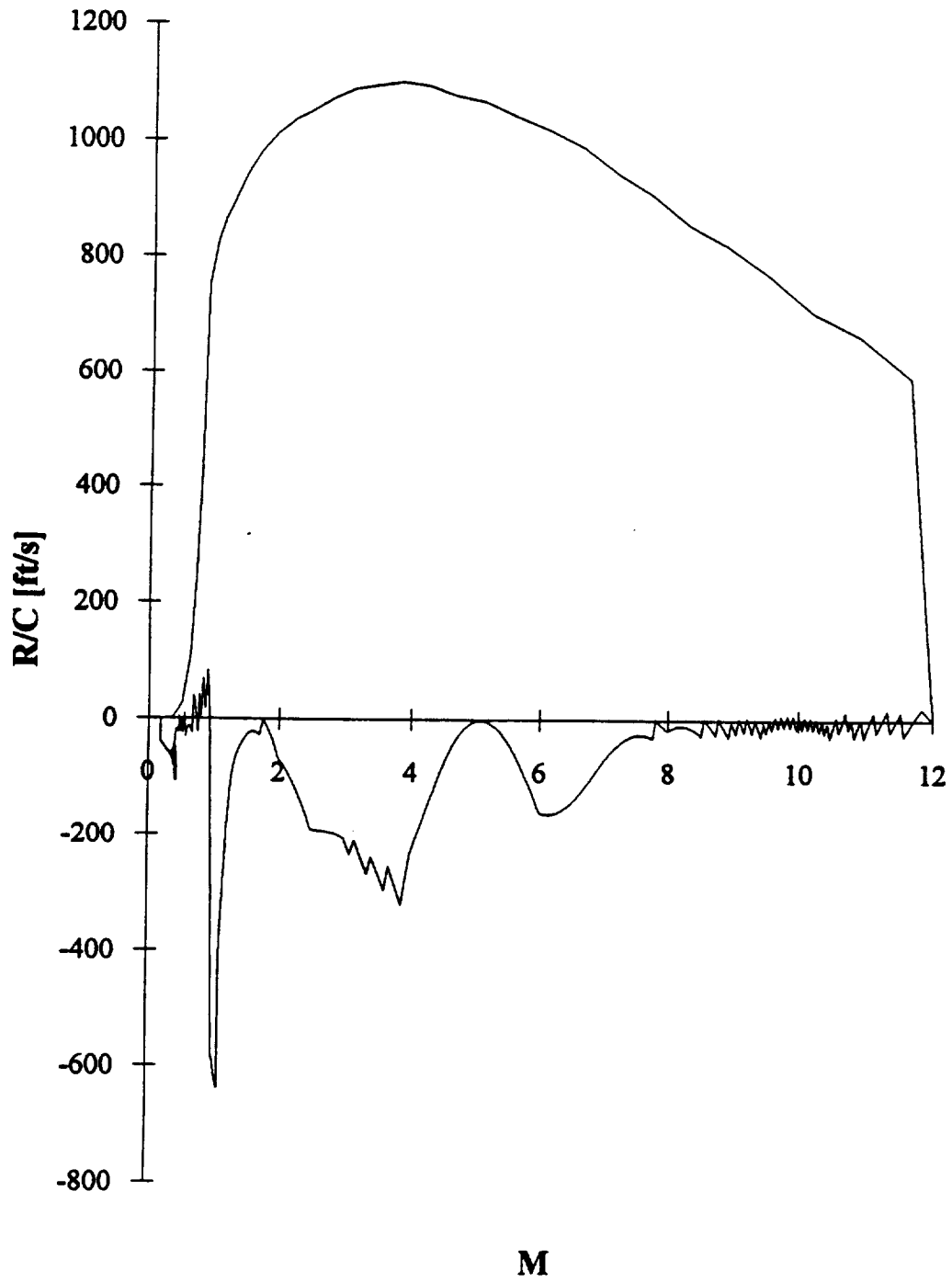


Figure 8.3. Altitude vs Distance

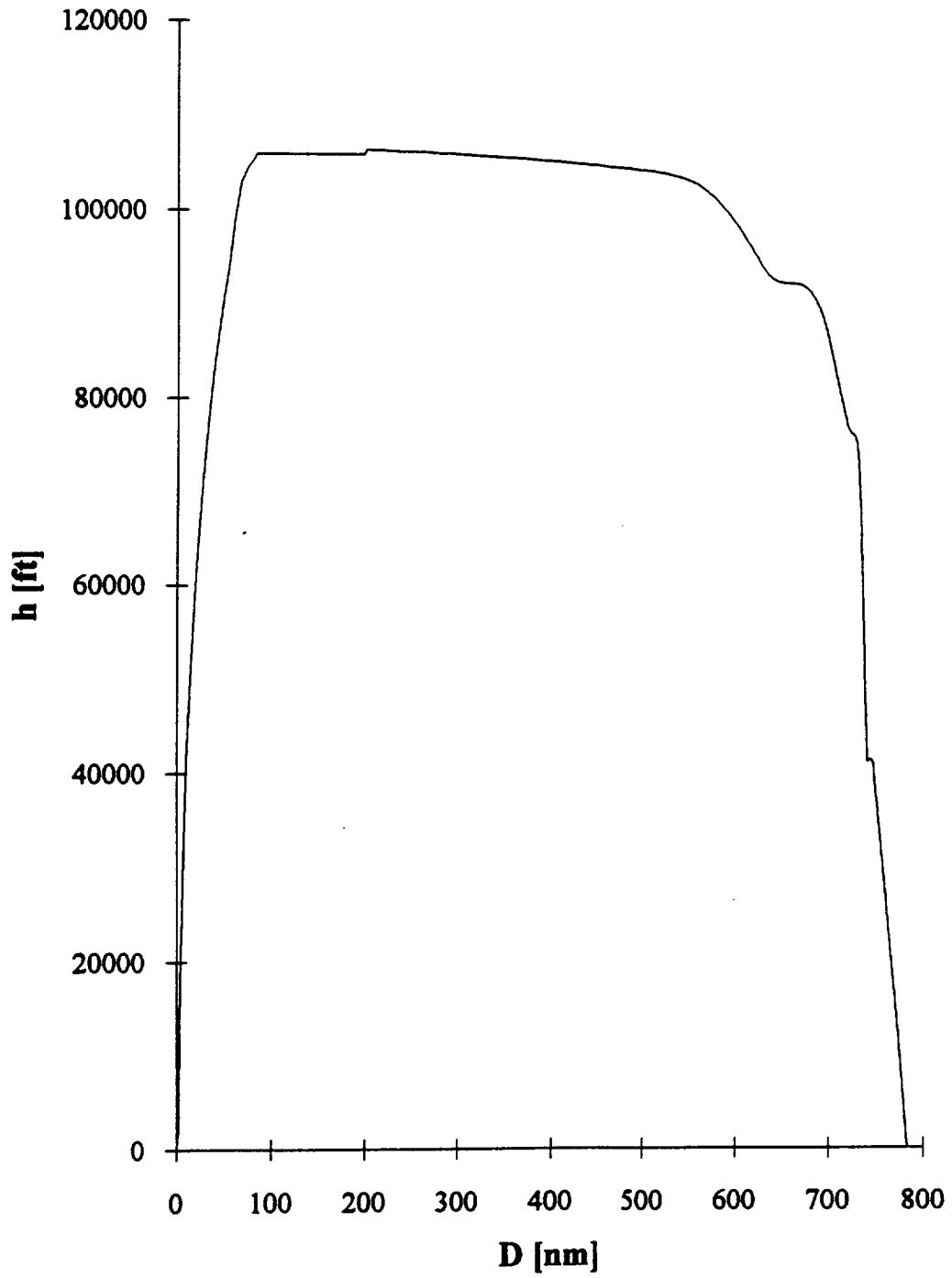


Figure 8.4. Thrust Available and Required vs Mach Number

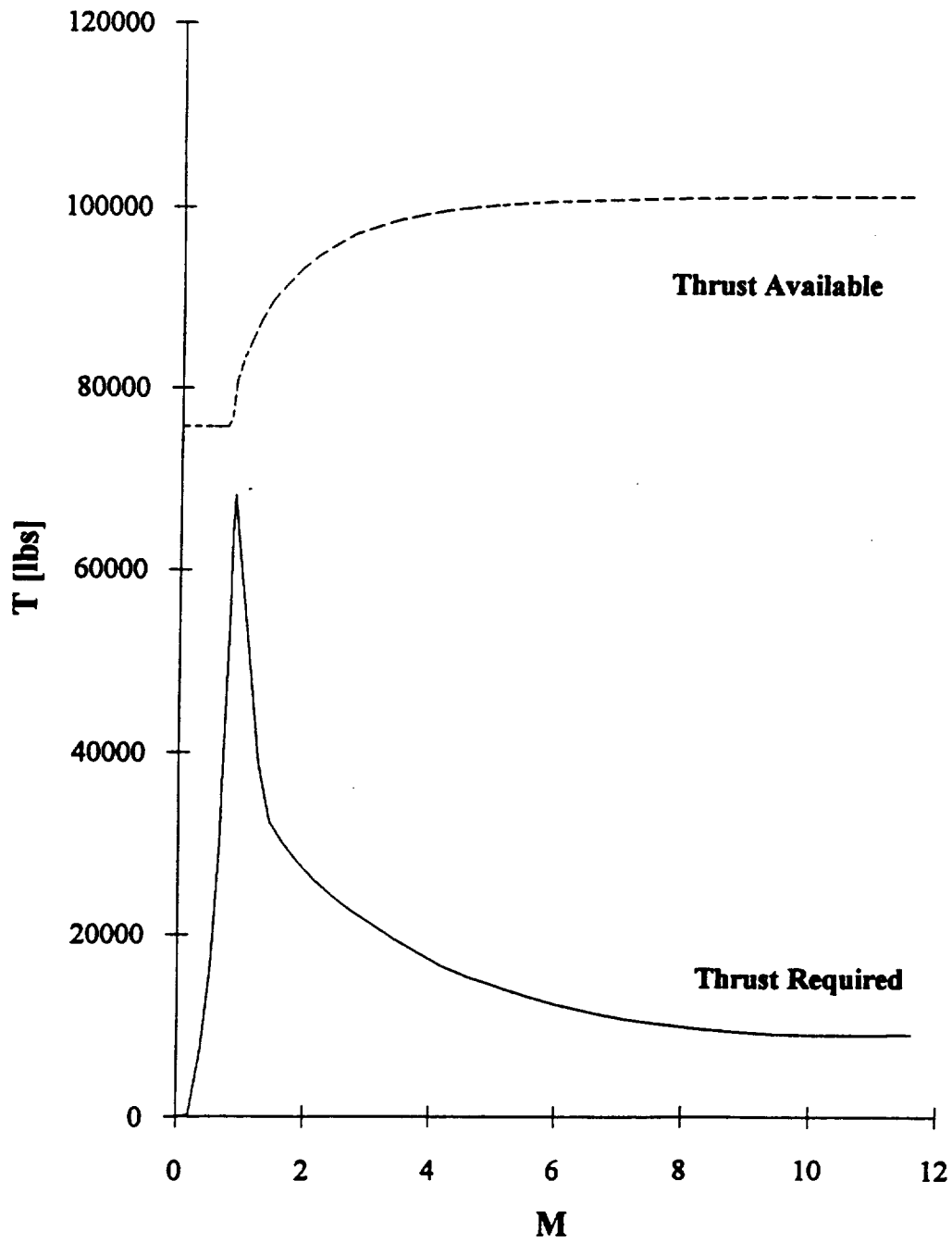


Figure 8.5. Altitude vs Mach Number

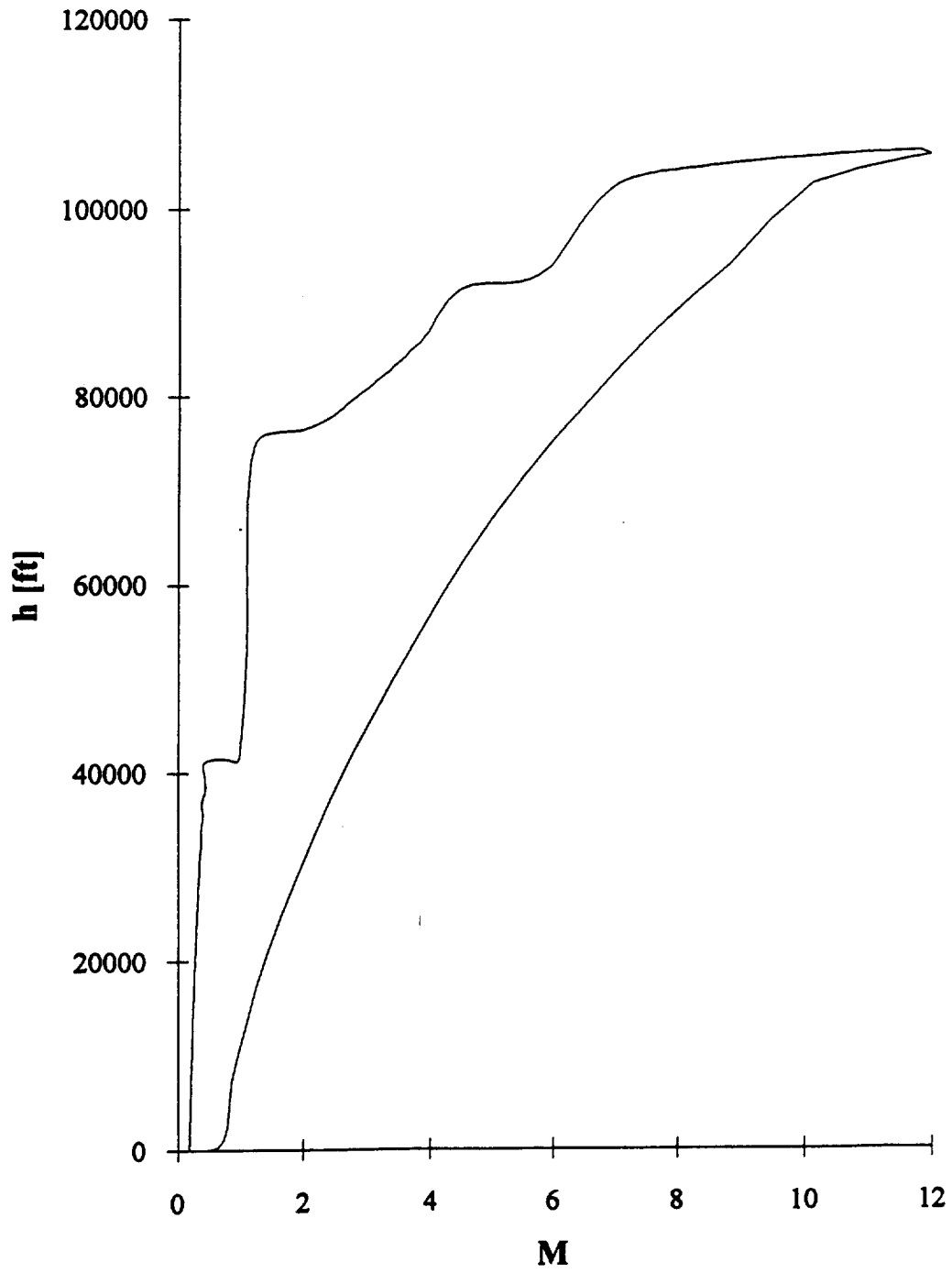
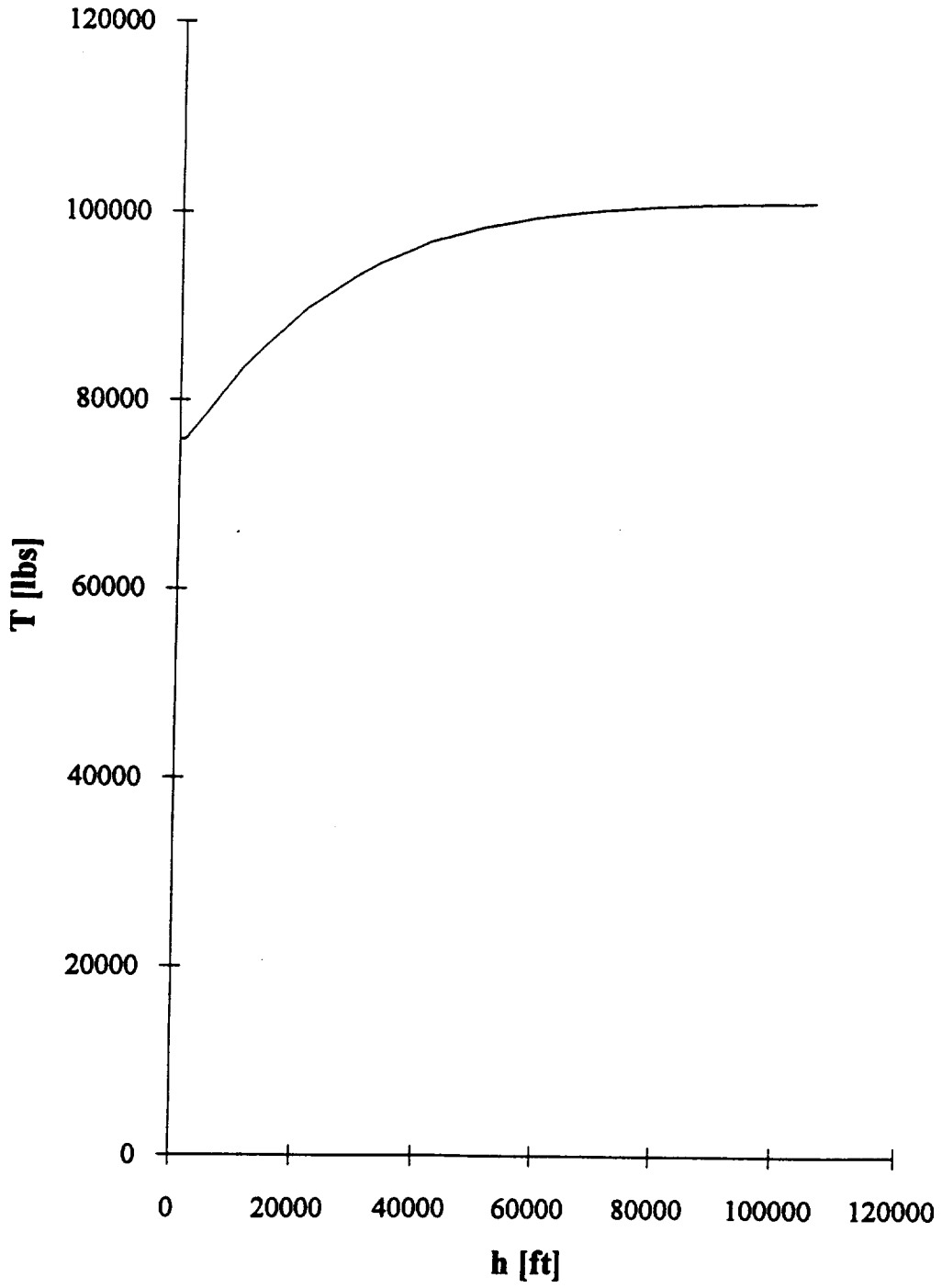


Figure 8.6. Thrust Available vs Altitude



7. ETO Input Listing

INPUT DATA FILE "SORT.DAT"/5MAY93/ROCKET SSTO
PROGRAM ETO
TABLE XISPA
0 0 0 0 0
1 4 0 0
0.0, .9,1.5,15.0
4000, 3000,2000,1000
TABLE XPHIMAX
0,0,0,0,0
1, 4 ,0 ,0
0.0,.9,1.5,15.0
1.0,1.0,1.0,3.0
TABLE XCDO
0,0,0,0,0
1,14, 0 ,0
0.0,0.1,0.3,0.5,0.7,0.9,1.1,1.3,1.5,2.0,4.0,6.0,8.0,10.0,12.0
0.0,.00549,.00533,.00566,.00631,.00723,.02737,.00884,.00809,.00704,.00523,.00453
.00418,.00398,.00385
TABLE XDELCD
0,0,0,0,0
1,13,0 ,0
0.0, 1000., 11000., 21000., 31000., 41000., 51000., 61000., 71000., 81000.
91000.,101000.,111000.
0.0,0.0021,0.0022,0.0022,0.0023,0.0024,0.0026,0.0027,0.0029,0.0030,0.0032
0.0035,0.0037
TABLE XCLALPHA
0,0,0,0,0
1,15 , 0 , 0
0.0,0.1,0.3,0.5,0.7,0.9,1.1,1.3,1.5,2.0,4.0,6.0,8.0,10.0,12.0
.005,.005,.005,.005,.005,.005,.010,.008,.008,.008,.009,.007,.006,.006,.006
TABLE XK
0,0,0,0,0
1,15 , 0 , 0
0.0,0.1,0.3,0.5,0.7,0.9,1.1,1.3,1.5,2.0,4.0,6.0,8.0,10.0,12.0
3.3855,3.3855,3.4036,3.4413,3.5027,3.5965,2.0971,2.2433,2.3399,2.3243,2.1479
2.6083,2.8917,3.0752,3.1992
TABLE XA0AC
0,0,0,0,0
2,4 ,3,0
0.0,0.8,1.0,15.0
-10.0,0.0,10.0

80.0,.15,.15,1.0
80.0,.15,.15,1.0
80.0,.15,.15,1.0
TABLE XISPR
0,0,0,0,0
1,12,0,0
1000.0, 11000.0, 21000.0, 31000.0, 41000.0, 51000.0, 61000.0, 71000.0
81000.0, 91000.0,101000.0,111000.0
308.5,341.9,366.3,383.6,395.4,402.9,407.5,410.3,412.1,413.2,413.8,414.3
TABLE XWDOTPMAX
0,0,0,0,0
1,4,0,0
0.0,2.0,8.0,13.0
245.783,245.783,245.783,245.783
AIRBREATHER-----
AC AREF FASTOIC
0.0, 625.0, .0292
VEHICLE-----
WLAUNCH WFUEL WFINAL VFINAL STAGE
47810., 33750., 14060., 11981., 1
INITIAL CONDITIONS-----
M0 H0 GAMMA ALPHA DT DELPRINT TIMEX
0.001,0.001,0.0,0.0,0.5,10,0.0
PHASE 1-----
VTAKEOFF
350.0
PHASE 2-----
ALPHA2MAX LOADFAC GAMMAMAX ACCCOMD V02 H02
25.0,6.0,45.0,9.0,900.0,3000.0
PHASE3-----
ALPHAMIN ALPHAMAX Q0COMD V0TEMP Q0FINAL GAINQ3 GAINGAM3
-15.0,10.0,549.,900.0,820.,10.0,1.0
PHASE 4-----
SWITCH4 V0CRUISE GAINH04 GAINGAM4 GAINQ4
0,0.0,-20.0,0.0,5.0
PHASE 5-----
SWITCH5 V05 ALPHA5MAX GAMMA5 ACCCOMD5 ENDFILE1
1,899.0,25.0,54.00,9.0,9999

Appendix 9: Dynamic Analysis of the Wing

1. **Figure 9.1. FEM on Wing**
2. **Figure 9.2. First Natural Frequency and Mode Shape**
3. **Figure 9.3. Second Natural Frequency and Mode Shape**
4. **Figure 9.4. Third Natural Frequency and Mode Shape**
5. **Figure 9.5. Fourth Natural Frequency and Mode Shape**

Figure 1: FEM on Wing

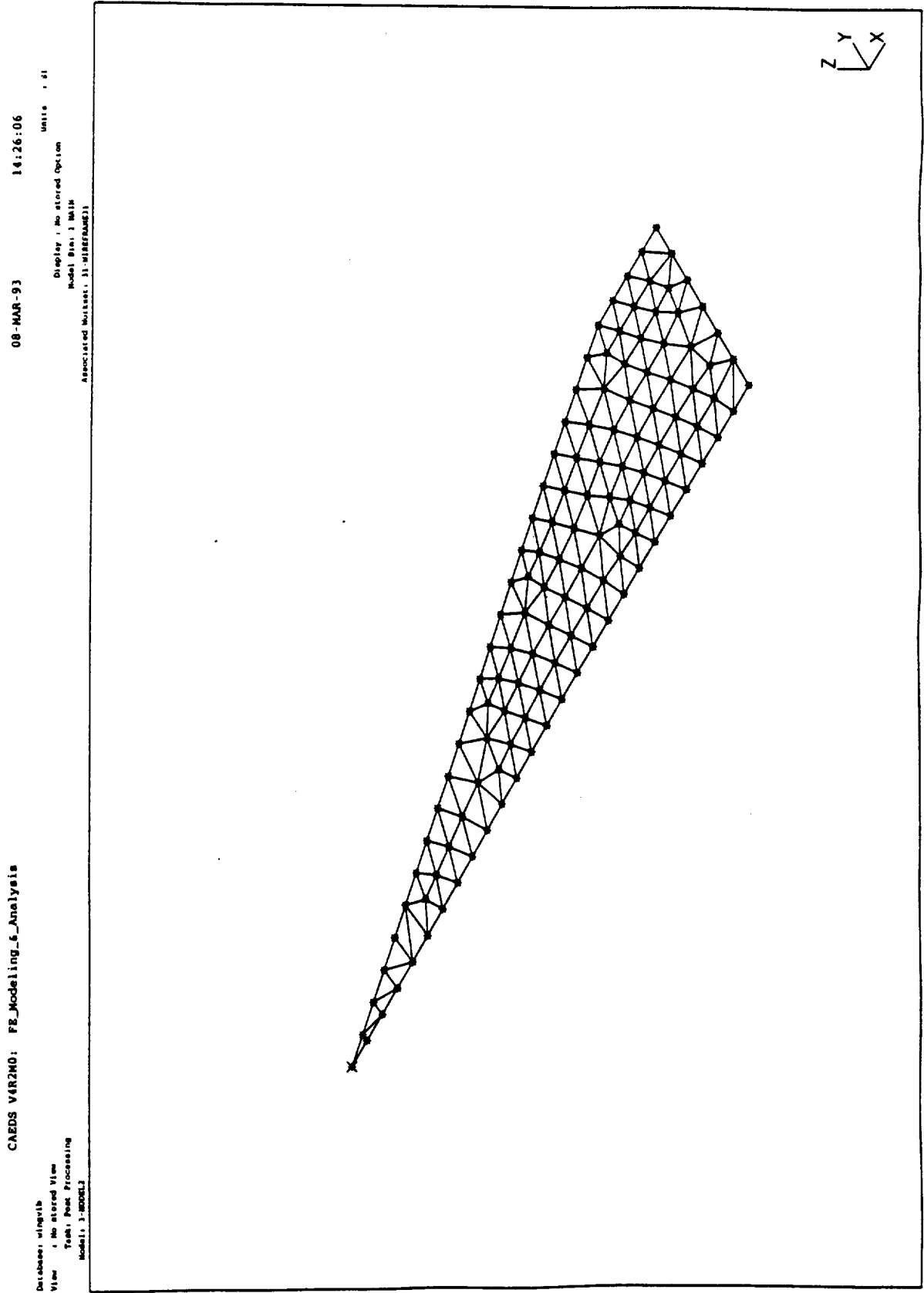


Figure 2 : First Natural Freq. and Mode Shape

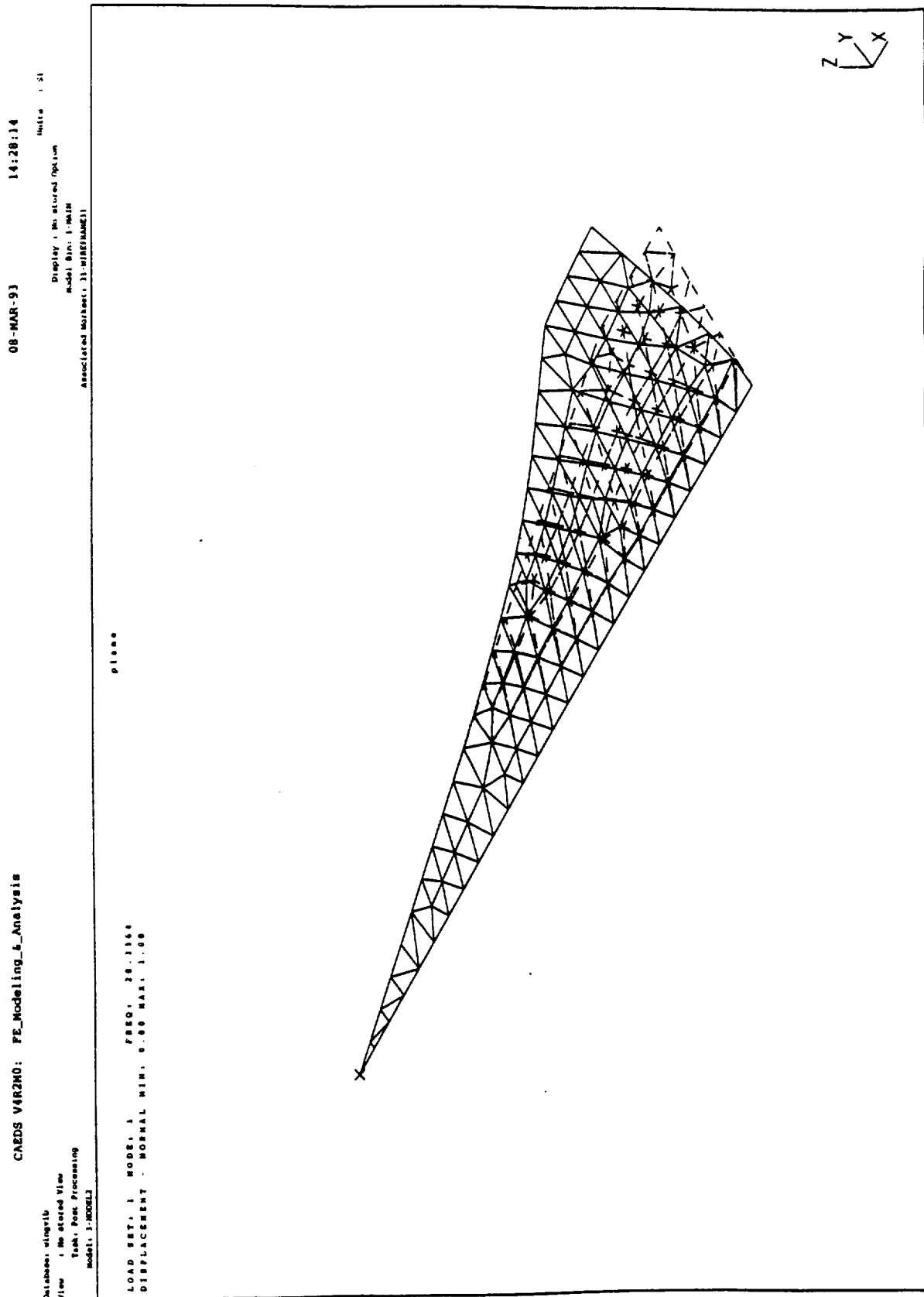


Figure 3 : Second Natural Freq. and Mode Shape

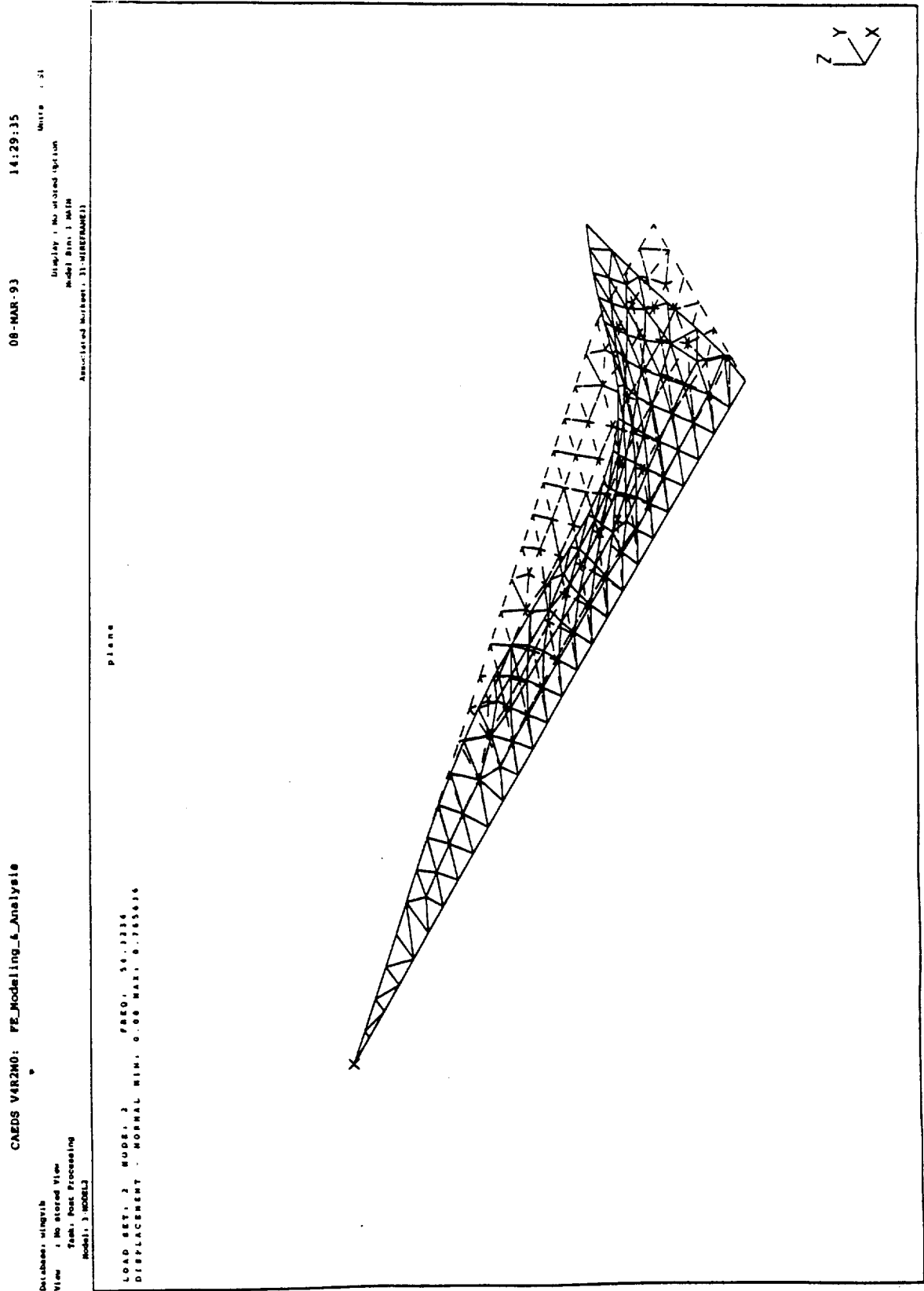
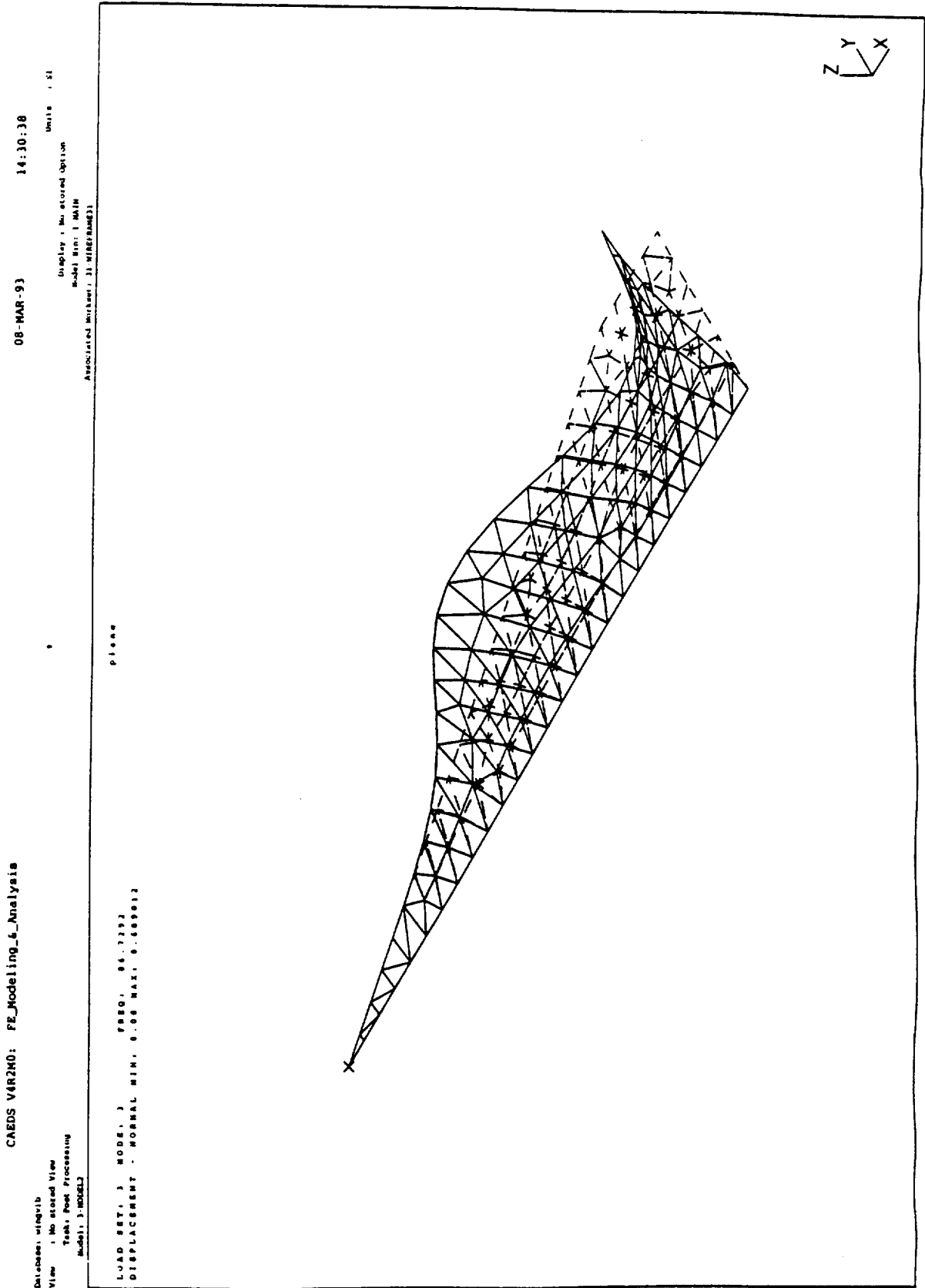


Figure 4: Third Natural Freq. and Mode Shape



Appendix 10. Proogram Listings

1. Propulsion Trade Study 1
2. Propulsion Trade Study 2
3. Glide Program
4. ETO Sort Program

Propulsion Trade Study 1

```
program a515;

const tsfch = 8.4;
    tsfcj = 12.2;
    dh = 19.97;
    djp = 64.29;
    ld = 2.5;

var iv,fv,gw,ts,tavail:real;

procedure fuelwt (tsfc,den,iv,fv,gw,ts,tavail:real);
var t,v,acc,w,fwt,accg: real;
begin
    v:=iv;
    t:=0;
    w:=gw;
    fwt:=0;
    acc:=(tavail-w/ld)/w*32.2;
    writeln ('time    acc    vel    g    fuelwt');
    accg:=acc/32.2;
    writeln (t:7:2,acc:7:2,v:10:2,accg:7:2,fwt:9:1);
    while v<fv do
    begin
        t:=t+ts;
        acc:=((tavail-w/ld)/w*32.2+acc)/2;
        accg:=acc/32.2;
        v:=v+acc*ts;
        w:=w-tsfc/3600*tavail*ts;
        fwt:=fwt+tsfc/3600*tavail*ts;
        writeln (t:7:2,acc:7:2,v:10:2,accg:7:2,fwt:9:1);
    end;
    writeln;
    writeln ('Fuel Weight: ',fwt:9:0,' lbmass');
    writeln ('Empty Weight: ',w:9:0,' lbmass');
    writeln ('Fuel Fraction: ',(gw-w)/gw:5:3);
    writeln ('Fuel Volume: ',(gw-w)/den:7:2,' ft^3');
    writeln;
    writeln ('Hit Enter to Continue');
    readln;
end;

begin
    write ('Input Initial Velocity: ');
```

```
readln (iv);
write ('Input Final Velocity: ');
readln (fv);
write ('Input Thrust Available: ');
readln (tavail);
write ('Input Gross Weight: ');
readln (gw);
write ('Input Time Step: ');
readln (ts);
writeln;
writeln ('Hydrogen Oxygen Rocket');
writeln;
fuelwt (tsfch,dh,iv,fv,gw,ts,tavail);
writeln;
writeln ('JP Oxygen Rocket');
writeln;
fuelwt (tsfcj,djp,iv,fv,gw,ts,tavail);
end.
```

□

Propulsion Trade Study 2

```
program a515;

const tsfch = 9.83;
    tsfcj = 12.2;
    dh = 19.97;
    djp = 64.29;
    ld = 1.5;

var iv,fv,gw,ts,tavail,theta:real;
    te,p:real;

procedure fuelwt (tsfc,den,iv,fv,gw,ts,tavail1,theta:real);
var t,v,acc,w,fwt,accg,h,dhdt: real;
begin
    v:=iv;
    t:=0;
    w:=gw;
    fwt:=0;
    h:=0;
    acc:=(tavail1-w/ld)/w*32.2;
    writeln ('time acc vel g fuelwt');
    accg:=acc/32.2;
    writeln (t:7:2,acc:7:2,v:10:2,accg:7:2,fwt:9:1,h:8:0);
    while v<fv do
    begin
        t:=t+ts;
        te:=518.69-h*3.58e-3;
        if (h > 37500) and (h < 65000) then te:=389.97;
        if h > 65000 then te:=389.97+5.45e-4*h;
        p:=2.1162e3*exp(-32.2/1716/te*h);
        tavail:=tavail1-p*3.977;
        acc:=((tavail-w*cos(theta)/ld-w*sin(theta))/w*32.2+acc)/2;
        dhdt:=v*sin(theta);
        h:=h+dhdt*ts;
        accg:=acc/32.2;
        v:=v+acc*ts;
        w:=w-245.76*ts;
        fwt:=fwt+245.76*ts;
        writeln (t:7:2,acc:7:2,v:10:2,accg:7:2,fwt:9:1,h:8:0,tavail:8:0,p:5:0,te:4:0);
    end;
    writeln;
    writeln ('Fuel Weight: ',fwt:9:0,' lbmass');
    writeln ('Empty Weight: ',w:9:0,' lbmass');
    writeln ('Fuel Fraction: ',(gw-w)/gw:5:3);
    writeln ('Fuel Volume: ',(gw-w)/den:7:2,' ft^3');
```

```
writeln;
writeln ('Hit Enter to Continue');
readln;
end;

begin
  write ('Input Initial Velocity: ');
  readln (iv);
  write ('Input Final Velocity: ');
  readln (fv);
  write ('Input Thrust Available: ');
  readln (tavail);
  write ('Input Gross Weight: ');
  readln (gw);
  write ('Input Time Step: ');
  readln (ts);
  write ('Input climb angle: ');
  readln (theta);
  theta:=theta*3.1415/180;
  writeln;
  writeln ('Hydrogen Oxygen Rocket');
  writeln;
  fuelwt (tsfch,dh,iv,fv,gw,ts,tavail,theta);
  writeln;
  writeln ('JP Oxygen Rocket');
  writeln;
  fuelwt (tsfcj,djp,iv,fv,gw,ts,tavail,theta);
end.
```

□

Glide Program

```
PROGRAM GLIDE
IMPLICIT DOUBLE PRECISION (A-G,K-Y)
DOUBLE PRECISION ALT(112),P(112),T(112),CL(25,20,7)
+ ,CD(25,20,7)
DOUBLE PRECISION ALMAX(25,20)
INTEGER H,I,J,Z,IA,ZF
OPEN(UNIT=1,FILE='ATMOS.DAT',STATUS='OLD')
OPEN(UNIT=4,FILE='MOD1.DAT',STATUS='OLD')
OPEN(UNIT=7,FILE='AOUT1.DAT',STATUS='OLD')
OPEN(UNIT=2,FILE='MOD2.DAT',STATUS='OLD')
OPEN(UNIT=3,FILE='AOUT2.DAT',STATUS='OLD')
PI=3.141592654D0
WRITE(6,10)
10 FORMAT('ENTER TIME INCREMENT: ')
READ(5,*) DT
DATA GAMA,G,R,ZF/1.387D0,3.216D+1,1.716D+3,1/
DATA S,MUR,B,TIME,E/6.25D+2,2D-1,2.5D+1,1.97D+2,8.5D-1/
AR=B*B/S
DO 30 I=1,12
DO 28 J=1,8
READ(7,*) DU49,XM9,ALMAX(I,J),LDMX,CD09,E5TOT
DO 27 H=1,6
READ(4,*)DUANE4,XM1,ALPHA9,CL(I,J,H),CD(I,J,H)
+ ,CLCD,EE59
27 CONTINUE
28 CONTINUE
30 CONTINUE
READ(7,*) ENDM
READ(4,*) ENDM2
WRITE(6,*) ENDM,ENDM2
CLOSE(UNIT=7)
CLOSE(UNIT=4)
DO 60 I=1,12
DO 58 J=9,14
READ(3,*) D4,XM9,ALMAX(I,J),LDMX,CD09,E5TOT
DO 57 H=1,6
READ(2,*)DUANE4,XM1,ALP,CL(I,J,H),CD(I,J,H)
+ ,CLCD,EE59
57 CONTINUE
58 CONTINUE
60 CONTINUE
```

```

READ(3,*)ENDM
READ(2,*)ENDM2
WRITE(6,*)ENDM,ENDM2
CLOSE(UNIT=3)
CLOSE(UNIT=2)
DO 100 I=1,111
  READ(1,*) ALT(I),T(I),P(I),RHO
100 CONTINUE
  CLOSE(UNIT=1)
  OPEN(UNIT=1,FILE='DEC.DAT',STATUS='UNKNOWN')
  DO 99 I=1,12
    ALMAX(I,15)=ALMAX(I,14)
    DO 98 Z=1,6
      CL(I,15,Z)=CL(I,14,Z)
      CD(I,15,Z)=CD(I,14,Z)
98 CONTINUE
99 CONTINUE
    DO 96 I=1,12
      DO 97 J=1,15
        CL(I,J,7)=CL(I,J,6)
        CD(I,J,7)=CD(I,J,6)
97 CONTINUE
96 CONTINUE
    TR=0D0
    DATA THETMX,THET,W/0D0,0D0,1.37D+4/
    DATA ALFMX,THETMN,M,Y,X/2.4D+1,-8D-2,1.2D+1,1.064256D+5,
+ 1.21314D+6/
    V1=M*DSQRT(GAMA*R*T(101))
    VY=0D0
    VX=V1
    L=W
80 IA=INT(Y/1000)+1
    MIA=Y/1000-IA+1D0
    IF(Y.LT.1D+1)GOTO 500
    P1=P(IA)+MIA*(P(IA+1)-P(IA))
    T1=T(IA)+MIA*(T(IA+1)-T(IA))
    RHO=P1/R/T1
    I=INT((Y-1D+3)/1D+4)+1
    MI=(Y-1D+3)/1D+4-I+1D0
    IF(Y.LT.1D+3)THEN
      I=1
      MI=0D0
    ENDIF
    IF(M.LT.1.5D0)THEN
      J=INT((M-1D-1)/2D-1)+1

```

```

    MJ=(M-1D-1)/2D-1-J+1D0
ELSEIF(M.LT.2D0)THEN
    J=8
    MJ=(M-1.5D0)/5D-1
ELSE
    J=INT((M-2D0)/2D0)+9
    MJ=(M-2D0)/2D0-J+9
ENDIF
AL1=ALMAX(I,J)+MI*(ALMAX(I+1,J)-ALMAX(I,J))
ALFA=AL1+MJ*(ALMAX(I,J+1)-ALMAX(I,J))
IF(THET.GT.THETMX)THEN
    ALFA=0D0
ELSEIF(THET.LT.THETMN)THEN
    ALFA=ALFMX
ENDIF
Z=INT(ALFA/5D0)+1
MZ=ALFA/5D0-Z+1D0
CL2=CL(I,J,Z)+MI*(CL(I+1,J,Z)-CL(I,J,Z))/3D0
CL3=CL2+MJ*(CL(I,J+1,Z)-CL(I,J,Z))/3D0
CLA=CL3+MZ*(CL(I,J,Z+1)-CL(I,J,Z))/3D0
CD2=CD(I,J,Z)+MI*(CD(I+1,J,Z)-CD(I,J,Z))/3D0
CD3=CD2+MJ*(CD(I,J+1,Z)-CD(I,J,Z))/3D0
CDA=CD3+MZ*(CD(I,J,Z+1)-CD(I,J,Z))/3D0
CL1=CLA
IF(THET.GT.THETMX)THEN
    CL1=0D0
ELSEIF(THET.LT.THETMN)THEN
    CL1=CLA
ENDIF
CD1=CDA
IF(M.LT.1.0D0.AND.ALFA.GT.0D0)THEN
    CL1=4.5D-1
    CD1=9.0D-2
ENDIF
IF(Y.LT.5.5D+4)THEN
    THETMN=3.7D-2
    THETMX=0D0
ENDIF
IF(Y.LT.1D+3)THEN
    FI=(16D0*Y/B)**2
    CD1=CDA-1D0/(1D0+FI)*CL1*CL1/PI/E/AR
    THETMN=2.9D-2
    THETMX=0D0
IF(Y.GT.5D+1)THEN
    T50=TIME

```

```

X50=X
V50=V1
ENDIF
ENDIF
Q0=RHO/2D0*V1*V1
L=RHO/2D0*V1*V1*S*CL1
D=RHO/2D0*V1*V1*S*CD1
AL=ALFA*PI/1.8D+2
AX=G/W*(TR*DCOS(THET+AL)-D*DCOS(THET)-
+ L*DSIN(THET))
AY=G/W*(TR*DSIN(THET+AL)-D*DSIN(THET)+
+ L*DCOS(THET))-G
X=X+(VX+VX+AX*DT)/2D0*DT
Y=Y+(VY+VY+AY*DT)/2D0*DT
VX=VX+AX*DT
VY=VY+AY*DT
V1=DSQRT(VX*VX+VY*VY)
M=V1/DSQRT(GAMA*R*T1)
A=DSQRT(AX*AX+AY*AY)
THET=DATAN(VY/VX)
TIME=TIME+DT
IF(ZF.EQ.1)THEN
WRITE(1,300) TIME,M,Y,X/6.0761033D+3,TR,Q0,ALFA,VY,W
+ ,L/D,D
300 FORMAT(F6.1,1X,F6.3,1X,F7.0,1X,F6.2,1X,F7.0,1X,F6.1,1X,
+ F4.1,1X,F6.1,1X,F7.1,1X,F6.3,1X,F7.1)
ZF=2
ELSE
ZF=1
ENDIF
GOTO 80
500 OPEN(UNIT=2,FILE='TSUM.DAT',STATUS='UNKNOWN')
Y=0D0
VY=0D0
DATA CLAL,ALDOT/1.8D-2,-8.33D0/
P1=P(1)
T1=T(1)
TR=0D0
RHO=P1/R/T1
FI=0D0
TL=TIME
XL=X
VL=VX
40 IF(J.LT.1)THEN
J=1

```

```

ENDIF
ALFA=ALFA+ALDOT*DT
CLTO=ALFA*CLAL
J=INT((M-1D-1)/2D-1)+1
CDTO=CD(1,J,1)
D=RHO/2D0*VX*VX*S*(CDTO-1D0/(1D0+FI)*CLTO*CLTO/PI/E/AR)
L=RHO/2D0*VX*VX*S*CLTO
Q0=RHO*VX*VX/2D0
IF(VX.LT.1D0)GOTO 888
IF(ALFA.GE.1D-3)THEN
  TND=TIME
  XND=X
  VND=VX
ELSEIF(ALFA.LT.1D-3)THEN
  ALDOT=0D0
  ALFA=0D0
ENDIF
IF(ZF.EQ.1)THEN
  WRITE(1,50) TIME,M,Y,X/6.0761033D+3,TR,Q0,ALFA,VY,W
  + ,L/D,D
50 FORMAT(F6.1,1X,F6.3,1X,F7.0,1X,F6.2,1X,F7.0,1X,F6.1,1X,
  + F4.1,1X,F6.1,1X,F7.1,1X,F6.3,1X,F7.1)
  ZF=2
ELSE
  ZF=1
ENDIF
AL=ALFA*PI/1.8D+2
AX=G/W*(-D-MUR*(W-L))
DVX=DT*AX
X=X+(DVX+VX+VX)/2D0*DT
TIME=TIME+DT
VX=VX+DVX
M=VX/DSQRT(GAMA*R*T1)
GOTO 40
888 WRITE(2,65) V50,XL-X50,VL,XND-XL,VND,X-XND,X-X50
65 FORMAT('V50= ',F7.2,5X,'XAP= ',F6.0,5X,'VL= ',F7.2,5X,
  + 'XROLL= ',F6.0,/,',VND= ',F7.2,5X,'XBR= ',F6.0,5X,
  + 'XLAND= ',F6.0)
STOP
END

```

ETO Sort Program

```
PROGRAM SORT
IMPLICIT DOUBLE PRECISION (A-G,K-Z)
DOUBLE PRECISION ALT(112),P(112),T(112),CL(25,20,7)
+ ,CD(25,20,7),ZEE5(25,20,7),DU4(25),XM(20),CD0(25,20)
+ ,ALPHA(7),K(20),DELCD(25),CLAL(20),XISP(250),ALT1(25)
INTEGER H,I,J
OPEN(UNIT=1,FILE='ATMOS.DAT',STATUS='OLD')
OPEN(UNIT=4,FILE='MOD3.DAT',STATUS='OLD')
OPEN(UNIT=7,FILE='AOUT3.DAT',STATUS='OLD')
OPEN(UNIT=2,FILE='MOD4.DAT',STATUS='OLD')
OPEN(UNIT=3,FILE='AOUT4.DAT',STATUS='OLD')
OPEN(UNIT=6,FILE='MSFOR\SORT.144',STATUS='UNKNOWN')
PI=3.141592654D0
WRITE(6,10)
10 FORMAT('INPUT DATA FILE "SORT.DAT"/5MAY93/ROCKET SSTO'
+ ,/, 'PROGRAM ETO',/, 'TABLE XISPA',/, '0 0 0 0 0'
+ ,/, '1 4 0 0',/, '0.0, .9,1.5,15.0')
WRITE(6,11)
11 FORMAT('4000, 3000,2000,1000',/, 'TABLE XPHIMAX',/,
+ '0,0,0,0,0',/, '1, 4 ,0 ,0',/, '0.0,.9,1.5,15.0',/, '1.0,1.0,1.0,3.0'
+ ,/, 'TABLE XCD0',/, '0,0,0,0,0',/, '1,14, 0 ,0')
DO 30 I=1,12
DO 28 J=1,8
READ(7,4001) DU4(I),XM(J),ALMAX,LDMX,CD0(I,J),ESTOT
4001 FORMAT(F8.1,F7.4,F6.3,F6.3,
+ F8.5,F7.4)
DO 27 H=1,6
READ(4,26)DUANE4,XM1,ALPHA(H),CL(I,J,H),CD(I,J,H)
+ ,CLCD,ZEE5(I,J,H)
26 FORMAT(F8.1,F7.4,F7.2,F7.3,F7.3,F7.3,F9.5)
27 CONTINUE
28 CONTINUE
30 CONTINUE
CLOSE(UNIT=7)
CLOSE(UNIT=4)
DO 60 I=1,12
DO 58 J=9,14
READ(3,4031) D4,XM(J),ALMAX,LDMX,CD0(I,J),ESTOT
4031 FORMAT(F8.1,F7.4,F6.3,F6.3,
+ F8.5,F7.4)
DO 57 H=1,6
```

```

      READ(2,56)DUANE4,XM1,ALP,CL(I,J,H),CD(I,J,H)
+   ,CLCD,ZEE5(I,J,H)
56   FORMAT(F8.1,F7.4,F7.2,F7.3,F7.3
+   ,F7.3,F9.5)
57   CONTINUE
58   CONTINUE
60   CONTINUE
      CLOSE(UNIT=3)
      CLOSE(UNIT=2)
      DO 100 I=1,111
          READ(1,*) ALT(I),T(I),P(I),RHO
100  CONTINUE
          CLOSE(UNIT=1)
          WRITE(6,101) (XM(J),J=1,14)
101  FORMAT('0.0',12(F3.1,''),F4.1,'',F4.1)
          WRITE(6,102) (CD0(1,J),J=1,14)
102  FORMAT('0.0',10(F6.5,''),F6.5,/,2(F6.5,''),F6.5,/,
+   ' TABLE XDELCD',/, '0,0,0,0,0',/, '1,13,0,0')
          DO 210 J=1,14
              CDN=1D+2
              DO 200 H=1,6
                  IF(CD(1,J,H).LE.CDN)THEN
                      K(J)=ZEE5(1,J,H)
                  ENDIF
200  CONTINUE
210  CONTINUE
          DO 220 I=1,12
              DSUM=0D0
              DO 215 J=1,14
                  DO 211 H=1,6
                      DCD=CD(I,J,H)-K(J)*CL(I,J,H)**2D0-CD0(1,J)
                      DSUM=DSUM+DCD
211  CONTINUE
215  CONTINUE
              DELCD(I)=DSUM/8.4D+1
220  CONTINUE
          WRITE(6,240) (DU4(I),I=1,12)
240  FORMAT('0.0',9(' ',F7.0),/,2(F7.0,' '),F7.0)
          WRITE(6,250) (DELCD(I),I=1,12)
250  FORMAT('0.0',10(' ',F6.4),/,F6.4,' ',F6.4,/, 'TABLE XCLALPHA'
+   ,/, '0,0,0,0,0',/, '1,15 , 0, 0')
          DO 270 J=1,14
              CASUM=0D0
              DO 265 I=1,12
                  CAL=(CL(I,J,5)-CL(I,J,1))/(ALPHA(5)-ALPHA(1))

```

```

      CASUM=CASUM+CAL
265  CONTINUE
      CLAL(J)=CASUM/1.2D+1
270  CONTINUE
      WRITE(6,280) (XM(J),J=1,14)
280  FORMAT('0.0',12(F3.1,''),F4.1,'',F4.1)
      WRITE(6,290) CLAL(1),(CLAL(J),J=1,14)
290  FORMAT(F4.3,14(',F4.3),/, 'TABLE  XK',/, '0,0,0,0,0',/,
+ '1,15,0,0')
      WRITE(6,300) (XM(J),J=1,14)
300  FORMAT('0.0',12(F3.1,''),F4.1,'',F4.1)
      WRITE(6,310) K(1),(K(J),J=1,14)
310  FORMAT(F6.4,10(',F6.4),/F6.4,3(',F6.4),/,
+ 'TABLE  XA0AC',/, '0,0,0,0,0',/, '2,4,3,0',/,
+ '0.0,0.8,1.0,15.0',/, '-10.0,0.0,10.0',/, '80.0,.15,.15,1.0')
      WRITE(6,320)
320  FORMAT('80.0,.15,.15,1.0',/, '80.0,.15,.15,1.0',/,
+ 'TABLE  XISPR',/, '0,0,0,0,0',/, '1,12,0,0')
      DO 340 I=1,12
      IC=(I-1)*10+1
      TR=3.4D+4-P(IC)/4D0*PI*(2.8D+1/1.2D+1)**2D0
      XISP(I)=TR/8.192771084D+1
      ALT1(I)=ALT(IC)
340  CONTINUE
      WRITE(6,350) (ALT1(I),I=1,12)
350  FORMAT(F8.1,7(',F8.1),/F8.1,3(',F8.1))
      WRITE(6,360) (XISP(I),I=1,12)
360  FORMAT(F5.1,11(',F5.1),/ 'TABLE  XWDOTPMAX',/, '0,0,0,0,0',/
+ ',1,4,0,0',/, '0.0,2.0,8.0,13.0',/, '245.783,245.783,245.783',
+ ',245.783',/, 'AIRBREATHER-----',/, 'AC AREF FASTOIC')
      WRITE(6,370)
370  FORMAT('0.0, 625.0, .0292',/, 'VEHICLE-----',/
+ 'WLAUNCH WFUEL WFINAL VFINAL STAGE',/
+ '48000., 35000., 13000., 11981., 1')
      WRITE(6,380)
380  FORMAT('INITIAL CONDITIONS-----',/
+ 'M0 H0 GAMMA ALPHA DT DELPRINT TIMEX',/
+ '0.001,0.001,0.0,0.0,1.0,10,0.0')
      WRITE(6,390)
390  FORMAT('PHASE 1-----',/, 'VTAKEOFF',/, '375.0',/
+ 'PHASE 2-----',/
+ 'ALPHA2MAX LOADFAC GAMMAMAX ACCCOMD V02 H02')
      WRITE(6,400)
400  FORMAT('20.0,8.0,30.0,9.0,900.0,18000.0',/
+ 'PHASE3-----',/

```

```
+ 'ALPHAMIN ALPHAMAX Q0COMD V0TEMP Q0FINAL GAINQ3
GAINGAM3')
  WRITE(6,410)
410 FORMAT('-5.0 ,5.0 , 549. ,1200.0 ,2305. ,10.0 ,1.0',/
+ 'PHASE 4-----',/
+ 'SWITCH4 V0CRUISE GAINH04 GAINGAM4 GAINQ4')
  WRITE(6,420)
420 FORMAT('0 ,0.0 ,-20.0 ,0.0 ,5.0',/,'PHASE 5-----',/
+ 'SWITCH5 V05 ALPHA5MAX GAMMA5 ACCCOMD5 ENDFILE1',/
+ '0 ,0.0 ,0.0 ,0.0 ,0.0 ,9999')
  STOP
  END
```





